University of Virginia
Automobile Safety Laboratory

Out-of-Position Occupant Testing (OOPS3 Series)

Cameron R. Bass
Jeff R. Crandall
Walter D. Pilkey

September 1998 Report OOPS3

TABLE OF CONTENTS

1: INTRODUCTION AND OBJECTIVES 1

1.1: REFERENCES 2

2: TEST DESCRIPTION 3

2.1: TEST SETUP 3
2.1.1: MECHANICAL EQUIPMENT 3
2.1.2: PHOTOGRAPHY EQUIPMENT 4
2.1.3: DATA ACQUISITION SYSTEM 5
2.1.4: INSTRUMENTATION 5
2.2: TEST PROCEDURE 11
2.2.1: OCCUPANT PREPARATION 11
2.2.2: DESCRIPTION OF TEST PROCEDURE 11
2.2.3: OCCUPANT POSITIONING 12
2.2.3.1: POSITIONING LOCATIONS 15
2.2.4: ENVIRONMENT 22
2.2.5: PHOTOGRAPHY 22
2.2.6: DATA ACQUISITION 23
2.2.7: DATA PROCESSING 23

3: TEST RESULTS 24

3.1: DESCRIPTION OF RESULTS 24
3.2: SENSOR DATA 24
3.3: THORACIC DATA 41
3.3.1: CHEST DISPLACEMENT DATA 49
3.3.1.1: CRUX PERFORMANCE 51
3.3.1.2: CHESTBAND PERFORMANCE 55
3.3.2: DYNAMIC CHEST V*C DATA 56
3.4: PHOTOGRAPHIC RESULTS 57
3.5: SENSOR AND TEST FAILURES 58
3.6: DISCUSSION OF RESULTS 59
3.6.1: SKIN/DISTANCE FROM MODULE STUDY 59
3.6.2: POSITIONING STUDY 61
3.6.3: COMPARISON WITH PREVIOUS ISO-2 TESTS AT ASL 64

4: CONCLUSIONS 66

1: INTRODUCTION AND OBJECTIVES

Although the use of air bag systems as supplemental restraints has significantly decreased the overall risk of fatality in automobile collisions, there is evidence of increased risk of severe and fatal injuries to out-of-position small female and child occupants. For example, surveys of crash data (NHTSA Special Crash Investigation Summary - 4/1/98) and laboratory tests conducted by NHTSA indicate that small female occupants are most likely to be injured by driver-side air bags owing to their stature and proximity to the steering wheel and air bag module. Recently, automobile manufacturers have begun 'depowering' driver- and passenger-side air bags as the result of concerns for these small female and child occupants.

The tests described in this report were designed to evaluate the relationship between air bag inflation aggressivity and occupant injury and response for a depowered driver-side air bag. Depowered driver-side air bags were deployed into the chest of a 5th Percentile Female Hybrid III dummy positioned against the cover of the air bag module in an effort to simulate worst-case chest loading. The occupant, air bags, and test conditions for the tests are summarized in *Table 1.1*. The tests assessed the ability of chestband contours, thoracic accelerations, and head accelerations to predict injury and to quantify air bag aggressivity in terms of measured occupant response parameters.

This report presents the results and analysis of nineteen air bag deployment tests with out-of-position occupants (OOPS) positioned according to the ISO-2 standard. The tests may be considered as two subseries. The first subseries is a study of the effect of skin conditions on the dummy response. These tests, OOPS3.1-OOPS3.6, comprise three different skin conditions repeated twice. These tests are skin on with breast forms on in OOPS3.1-OOPS3.2, skin on with breast forms off in OOPS3.3-OOPS3.4, and skin off in tests OOPS3.5-OOPS3.6.

The second subseries, OOPS3.7-OOPS3.19, is a lateral and vertical positioning study. Positions investigated include the dummy thorax centered on the air bag module, vertically displaced 2 cm and 4 cm upwards with respect to the steering wheel center, and laterally displaced 4 cm left with respect to the steering wheel module. A test matrix for the entire OOPS3 test series is shown in *Table 1.1* below.

Goals of this research include evaluation of the position sensitivity of out-of-position deployment into a 5th Percentile Female Hybrid III dummy thorax as a part of a larger series in which occupant response and injury are being evaluated for a variety of occupant initial positions and air bag systems. Based upon data from these tests, a risk function that correlates observed cadaver injury with cadaver and dummy response is being developed using existing and future tests. The objective of this research is to develop a relationship between air bag inflation characteristics, occupant position, and cadaver injury. Using this relationship, guidelines will be established for air bag aggressivity thresholds and occupant position versus risk of injury.

The tests were conducted at the Automobile Safety Laboratory (ASL), operated by the Department of Mechanical, Aerospace, and Nuclear Engineering at the University of Virginia, Charlottesville, Virginia. Research is conducted under Cooperative Agreement No. DTNH22-93Y-07028 with the National Highway Traffic Safety Administration (NHTSA) of the U.S. Department of Transportation.

TABLE1.1: OOPS3 TEST MATRIX					
Study	**OOPS Test**	**Skin**	**Horizontal Position①**	**Vertical Position①**	**Comments②**
Skin Study	3.1	On with breasts	Center	Center	'Nominal ISO-2'
	3.2	On with breasts	Center	Center	'Nominal ISO-2'
	3.3	On without breasts	Center	Center	'Nominal ISO-2'
	3.4	On without breasts	Center	Center	'Nominal ISO-2'
	3.5	Off	Center	Center	'Nominal ISO-2'
	3.6	Off	Center	Center	'Nominal ISO-2'
Position Study	3.7	On with breasts	Center	Center	'Chest on Module', No chestbands
	3.8	On with breasts	Center	Center	'Chest on Module'
	3.9	On with breasts	Center	Center	'Chest on Module'
	3.10	On with breasts	Center	Center	'Chest on Module'
	3.11	On with breasts	Center	4 cm up	'Chest on Module'
	3.12	On with breasts	Center	4 cm up	'Chest on Module'
	3.13	On with breasts	4 cm left	Center	'Chest on Module', air bag tear
	3.14	On with breasts	4 cm left	Center	'Chest on Module', air bag tear
	3.15	On with breasts	4 cm left	Center	'Chest on Module'
	3.16	On with breasts	4 cm left	Center	'Chest on Module'
	3.17	On with breasts	Center	2 cm up	'Chest on Module'
	3.18	On with breasts	Center	2 cm up	'Chest on Module'
	3.19	On with breasts	Center	2 cm up	'Chest on Module'

NOTES:

① Horizontal and Vertical Position refer to dummy sternum center positions relative to steering wheel center in the local axis system tangential to the steering wheel plane.

② Comments are described in subsequent sections.

TABLE1.2: OOPS ISO-2 SERIES 3 TEST SUMMARY	
TEST NUMBER	**OOPS3.1 – OOPS3.19**
OCCUPANT	
Type	5th % Female Hybrid III
Number	VRTC 145
STEERING WHEEL AND AIR BAG	
Type	1998 Ford
Model	Taurus

1.1: REFERENCES

All Appendix references in this document are found in the ASL ***Descriptions and Procedures Manual***. To ensure conformity of data with other test facilities and between tests conducted at the ASL, standard conventions have been adopted for test procedures and data analysis procedures. The primary standards used are listed in Appendix A.1. Other references concerning equipment and procedures and relevant published literature are listed in Appendix B.

2: TEST DESCRIPTION

2.1: TEST SETUP

2.1.1: MECHANICAL EQUIPMENT

The static out-of-position tests were conducted in the Automobile Safety Laboratory's OOPS test fixture shown in *Figure 1*. The fixture incorporates a rigid dummy seat with an adjustable pelvis locating pin in the occupant centerline. The steering wheel angle is 25 degrees (+/- 1 degree) from laboratory vertical. The steering wheel is attached to a five-axis steering column load cell mounted to a plate with horizontal and vertical adjustment positions. These positions allow variation of steering wheel position relative to the locating pin in increments of +/- 2 cm and +/- 4 cm from the vertical center position and +2 cm and +4 cm right of the horizontal center position. The center position of the steering wheel was selected to align the center of the sternum with the center of the air bag module in a coordinate system aligned with the dummy seat. Ganged hydraulic adjustment pistons were used to move the steering wheel into position in the local X-axis. Finally, a plywood backboard, cushioned with foam and padding, was positioned behind the bench to limit the rearward translation of the occupant following interaction with the air bag.

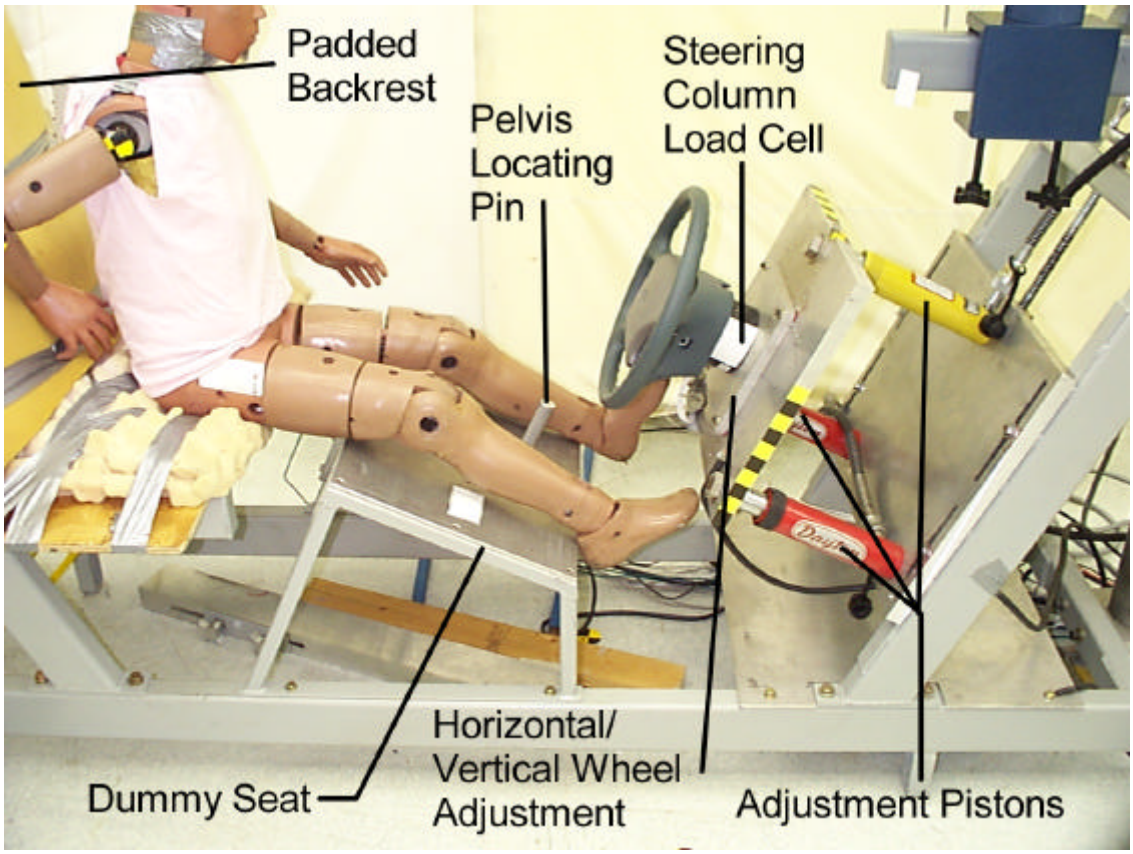

Figure 1: *Out-of-position Test Fixture*

The Ford Part numbers of the steering wheel and air bag assemblies used for the tests (refer to the test summary *Table 1.2*, above) are given in *Table 2.1.1.1*. A single bolt was used to attach the steering wheel to the center of the five-axis steering column load cell. Mating connectors, removed from steering column wiring harnesses, were used to connect the air bag modules to the ASL squib-firing circuitry. The connectors were brought out the backs of the steering wheels to facilitate connection and to protect the mating connectors from squib and inflator heat.

TABLE 2.1.1.1: EQUIPMENT PART NUMBERS

Part	1998 Ford Taurus
Steering Wheel	F7DC-3600-BAW
Air bag	F8DB-54043B13-ABW*DP

2.1.2: PHOTOGRAPHY EQUIPMENT

The tests were all photographed with the same set of one high-speed motion picture film camera and two high-speed solid-state video cameras. The equipment used is described in Appendix D. Lights, on portable and fixed stands, were positioned as necessary to ensure adequate lighting of the tests. Cameras, views, and settings are summarized in *Table 2.1.2.1* and the camera locations are shown schematically in *Figure 2*.

Synchronized photographic timing marks were recorded on the films in the film cameras, as described in Appendix D.1.4. Still photos were taken on Kodak Kodacolor 35mm ISO-200 color print film with a Nikon 6006AF single-lens reflex camera and with a Kodak DC-120 high-resolution digital still camera.

TABLE 2.1.2.1: HIGH-SPEED MOTION PICTURE CAMERAS

Camera					Lens		
#	Position ①	View	Type ②	Frame Rate ③	Focal Length	Aperture	Range
1	Offboard, Driver's Side	Analysis	R	2500	25.4 mm	f: 4	4.0 m
2	Offboard, Passenger's Side	Overall	K	1000	18.0 mm	f: 2.8	1.3 m
3	Onboard, Angled Overhead	Oblique	K	1000	13.0 mm	f: 2.8/4.0	1.0 m

NOTES:

① Camera positions are described in general in Appendix D.1.1. Also refer to Motion Picture Camera Position diagram, below.

② Camera types:

R = Redlake Hycam

K = Kodak RO High-Speed Video

③ Frame rate in exposures per second.

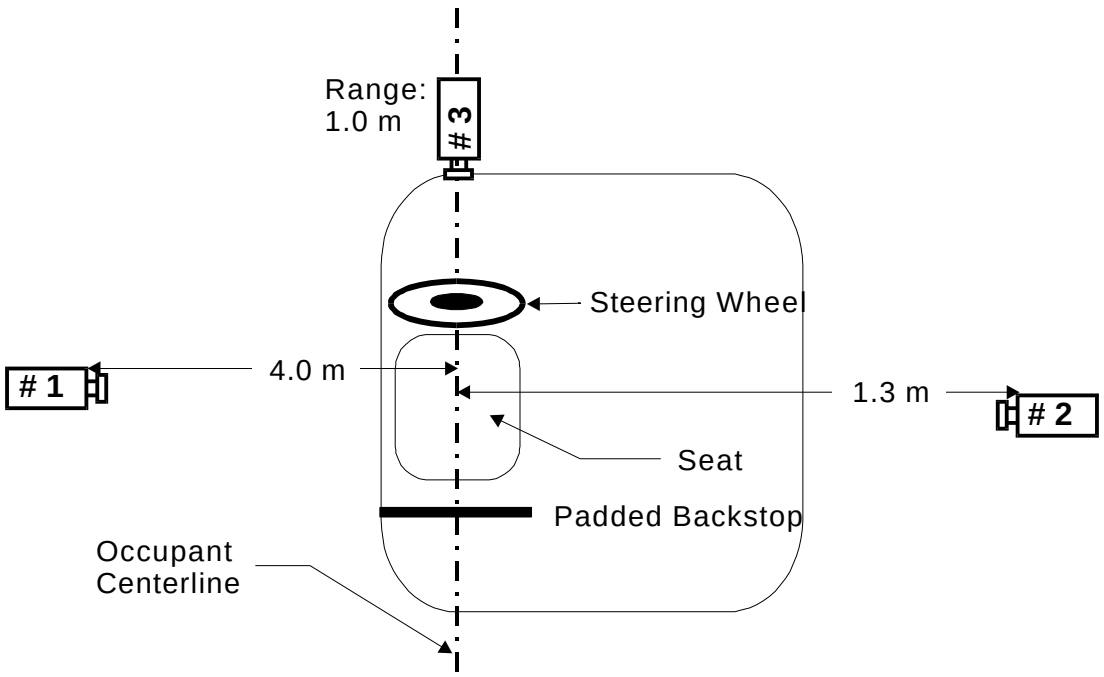

Figure 2: *Motion Picture Camera Position Diagram*

2.1.3: DATA ACQUISITION SYSTEM

Electronic signals from sensors mounted on the test fixture and within the test subject were recorded and converted to digital data by the ASL's 128-channel DSP Technology, model TRAQ-P, data acquisition system, which is described in detail in Appendix E.1. The data-collection process was controlled by DSP technology IMPAX 3.0 software, which is described in Appendix E.2. The post-test processing and conversion of the digital data to the NHTSA datatape format was done on IBM-compatible Pentium personal computers, using ASL software.

2.1.4: INSTRUMENTATION

The 5th Percentile Female Hybrid III was instrumented to acquire head, neck, and thoracic response during air bag deployment. The dummy instrumentation package included accelerometers at the conventional head and chest center-of-gravity locations. In addition, magnetohydrodynamic (MHD) angular rate sensors and accelerometers were attached to the posterior head and upper spine in locations analogous to those of cadaveric subjects tested in previous out-of-position tests. Data from the angular rate sensors allowed neck motion to be estimated from relative motion of the head and upper spine. Accelerometers on the second and fifth ribs recorded lateral acceleration of the rib cage. Upper and lower load cells recorded neck forces and moments. Chestbands were placed at the second and fifth ribs to determine local thoracic loading by the air bag systems. A sternal accelerometer and upper and lower sternum crux devices also recorded response of the anterior chest. In addition, contact forces between the occupant and the air bag were estimated from a five-axis load cell located at the upper end of the steering column. The sensors used are described in general, by type, in Appendix F.1 and

Appendix F.2. Table 2.1.4.1 lists the type, location, active axis, and model of the various sensors used in the tests.

In addition to the sensors discussed above, CRUX displacement sensors were used in the 5th Percentile Female Hybrid III thorax. Development of the CRUX displacement measurement unit was originally conducted by GESAC, Inc., as a component of the NHTSA THOR advanced frontal dummy development program. The CRUX concept provides continuous 3D measurement of sternal displacement with respect to the dummy spine, and has been designed to function reliably at sternal velocities anticipated in OOP airbag environments. The CRUX design is comprised of a two-bar linkage, with three rotational degrees of freedom, which are continuously measured by three precision rotary potentiometers. Using software calculations, these angular measurements are converted to X, Y, and Z sternal displacements with respect to the CRUX base coordinate system (which is attached to the dummy spine). The CRUX design in schematic form is shown in *Figure 3*, and a CRUX mechanical assembly as currently installed as standard equipment in the 50th percentile male THOR dummy is presented in *Figure 4*. The two CRUX assemblies utilized in the 5th Percentile Female Hybrid III dummy tests conducted at the University of Virginia were custom modified versions of these THOR units, to adapt the CRUX devices into the limited available thoracic volume in the 5th Percentile Female Hybrid III. The CRUX units were located at the level of the first rib (upper CRUX unit) and the sixth rib (lower CRUX unit). To facilitate mounting, the upper CRUX unit was located 1.1 cm left of the sternum centerline and the lower CRUX unit was located 1.1 cm right of the sternum centerline.

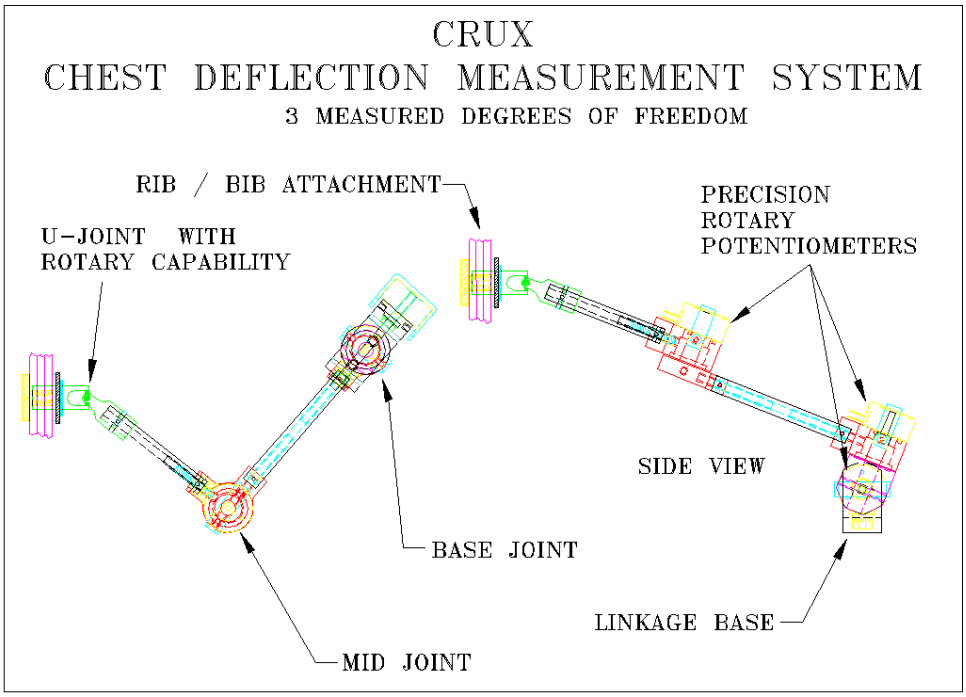

Figure 3: *CRUX Schematic*

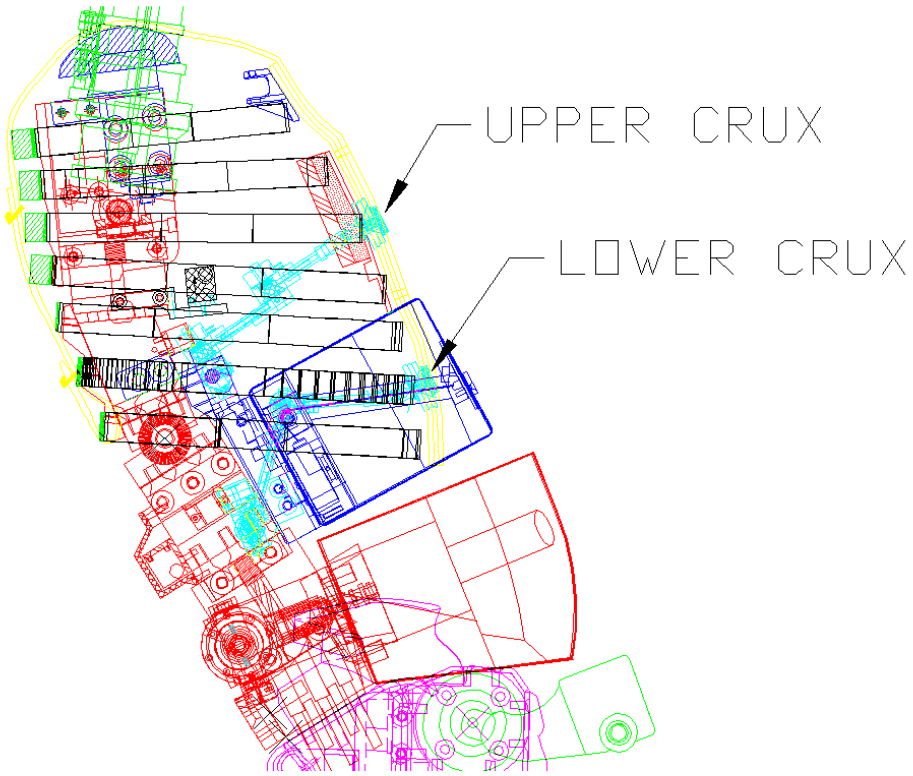

Figure 4: *CRUX Installed in THOR Dummy*

TABLE 2.1.4.1: SENSOR LIST- OOPS3

Measurement		Location	Axis ①	Type	Manuf.	Model
Steering Column	Load	Steering Column, Upper	X	5-Axis Load Cell	Denton	1765
			Y			
			Z			
	Moment		Y			
			Z			
5th % Female Hybrid III	Head Acceleration	Head CG	X	Accelerometer	Endevco	7264A
			Y	Accelerometer	Endevco	7264A
			Z	Accelerometer	Endevco	7264A
		Head, Rear, External ③	X	Accelerometer	Endevco	7264A
			Y	Accelerometer	Endevco	7264A
			Z	Accelerometer	Endevco	7264A
	Chest Acceleration	Chest CG	X	Accelerometer	Endevco	7264A
			Y	Accelerometer	Endevco	7264A
			Z	Accelerometer	Endevco	7264A
	Sternal Acceleration	Sternum, Upper	Y	Accelerometer	Endevco	7264A
		Sternum, Lower	X	Accelerometer	Endevco	7264A
	Spinal Acceleration	Spine, Upper, External ③	X	Accelerometer	Endevco	7264A
			Y	Accelerometer	Endevco	7264A
			Z	Accelerometer	Endevco	7264A
	Neck Load	Neck, Upper	X	6-Axis Load Cell	Denton	1716
			Y			
			Z			
		Neck, Lower	X	5-Axis Load Cell	Denton	2150
			Y			
			Z			
	Neck Moment	Neck, Upper	X	6-Axis Load Cell	Denton	1716
			Y			
			Z			
		Neck, Lower	X	5-Axis Load Cell	Denton	2150
			Y			
	Neck Rotation	Head, Rear & Spine, Upper, External ④	X	2 Triaxial MHD Angular Rate Sensors	ATA Sensors	ARS-04 Dynacube
			Y			
			Z			
	Sternum Deflection	Sternum, Lower & Upper	X	2 Triaxial Deformation Cruxes	GESAC	Crux
			Y			
			Z			
	Thorax Deflection	2nd Rib	⑤	Chestband	Denton	36-gauge
		5th Rib	⑤	Chestband	Denton	39-gauge

NOTES:

① Frame of reference is local to the part on which the sensor is mounted. See Appendix A.2 for definitions.
② Not applicable.
③ Accelerometers mounted on angular rate sensor cube faces. Angular rate sensor acceleration data is transformed to the local anatomical reference frame. See Appendix I.6 for a description of the procedure used.
④ Head and upper spine angular velocity data is used to compute neck rotation data, in the anatomical reference frame. See Appendix I.6 for a description of the procedure used.
⑤ Each chestband is wrapped around the exterior of the thorax at the location of the specified rib and measures local curvature at 37 or 38 points around the circumference of the thorax. See Appendix F.2 for a more detailed description of the chestband and Appendix H.3 for a description of the chestband installation procedure.
⑥ Head Y- and Z-axis and head angular rate sensor X-axis accelerometer data are used to compute head center-of-gravity acceleration data. See Appendix I.6 for a description of the procedure used.

2.1.5: OCCUPANT

The 5th Percentile Female Hybrid III dummy is a standard device, supplied to the ASL by NHTSA. The dummy, S/N #145, was received on 7 July 1996. A complete description of the dummy may be obtained from the reference listed in Appendix B.2. *Table 2.1.5.1* contains information about the clothing placed on the dummy during the tests. A grounded copper mesh shielding vest was used around the thorax, under the outer clothing layer, to shield the chestbands and internal instrumentation from possible electrical interference caused by static electrical discharges in the inflating air bag. A foam neck shield, supplied by First Technology Safety Systems, was installed around the Hybrid III neck to generally simulate a realistic neck diameter and to prevent entrapment of the air bag beneath the chin.

Special mounts were required for attaching the MHD angular rate sensors, used to measure neck flexion, to the Hybrid III dummy. The head rear mount consisted of a rectangular aluminum plate, approximately 9.5 mm thick, installed in place of the skull cover, and drilled and tapped to accept the MHD mounting screws. Spacers between the plate and the rear surface of the skull provided clearance for the internal head instrumentation cables. A removable cover protected the MHD sensor, but provided access for initial position measurements. The total mass of the mounting plate, cover assembly, mounting hardware, and sensor was adjusted to be approximately the same as that of the standard skull cover (including skin and mounting hardware). The upper spine MHD mount consisted of an aluminum bracket, which was attached to the top of the spine box by the four neck attachment bolts, and to which an aluminum plate, drilled and tapped for the MHD mounting screws, was attached. This plate was also used as the locating device for the rigid dummy positioning arm for the out-of-position fixture.

TABLE 2.1.5.1:
OCCUPANT SUMMARY

TEST NUMBER	**OOPS3.1 – OOPS3.19**
GENERAL INFORMATION	
Type	5th Percentile Hybrid III
Number	VRTC 145
Gender	Female
ANTHROPOMETRY	
Height (cm)	150.0
Weight (kg)	46.3
CLOTHING	
Upper Body Inner	Copper Mesh Shielding
Upper Body Outer	Cotton Shirt
Lower Body	None

2.2: TEST PROCEDURE

2.2.1: OCCUPANT PREPARATION

All Hybrid III instrumentation was installed, and the installation verified, before the tests. The standard Hybrid III head and spine center-of-gravity mounting blocks (designed for Endevco model 7264 miniature accelerometers) were used to mount the Endevco 7264A accelerometers used for these tests. Holes were drilled and tapped in the inner aluminum sternum plate of the Hybrid III for attachment of the lower sternal accelerometer to the inner surface. After removal of the rear head cover, the MHD angular rate sensor mounting plate was attached to the rear of the skull. The four lower neck attachment bolts were removed, and the upper spine MHD mounting bracket was attached to the top of the spine box using longer bolts. Grounding wires were connected to the spine box and skull.

2.2.2: DESCRIPTION OF TEST PROCEDURE

With the chestbands laid flat, static reference data was recorded at the beginning of each test. The dummy, prepared as described above, was placed next to the test fixture in a seated position, with the arms raised above the head. Chestbands were installed and static chest contours were generated and verified with measurements, as described in Appendix H.3. The remaining external instrumentation was installed, and individual sensor locations and polarities were confirmed. The occupant was dressed, the shielding mesh vest was installed, and the occupant was moved into the test position. The steering wheel and air bag were installed with the steering wheel fixture retracted from test position, with attention given to the correct orientation of the wheel.

The occupant was then attached to a rigid dummy-positioning arm as shown in *Figure 5*. For several tests in the series, measurements of chest stiffness were taken using a 2.54 cm diameter cylinder mounted at the steering wheel center to the steering column load cell as discussed in Section 3.5.2. After the occupant was positioned relative to the steering wheel, as described in Section 2.2.3, the steering wheel and air bag module were moved into test position. Following this, the rigid positioning arm was carefully removed so as not to disturb the dummy position. Final positioning measurements were taken as described below. In addition, the initial orientations of the MHD angular rate sensors were measured and noted, using the procedure described in Appendix H.2. Crosshair-type photographic targets were attached to the occupant at anatomical landmarks and their coordinates, relative to the reference target on the test fixture, were measured and noted using a Faro Arm positioning device. Measurements of head angles were also taken. (Refer to Table 2.2.3.2.) In addition, digital photographs of the final occupant positioning were taken.

After the air bag deployment, digital photographs were taken of the resting position of the occupant. The occupant was removed from the test fixture and the chestbands were removed and laid flat. The digital and high-speed video data were saved to computer disk. The various types of data were processed, as described in Section 2.2.7. The procedures used throughout the tests for motion picture photography and data acquisition are described in Sections 2.2.5 and 2.2.6.

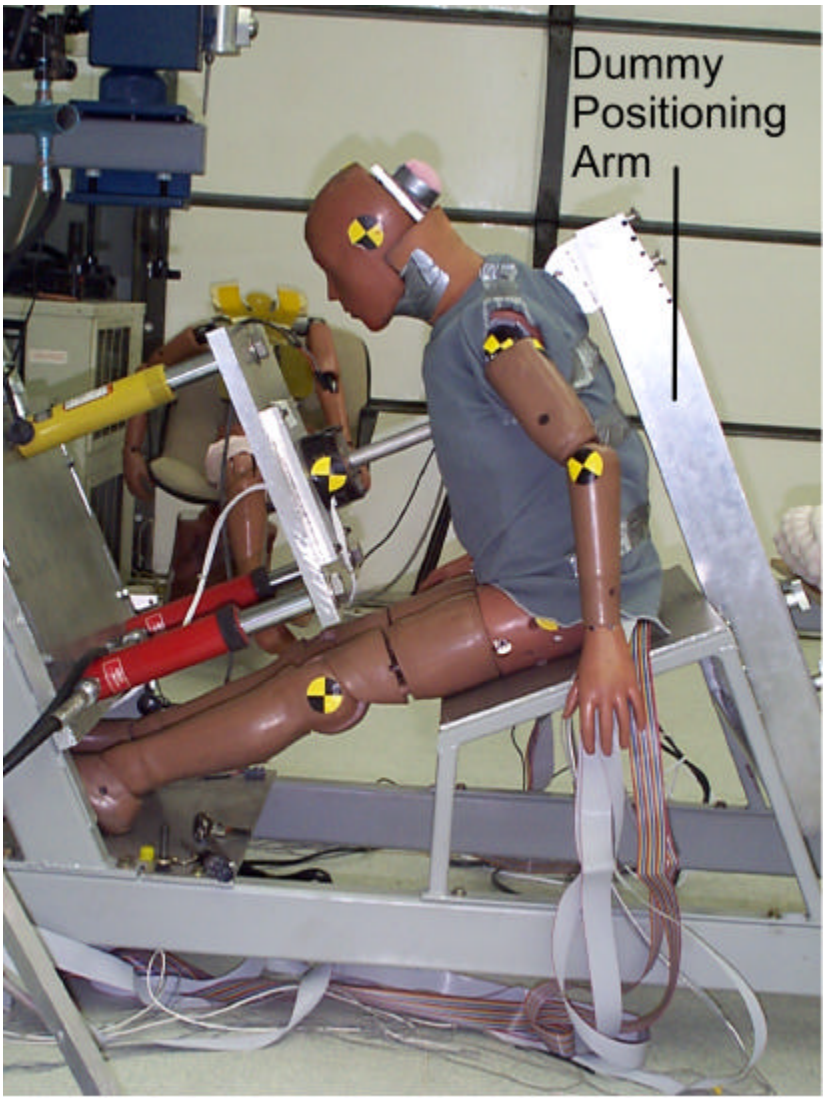

Figure 5: *Dummy on Rigid Positioning Arm*

2.2.3: OCCUPANT POSITIONING

The positioning guidelines for the ISO-2 tests came from the ISO DTR 10982 draft standard on "Road Vehicles - Test Procedures for Evaluating Out-of-Position Vehicle Occupant Interactions with Deploying Air Bags" (referenced in Appendix B.11). The 5th Percentile Female Hybrid III occupant used in this test series was positioned according to this procedure, briefly reviewed here. A general diagram of this position is presented in *Figure 9*.

There is some ambiguity in the interpretation of ISO-2 positioning. The presumed intention of the ISO-2 position is to investigate maximum thoracic loading of an out-of-position occupant. To achieve this position, the chin is placed just on top of the upper rim of the steering wheel, without hanging the head over the rim, and the chest is placed in direct contact with the air bag module with the spine parallel to the plane of the steering wheel. However, the breast forms of the 5th Percentile Female Hybrid III dummy allow several different interpretations of

this position depending on the maintenance of the chin position and spine angle, and force of the chest on the air bag module. So, this study used two different positioning criteria:

1. **Nominal ISO-2**:

   For **OOPS3.1 – 3.6:** The position was ISO-2 with chin on wheel but not hanging over the wheel. The chest is in close proximity to the air bag with the dummy spine parallel to the plane of the steering wheel. In subsequent text, this is termed "**Nominal ISO-2**" as shown in *Figure 6*.

   Using the 5th Percentile Female Hybrid III Dummy, this test condition places the dummy skin with breasts on the air bag module, but not deformed by the air bag module. Tests OOPS3.1-3.6 were a study of occupant response using different dummy skin conditions and the "Nominal ISO-2" position with the chin and spine positions the same for all tests. This implied that the thorax contact point moved away from the air bag, over 5 cm from the tests using the dummy skin with breasts to the dummy with no skin as is discussed in Section 3.8.1.

2. **Chest on Module**:

   For **OOPS3.7 - 3.19:** The ISO-2 position was relaxed for tests OOPS3.7-3.16 to put the chest in direct contact with the air bag module with some nominal force that allowed static equilibrium to be maintained between the dummy chest and the air bag module. In subsequent text, this is termed "**Chest On Module**" as shown in *Figure 7*.

   The Chest On Module positioning implies that the dummy breasts will be deformed by the air bag module. To ensure this, the dummy was positioned with the thorax pressing 100 N force on the air bag module as measured using the steering column load cell. In this position, the spine angle was maintained parallel to the plane of the steering wheel.

Occupant positioning was accomplished using an adjustable pin located between the thighs of the dummy, resting against the occupant pelvis. The chin was placed on the top of the steering wheel. For the Nominal ISO-2 position, the chin was placed in the middle of the steering wheel, not hanging over. For the Chest On Module position, the chin was allowed to hang over the steering wheel if necessary; for this position, a small wedge of foam padding was used to prevent the occupant chin from catching on the steering wheel under air bag deployment. For both positions, the spine angle was 25 degrees (+/- 1 degrees) from vertical (i.e. parallel to the steering wheel).

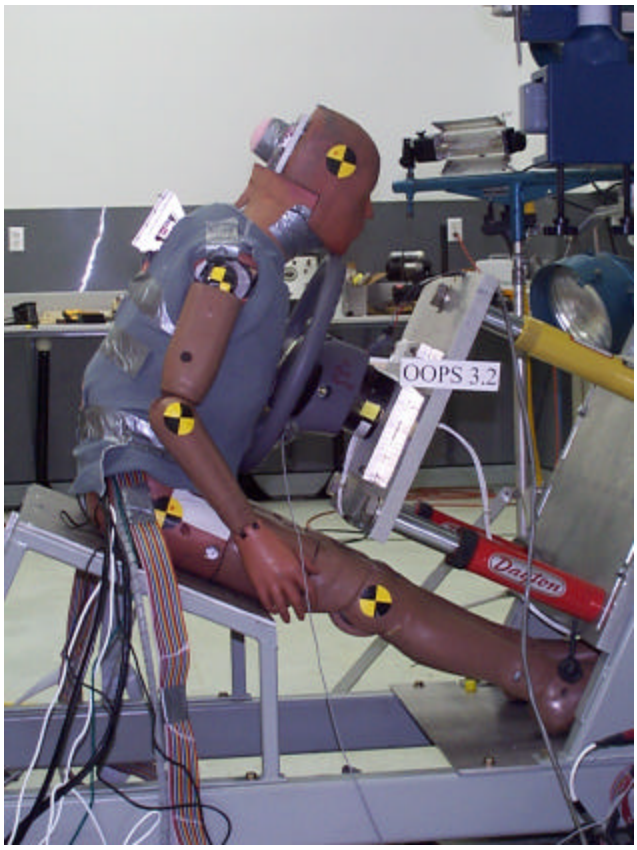

Figure 6: *Nominal ISO-2 Positioning - OOPS3.1 - OOPS3.6*

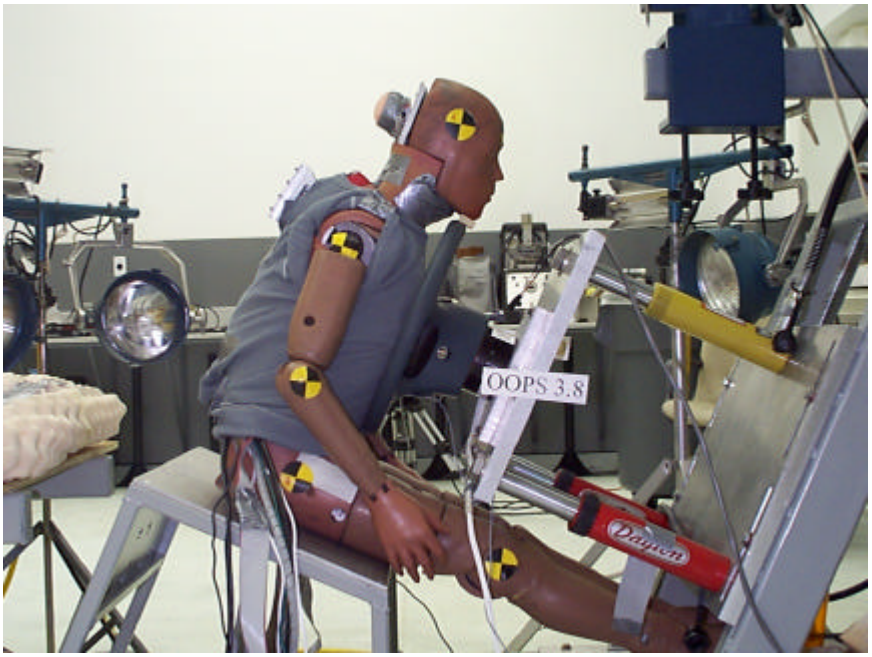

Figure 7: *Chest on Module Positioning - OOPS3.7 - OOPS3.19*

2.2.3.1: POSITIONING LOCATIONS

Fixed dummy location and photo target positioning locations for the Faro Arm measurement device are listed in *Table 2.2.3.1* and shown in *Figure 8*. Measurement positions range from photo target locations on the head and occupant H-point to bolts on the dummy to fixed locations on the test device. Position measurements taken at these locations are shown in *Table 2.2.3.2* below.

TABLE 2.2.3.1:
FARO ARM MEASUREMENT LOCATIONS

POINT #	DESCRIPTION
1	Right Head Photo Target
2	Left Head Photo Target
3	Upper Right Spine Bracket Bolt
4	Upper Left Spine Bracket Bolt
5	Lower Right Spine Bracket Bolt
6	Left Shoulder Bolt
7	Right Shoulder Bolt
8	Left H-Point Photo Target
9	Right H-Point Photo Target
10	Wheel Fixture Reference

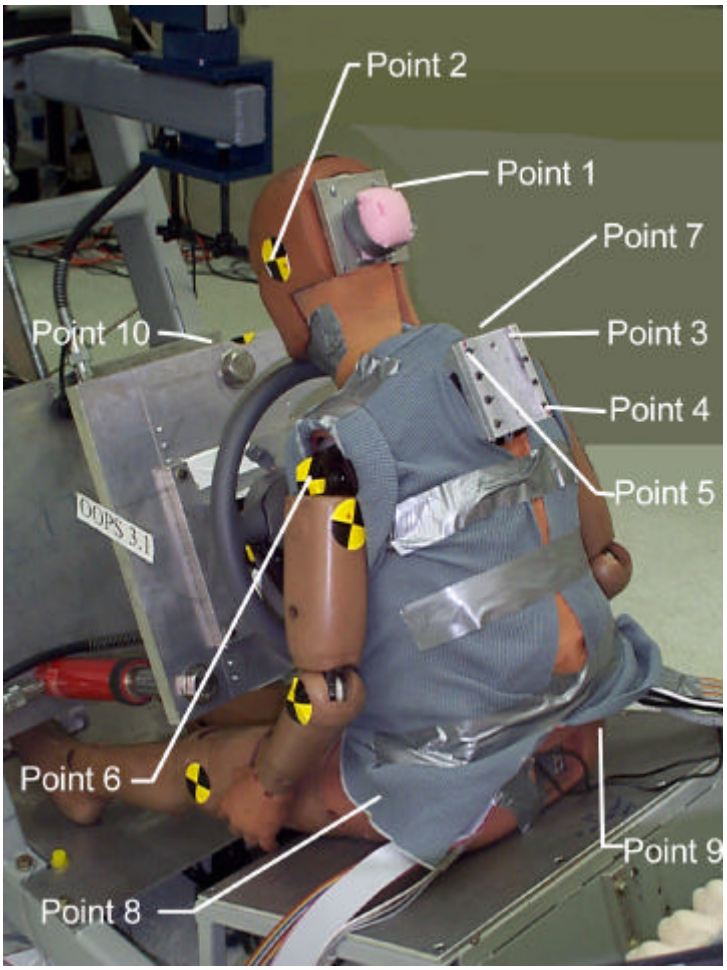

Figure 8: *Faro Arm Measurement Locations*

Since the head and H-point measurements were taken to photo targets and the location of the shoulder bolts depend on details of orientation of upper arm, the three fixed bolt positions represent most accurate determination of positioning tolerance for the runs. For runs OOPS3.1 – OOPS3.6, the positioning accuracy based on bolt locations was within +/- 0.37 cm in local X, +/- 0.29 cm in local Y, and +/-0.2 cm in local Z. For runs OOPS3.7 – OOPS3.19, the positioning accuracy based on bolt locations was +/-0.36 cm in local X, +/-0.5 cm in local Y, and +/-0.32 cm in local Z.

An indication of the intrinsic accuracy of the Faro Arm measurement is the positioning accuracy derived from measurements made to a fixed reference location. For this location, positioning accuracy was +/- 0.06 cm in local X, +/- 0.23 cm in local Y, and +/- 1.3 cm in local Z.

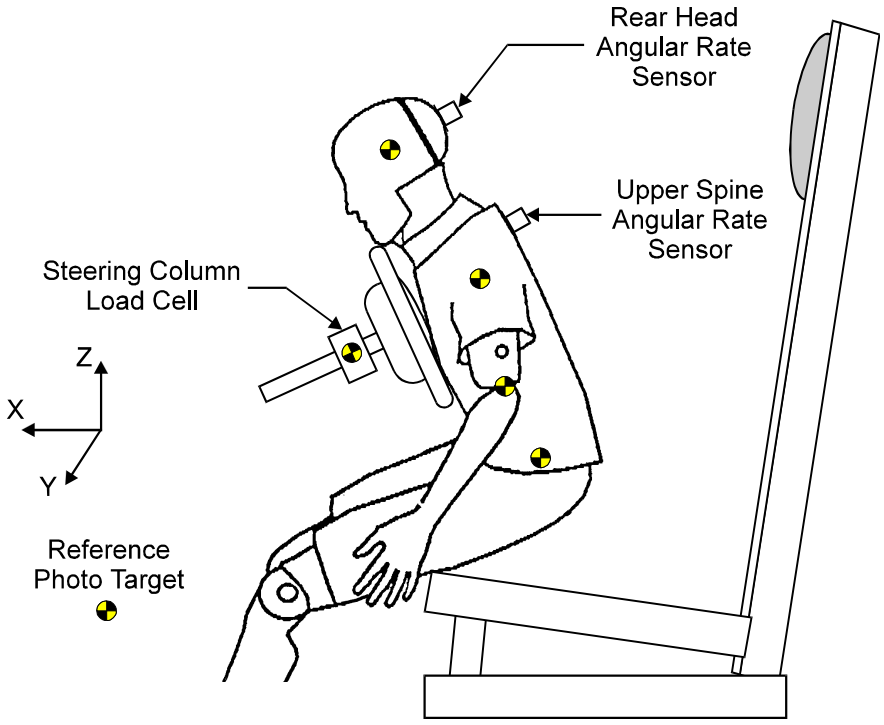

Figure 9: *Occupant Positioning Diagram*

TABLE 2.2.3.2: OCCUPANT POSITION DATA

POSITIONING COORDINATES (mm) ②

Location	Axis	Test Number					
		OOPS3.6	OOPS3.5	OOPS3.4	OOPS3.3	OOPS3.2	OOPS3.1
Head Right	X	222.7	225.5	222.6	224.9	223.6	222.5
	Y	-62.8	-67.1	-68.8	-71	-73	-71.5
	Z	684.6	686.2	683.5	682.9	684.9	684.5
Head Left	X	209.1	210.5	206.6	205.4	207.8	205.3
	Y	74.5	70.7	69	66.3	62.5	66.5
	Z	661.8	668.3	667.4	669.9	670.6	668.4
Bolt Upper Right	X	-2.4	-3.7	-7	-6	-6.8	-9.6
	Y	-34.3	-34.9	-33.7	-33.9	-37.8	-38.9
	Z	522	524.9	522.4	523.1	525.4	525.1
Bolt Upper Left	X	-3.3	-4.5	-7.3	-6.8	-7.3	-10.7
	Y	38.9	38.4	39.5	39.5	35.6	35.2
	Z	521.4	524.8	522.2	522.9	525.4	525.4
Bolt Lower Right	X	-15.4	-16.9	-19.3	-18.6	-19.1	-21.4
	Y	-35.2	-35	-33.3	-33.7	-37.8	-39.1
	Z	447.3	449.8	447.1	447.8	450.2	450.5
Shoulder Left	X	106.3	105.9	104.7	105.7	104.2	100.4
	Y	154.4	154.8	154.4	154.9	150.5	149.9
	Z	432.1	438.2	435.1	435.5	439.4	436.8
Shoulder Right	X	139.5	138.6	135.8	136.2	136.1	135.1
	Y	-151.2	-150.6	-150.1	-149.5	-155.5	-154.6
	Z	427.6	431.8	427.6	427.7	431.4	430.1
H-Point Left	X	199.3	195.3	200.1	198.9	187.2	172.4
	Y	154.2	154.9	154.6	154.8	339.3	339.7
	Z	85.2	82.8	83.7	85.1	82.7	80.5
H-Point Right	X	184.9	178.2	182.3	175.8	NA	184.5
	Y	-146.4	-146.4	-143	-146.4	NA	-342
	Z	81	78.7	79.2	77.7	NA	83.5
Steering Wheel Ref.	X	478.8	479.4	479.1	479.9	479.8	479.4
	Y	-1.4	-1.8	-0.4	-0.7	-0.2	-1.7
	Z	593.6	594	593.2	593.8	593.5	594.1

TABLE 2.2.3.2: OCCUPANT POSITION DATA (CONTINUED)

POSITIONING COORDINATES (mm) ②

Location	Axis	Test Number					
		OOPS3.12	OOPS3.11	OOPS3.10	OOPS3.9	OOPS3.8	OOPS3.7
Head Right	X	260.2	266.5	205.6	210.9	206	209.7
	Y	-69.5	-64.6	-69.4	-67.5	-69.1	-66.8
	Z	662.3	663.4	690.2	691.2	690.4	693.6
Head Left	X	264.7	244.5	199.8	200.7	199.3	202.5
	Y	-70.2	72.2	67.8	68.4	68.2	68.7
	Z	657.9	650.6	669.1	670.8	669.2	671
Bolt Upper Right	X	-7.5	-3.8	-9.3	-4.6	-6.7	-4.8
	Y	-39.2	-35.1	-35	-37.4	-36.8	-37.8
	Z	520.2	524.9	522.2	524.9	523.8	526.5
Bolt Upper Left	X	-8.4	-4	-9.2	-5.4	-7.6	-5.7
	Y	34.4	38	38.3	35.8	36.4	35.5
	Z	520.6	524.8	522.2	524.9	523.9	526.2
Bolt Lower Right	X	-20.7	-16.9	-21.7	-17.6	-19.4	-17.6
	Y	-39.1	-35.7	-34.8	-37.3	-36.9	-38.3
	Z	444.7	449.8	446.9	449.7	448.9	451.2
Shoulder Left	X	101.6	104.9	102.9	105.6	103.4	104.8
	Y	150.2	153.9	154.4	151.5	152.9	151.7
	Z	432.3	436.7	437.3	437.3	435	437.9
Shoulder Right	X	136.3	140.2	NA	138.5	137.1	138.9
	Y	-152.5	-151.8	NA	-153.8	-153.5	-152.6
	Z	425.9	431.9	NA	428.2	431.7	430.8
H-Point Left	X	187.4	187.2	187.5	187.1	189.1	188.6
	Y	155	154.8	154.3	154.7	153.9	152.8
	Z	82	83	82.6	82.5	79.4	81.2
H-Point Right	X	187.3	186.1	187.8	186.4	189	187.8
	Y	-150.2	-149.5	-150.1	-151	-151	-152.4
	Z	76.3	76.3	77.4	76.4	77.8	78.6
Steering Wheel Ref.	X	462.4	462.4	462.7	462.5	462.2	461.6
	Y	-1.5	-1.1	-1.3	-0.5	-0.8	-2.1
	Z	594.3	594.4	594.2	593.9	594	594.2

TABLE 2.2.3.2: OCCUPANT POSITION DATA (CONTINUED)

POSITIONING COORDINATES (mm) ②

Location	Axis	Test Number					
		OOPS3.18	OOPS3.17	OOPS3.16	OOPS3.15	OOPS3.14	OOPS3.13
Head Right	X	231.3	229	230.1	230.7	227.6	228
	Y	-63.6	-68.7	-63.5	-68.7	-59.5	-68
	Z	687.2	686.5	686.5	685.7	684.6	684
Head Left	X	215.2	213.8	215.3	214.8	212.2	210.6
	Y	72.8	67.3	72	67.7	76.7	68.5
	Z	662.6	666.4	662	663.7	661.7	665.1
Bolt Upper Right	X	-2.2	-2.4	-4.4	-3.6	-7.4	-5.5
	Y	-37.7	-38.3	-38.2	-39.1	-29.8	-37.2
	Z	524.7	525.8	523.6	524.7	524	524.1
Bolt Upper Left	X	-3.2	-3.3	-5	-4.1	-7	-6
	Y	35.6	35.1	35.6	34.4	43.4	35.9
	Z	524.3	525	524.1	525.4	522.8	524.1
Bolt Lower Right	X	-15	-14.8	-16.7	-16.6	-19.5	-18.6
	Y	-38.2	-38.8	-38.2	-39.6	-30.6	-36.7
	Z	449.4	450	449	449.1	448.5	449.2
Shoulder Left	X	106.7	107.1	105.3	105.8	104.3	105
	Y	151.5	150.5	150.7	150.1	156.4	150.1
	Z	435.6	436.2	434.9	437	433.5	430.9
Shoulder Right	X	141.3	141.5	140.9	141.4	136.1	137.1
	Y	-153.5	-153.2	-152.2	-153.3	-146.9	-152.9
	Z	429	430.6	429.8	429.1	430.6	433.4
H-Point Left	X	187.8	187.2	186.2	186.7	187	186.1
	Y	151.9	150.4	152.1	150.9	154.4	154.4
	Z	81.8	81.7	81.1	80.5	81.1	83.3
H-Point Right	X	189.1	188.3	189.2	185	187	187.1
	Y	-153.3	-154.5	-153.2	-155.3	-149.9	-149.8
	Z	75.7	74.7	74.5	74.9	80.3	77
Steering Wheel Ref.	X	462.5	462.6	462.3	462.3	462.6	462.6
	Y	-5.4	-5.4	-5.2	-4.8	-1.2	-1.7
	Z	592.9	593	592.3	591.9	594.4	594.3

TABLE 2.2.3.2: OCCUPANT POSITION DATA (CONTINUED)

POSITIONING COORDINATES (mm) ②		
Location	**Axis**	**Test Number OOPS3.19**
Head Right	X	230.7
	Y	-72.2
	Z	682.6
Head Left	X	213.1
	Y	64.6
	Z	667.5
Bolt Upper Right	X	-2.3
	Y	-39.7
	Z	525.4
Bolt Upper Left	X	-3.7
	Y	33.3
	Z	524.7
Bolt Lower Right	X	-15.9
	Y	-40.1
	Z	449.9
Shoulder Left	X	105.4
	Y	149.6
	Z	435.2
Shoulder Right	X	142
	Y	-153.8
	Z	427.1
H-Point Left	X	186.8
	Y	150.3
	Z	81.4
H-Point Right	X	189.4
	Y	-154
	Z	75.2
Steering Wheel Ref.	X	461.7
	Y	-5.2
	Z	592.8

NOTES:

② Coordinates are X-, Y- and Z-Axis distances from the test fixture reference locations in the local reference frame with the Z-Axis aligned with the vertical plane of the steering wheel. The local X-Axis is normal to the plane of the steering wheel directed from the face of the module into the steering wheel.

2.2.4: ENVIRONMENT

To minimize the effect of temperature variation on the response of the test dummy (c.f. DOT HS 806 722 "State-of-the-Art Dummy Selection"), tests were performed in a climate-controlled room. The dummy was placed in the room 10 hours before the tests to allow the mechanical structures to equilibrate with the ambient temperature. Less than 3 ^{0}C temperature variation was seen over this time. Environmental data at airbag initiation for the OOPS3.1 – OOPS3.19 tests is presented in *Table 2.2.4.1*. The average test-time temperature for all tests was 28.3 ^{0}C (+/- 1.1 ^{0}C standard deviation) with an average relative humidity of 65.5 % (+/- 3.5 % standard deviation).

TABLE 2.2.4.1: TEST ENVIRONMENTAL DATA

TEST	3.1	3.2	3.3	3.4	3.5	3.6	3.7	3.8	3.9	3.10	3.11	3.12	3.13	3.14	3.15	3.16	3.17	3.18	3.19
Date	Oct 23	Oct 23	Oct 24	Oct 24	Oct 24	Oct 24	Nov 7	Nov 7	Nov 10	Nov 10	Nov 11	Nov 11	Nov 11	Nov 11	Nov 18	Nov 18	Nov 20	Nov 20	Nov 20
Temperature (^{0} C)	28.3	29.3	27.0	28.9	30.2	29.4	28.9	28.6	28.4	27.8	27.0	28.3	28.9	28.0	28.3	29.1	28.1	28.8	25.1
Relative Humidity (%)	64	64	62	64	66	68	71	71	68	68	69	69	68	67	60	61	62	61	62

2.2.5: PHOTOGRAPHY

During the pre-impact phase of each test, the motion picture film cameras were test-run without film. The high-speed video cameras, photographic lighting system, and timing mark generator were activated in a simulation of the actual impact event, to test the various systems and the interconnections between them. After these tests, the film cameras were loaded with film.

When the occupant was positioned for the air bag impact, adhesive-backed crosshair-type photo targets were placed at important points on the occupant, to facilitate post-test motion picture analysis tracking of the various body segments. The global X-, Y-, and Z-axis coordinates of the occupant measurement points relative to the local reference frame of the test fixture were measured and recorded. The measured coordinates are listed in Section 2.2.3.2. The run number was posted on paper signs, visible in all camera views. Still photos of the final occupant position were taken before the air bag deployment was initiated and similar photos were taken immediately after the event. The pre- and post-deployment photos appear in Sections 2.2.4.1 and 3.1.3.2 respectively.

The impact event was initiated by manually activating the camera controller, which started the film cameras running. After a pre-programmed delay of approximately one second, the data acquisition system trigger circuitry was automatically activated, resulting in the simultaneous triggering of the high-speed video camera, timing mark generator, data acquisition system, and air bag deployment circuitry.

After the test series, the films were commercially developed and printed. The motion picture film images were edited to remove insignificant pre- and post-impact frames and the

remaining footage from all three cameras was spliced together into a single roll for each test. The motion picture originals and the still photo negatives were archived. The high-speed video images of each test were saved on computer disk and are available on disk or VHS videotape.

2.2.6: DATA ACQUISITION

Standard data acquisition procedures, as described in Appendix H.6, were used in the collection of pre-impact and impact data. Sensors used for these tests were verified to be working properly before the tests and were monitored during the pre-impact preparations, using the procedures described in Appendix F.3. All Hybrid III instrumentation was installed, and the installation verified, before each test. Correct installation and operation of the chestbands was confirmed after they had been installed on the occupant, using the procedure described in Appendix H.3.

During the pre-impact phase of each test, the trigger circuitry, photographic timing mark generator, air bag squib-firing circuitry, camera controller, and high-speed video systems were activated in a simulation of the actual impact event, to test the various systems and the interconnections between them.

The various system settings used for the impact data collection are summarized in *Table 2.2.6.1*. The system was triggered manually through the camera controller, which introduced a delay of approximately one second to allow the motion picture camera to reach operating speed. After the delay, the trigger circuitry was automatically activated and simultaneously triggered the data acquisition system, photographic timing mark generator, and high-speed video system, and initiated deployment of the air bag.

TABLE 2.2.6.1:
DATA ACQUISITION PARAMETERS

Number of Channels Used	118
Sampling Rate	10,000 samples/ second
Pre-Trigger Samples	1,280 / channel
Post-Trigger Samples	8,960 / channel
Total Samples	10,240 / channel ①
Pre-Trigger Duration	128 ms.
Post-Trigger Duration	896 ms.
Total Duration	1,024 ms.
Anti-Aliasing Filter Cutoff Frequency	3300 Hz. ①

NOTE:
① See Appendix I.1 for a discussion of record length and the frequency content of the data, as presented on the datatape.

2.2.7: DATA PROCESSING

Standard procedures, described in Appendix I, were used for all post-test data processing.

Appendix I.1 covers the processing done to all the data. Resultant accelerations were calculated from their orthogonal components, as described in Appendix 1.3. Neck flexion angles were computed using data from the head rear and upper spinal MHD angular rate sensors. The processes used are described in Appendix I.7. Finally, standard NHTSA datatape files were created, as described in Appendix I.2, and a set of IBM-compatible diskettes, which constitute the datatape, were prepared for delivery to NHTSA.

3: TEST RESULTS

3.1: DESCRIPTION OF RESULTS

In addition to the datatape, motion pictures, and high-speed video, data from the tests is presented in several different forms in this section. Minima and maxima and the times at which they occurred from sensor channels is presented and discussed in Section 3.2. In Section 3.3, thoracic data measured and calculated from various sensors is discussed. This discussion includes an examination of thoracic injury criteria including sternal displacements and sternal viscous response. Photographic results are presented in Section 3.4 and include a summary of the occupant response and kinematics from high-speed video and film. Sensor and test failures are discussed in Section 3.5, and a discussion of test results is presented in Section 3.6. This discussion includes the effect of dummy skin and distance from the module on occupant response, and the effect of position on dummy and occupant response.

3.2: SENSOR DATA

A summary of maximum and minimum values of accelerometer and load cell sensor data is presented in *Table 3.2.3*. The steering axial column load (Steering Column Load X-axis) measured in the tests shows a large variation among tests that correlates with occupant response, generally lower in value with lower occupant response and higher in value with higher occupant response. Steering column moment values represent vertical and lateral oscillations in the air bag as it interacts with the occupant.

Head center-of-gravity acceleration values seen in *Table 3.2.3* are well below injury tolerance values as expected for these predominantly thoracic out-of-position tests. Peak resultant values for all tests are significantly below 60 g's, the standard injury tolerance value for a 50th Percentile Male Hybrid III dummy. Head injury criterion (HIC) calculated for each test is presented in *Table 3.2.1*. HIC values for all tests peak within 20 ms of air bag deployment, and are all substantially lower than the 50th Percentile Male Hybrid III dummy head injury tolerance value of 1000.

TABLE 3.2.1: HEAD INJURY CRITERION (HIC)

TEST	3.1	3.2	3.3	3.4	3.5	3.6	3.7	3.8	3.9	3.10	3.11	3.12	3.13	3.14	3.15	3.16	3.17	3.18	3.19
Peak HIC	11	11	10	9	14	17	27	34	25	25	23	24	18	8	22	21	32	25	50
@ Time (ms)	10.7	10.2	10.3	10.5	19.9	15.0	10.3	10.8	10.5	10.8	11.5	11.5	10.0	9.5	17.8	10.3	10.3	10.1	12.3

Accelerometers mounted externally on an MHD angular rate sensor attached to the back of the dummy head show similar peak acceleration values as the head center-of-gravity accelerometers. In no case does the local acceleration value go above 60 g's.

The chest center-of-gravity acceleration resultant for the test series is shown in *Table 3.2.2*. The peak chest CG resultant acceleration values are above the 60 g level for the tests OOPS3.8 – OOPS3.10 with the dummy sternum centered on the air bag module in the Chest on Module position. In addition, this average peak CG acceleration is 44% larger for the Chest on

Module tests (OOPS3.7 – OOPS3.10) with the dummy centered on the air bag module than the Nominal ISO-2 tests (OOPS3.1 – OOPS3.2). Significant differences in average peak accelerations are seen among the different conditions tested as discussed in Section 3.6.2 below.

TABLE 3.2.2: CHEST CG RESULTANT ACCELERATION PEAK

TEST	3.1	3.2	3.3	3.4	3.5	3.6	3.7	3.8	3.9	3.10	3.11	3.12	3.13	3.14	3.15	3.16	3.17	3.18	3.19
Peak Accel. (g's)	32	33.6	28.1	28.5	22.6	22.7	51.4	60.8	60.5	61.8	40.1	38.9	25.1	19	31.8	30.7	50.7	56.2	50.7
@ Time (ms)	13.1	13.5	13.6	13.8	11	11.3	13.3	13.3	13.4	13.8	12.8	12.9	13.2	12.5	12.3	12.6	12.7	12.3	13.5

Owing to electrical noise, a substantial number of neck load and neck moment sensors shown in *Table 3.2.3* have questionable data during the test. However, two tests, the sternum-centered case of OOPS3.9 and the sternum up 4 cm case of OOPS3.11, are expected to be the limiting cases for neck injury. These tests have good data on all neck load cell channels. Both Chest on Module tests show upper and lower neck axial tension loads of less than 1600 N. Also, neck shear values for both tests are well below 2000 N. Similarly, neck moments in flexion for both the upper and lower neck are relatively small. Relatively large neck moment values in extension for these tests occur after occupant/air bag interaction upon rebound. These values, however, are obtained outside the region of primary air bag/occupant interaction investigated in this study.

Magnetohydrodynamic (MHD) angular rate sensors were used to determine neck flexion for all tests. Similar time histories of neck flexion were seen for the occupant-centered tests in OOPS3.1-OOPS3.7 and OOPS3.9 shown in *Figure 10*. Data spikes in MHD channels in OOPS3.8, OOPS3.10-OOPS3.12, and OOPS3.17-OOPS3.19 prevented comparison of processed MHD data from those tests. In contrast, spine flexion is lower for tests in which the dummy is offset 4 cm to the left of the air bag center. *Figure 11* shows a comparison of the dummy-centered tests of OOPS3.1 and OOPS3.2 with the dummy-offset-left tests of OOPS3.15 and OOPS3.16. In the dummy-offset tests, the spine flexion is initially steeper. Owing to lower total occupant forcing, however, the time evolution of the flexion is ultimately shallower than with the occupant centered on the air bag.

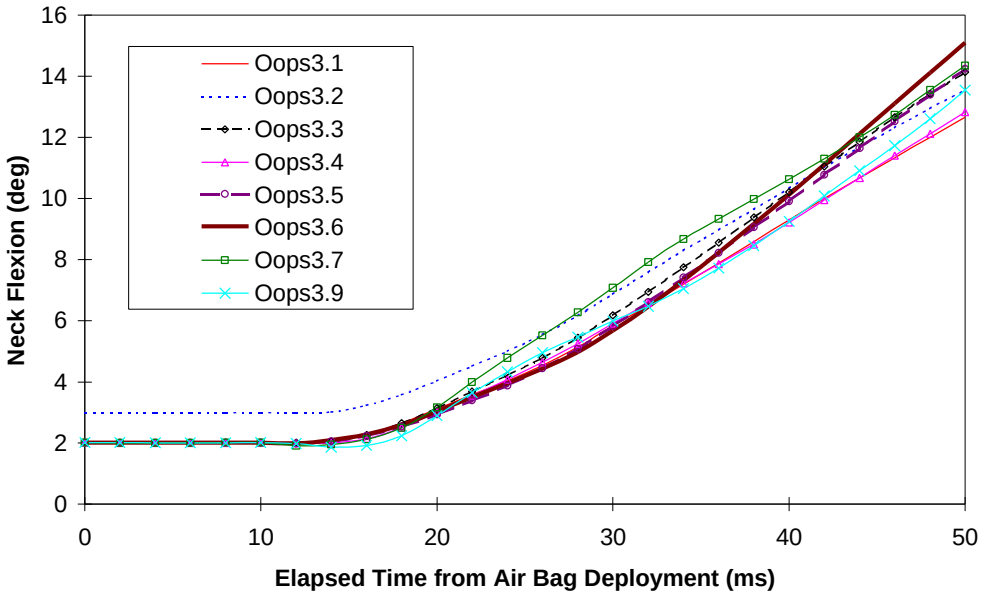

***Figure 10**: Neck Y Flexion from MHD Data - Dummy Sternum Centered on Air Bag Module*

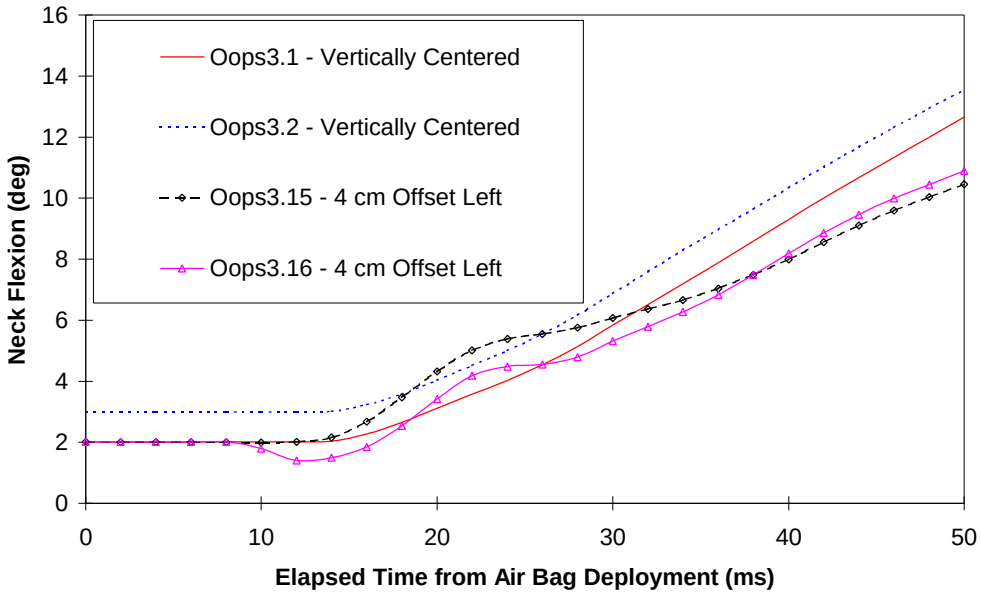

***Figure 11:** Neck Y Flexion from MHD Data - Effect of Dummy Sternum Position*

TABLE 3.2.3: SENSOR DATA SUMMARY

Measurement	Sensor Location	Unit	Filter Class	Axis ①	Test②	Minimum④		Maximum④	
						Value	Time	Value	Time
Steering Column									
Steering	Steering	N	600	X	OOPS3.1	-136.17	6.50	6716.40	9.20
Column	Column,	N	600		OOPS3.2	-440.05	6.30	7485.60	9.90
Load	Upper	N	600		OOPS3.3	-476.02	6.20	6572.60	8.30
		N	600		OOPS3.4	-357.91	6.30	6119.20	9.70
		N	600		OOPS3.5	-607.94	7.40	4730.90	8.80
		N	600		OOPS3.6	-73.31	94.60	4361.10	30.30
		N	600		OOPS3.7	-147.9⑤	90.3	8348.6⑤	10.9
		N	600		OOPS3.8	-96.9	75.2	9815.7	10.0
		N	600		OOPS3.9	-140.3	96.4	6678.5	9.6
		N	600		OOPS3.10	-47.4	98.5	8098.3	10.5
		N	600		OOPS3.11	-412.8	99.3	5664.3	11.3
		N	600		OOPS3.12	-310.2	99.4	6494.8	10.5
		N	600		OOPS3.13	-156.7⑤	74.3	7175.1⑤	9.4
		N	600		OOPS3.14	-79.0⑤	98.1	6726.9⑤	8.4
		N	600		OOPS3.15	-293.0	99.2	6449.2	10.1
		N	600		OOPS3.16	-198.1	99.3	6127.9	9.9
		N	600		OOPS3.17	-175.8	94.5	9146.8	10.1
		N	600		OOPS3.18	-167.0	98.2	9063.6	9.7
		N	600		OOPS3.19	-204.1	65.6	5873.2	11.8
		N	600	Y	OOPS3.1	-359.67	13.50	302.31	12.60
		N	600		OOPS3.2	-554.91	9.20	459.58	15.30
		N	600		OOPS3.3	-525.01	22.90	306.67	17.10
		N	600		OOPS3.4	-521.38	28.90	230.46	36.10
		N	600		OOPS3.5	-527.67	21.30	468.54	27.20
		N	600		OOPS3.6	-362.36	28.20	303.33	25.10
		N	600		OOPS3.7	-490.6	10.6	388.3	15.1
		N	600		OOPS3.8	-2386.1⑤	9.7	737.6⑤	18.4
		N	600		OOPS3.9	-527.5	23.2	766.9	14.9
		N	600		OOPS3.10	-2189.9⑤	13.4	540.5⑤	23.2
		N	600		OOPS3.11	-614.9	12.2	540.8	24.7
		N	600		OOPS3.12	-513.1⑤	22.0	507.5⑤	10.9
		N	600		OOPS3.13	-2496.9⑤	9.4	620.9⑤	11.6
		N	600		OOPS3.14	-2338.6⑤	9.0	361.0⑤	13.6
		N	600		OOPS3.15	-1109.6	31.8	660.7	11.6
		N	600		OOPS3.16	-1463.0	35.1	409.5	12.1
		N	600		OOPS3.17	-1848.3⑤	10.1	483.8⑤	30.0
		N	600		OOPS3.18	-3105.5⑤	9.6	470.9⑤	16.7
		N	600		OOPS3.19	-435.3	27.0	609.3	17.8
		N	600	Z	OOPS3.1	-992.92	10.10	1354.80	8.70
		N	600		OOPS3.2	-1437.00	10.10	1599.40	8.80
		N	600		OOPS3.3	-1517.50	9.90	1528.80	8.40
		N	600		OOPS3.4	-1403.40	9.80	1538.70	8.40

TABLE 3.2.3: SENSOR DATA SUMMARY

Measurement	Sensor Location	Unit	Filter Class	Axis ①	Test②	Minimum④		Maximum④	
						Value	Time	Value	Time
		N	600		OOPS3.5	-786.38	10.60	1213.40	8.80
		N	600		OOPS3.6	-1152.90	10.70	991.06	34.50
		N	600		OOPS3.7	-1935.1	10.7	1407.1	9.0
		N	600		OOPS3.8	-3638.6⑤	10.6	1356.4⑤	8.6
		N	600		OOPS3.9	-963.2	26.4	935.1	8.5
		N	600		OOPS3.10	-2984.8⑤	11.0	1242.1⑤	37.2
		N	600		OOPS3.11	-736.2	14.1	1436.3	8.9
		N	600		OOPS3.12	-1037.2⑤	6.5	1657.7⑤	8.8
		N	600		OOPS3.13	-3173.1⑤	8.4	1122.9⑤	20.0
		N	600		OOPS3.14	-2576.7⑤	7.9	973.5⑤	5.0
		N	600		OOPS3.15	-1047.0	10.4	1379.3	8.4
		N	600		OOPS3.16	-1486.8	9.9	1137.3	8.4
		N	600		OOPS3.17	-1812.8⑤	10.2	978.0⑤	8.4
		N	600		OOPS3.18	-2893.3⑤	9.7	1177.3⑤	8.6
		N	600		OOPS3.19	-1073.1	14.4	884.6	9.2
Steering		Nm	600	Y	OOPS3.1	-206.28	26.80	32.98	5.20
Column		Nm	600		OOPS3.2	-243.28	25.50	41.47	62.10
Moment		Nm	600		OOPS3.3	-269.79	27.10	36.83	34.10
		Nm	600		OOPS3.4	-219.93	13.60	60.83	20.10
		Nm	600		OOPS3.5	-126.04	25.30	79.84	32.30
		Nm	600		OOPS3.6	-132.32	10.20	144.88	32.60
		Nm	600		OOPS3.7	-346.3	27.7	55.2	21.7
		Nm	600		OOPS3.8	-430.3⑤	25.7	31.7⑤	5.5
		Nm	600		OOPS3.9	-309.3	26.5	39.5	88.1
		Nm	600		OOPS3.10	-367.3⑤	11.4	26.2⑤	5.5
		Nm	600		OOPS3.11	-303.9	14.1	103.4	99.7
		Nm	600		OOPS3.12	-310.6⑤	14.9	83.9⑤	99.7
		Nm	600		OOPS3.13	-369.6⑤	9.4	91.8⑤	48.4
		Nm	600		OOPS3.14	-321.7⑤	9.0	113.0⑤	43.3
		Nm	600		OOPS3.15	-194.3	28.3	78.3	38.5
		Nm	600		OOPS3.16	-244.9	9.8	71.0	42.7
		Nm	600		OOPS3.17	-444.4⑤	14.1	26.4⑤	5.1
		Nm	600		OOPS3.18	-488.1⑤	9.6	29.3⑤	4.5
		Nm	600		OOPS3.19	-264.1	14.4	71.0	22.5
		Nm	600	Z	OOPS3.1	-53.15	30.00	33.57	13.40
		Nm	600		OOPS3.2	-62.10	32.30	52.57	42.50
		Nm	600		OOPS3.3	-42.26	24.50	48.02	20.90
		Nm	600		OOPS3.4	-46.98	35.90	114.09	28.10
		Nm	600		OOPS3.5	-129.19	27.20	82.56	36.00
		Nm	600		OOPS3.6	-57.81	35.60	52.38	41.80
		Nm	600		OOPS3.7	-41.4	16.1	66.0	34.7
		Nm	600		OOPS3.8	-97.5⑤	17.2	36.3⑤	42.7
		Nm	600		OOPS3.9	-177.5	30.5	24.3	22.9
		Nm	600		OOPS3.10	-67.9⑤	10.9	38.1⑤	29.2

TABLE 3.2.3: SENSOR DATA SUMMARY

Measurement	Sensor Location	Unit	Filter Class	Axis ①	Test②	Minimum④		Maximum④	
						Value	Time	Value	Time
		Nm	600		OOPS3.11	-193.4	22.1	18.6	5.9
		Nm	600		OOPS3.12	-39.9⑤	10.9	70.4⑤	22.0
		Nm	600		OOPS3.13	-82.6⑤	8.4	284.5⑤	17.5
		Nm	600		OOPS3.14	-99.1⑤	7.8	360.1⑤	23.7
		Nm	600		OOPS3.15	-19.2	8.0	287.6	31.8
		Nm	600		OOPS3.16	-18.7	8.0	363.9	35.5
		Nm	600		OOPS3.17	-142.2⑤	17.9	23.4⑤	25.9
		Nm	600		OOPS3.18	-82.2⑤	9.4	48.8⑤	24.6
		Nm	600		OOPS3.19	-85.1	19.1	94.6	26.9
Head									
Head Acceleration	Head, Center of Gravity	g's	180	X	OOPS3.1	-14.60	20.50	0.50	8.50
		g's	180		OOPS3.2	-17.39	21.00	0.55	8.60
		g's	180		OOPS3.3	-16.41	17.80	0.58	8.60
		g's	180		OOPS3.4	-13.27	17.50	0.80	8.70
		g's	180		OOPS3.5	-15.07	22.30	0.65	8.40
		g's	180		OOPS3.6	-13.08	22.70	0.84	8.30
		g's	180		OOPS3.7	-25.2	31.8	0.1	6.9
		g's	180		OOPS3.8	-27.7	27.9	0.3	8.3
		g's	180		OOPS3.9	-22.8	30.5	0.1	7.7
		g's	180		OOPS3.10	-21.5	21.9	0.2	8.1
		g's	180		OOPS3.11	-21.9	30.2	0.3	7.4
		g's	180		OOPS3.12	-18.8	33.8	0.2	7.3
		g's	180		OOPS3.13	-16.6	31.7	0.9	60.4
		g's	180		OOPS3.14	-15.3	26.9	0.1	6.3
		g's	1000		OOPS3.15	-21.8	25.1	0.3	6.3
		g's	1000		OOPS3.16	-20.5	21.4	0.3	6.4
		g's	1000		OOPS3.17	-22.9	31.4	0.3	6.6
		g's	1000		OOPS3.18	-18.4	20.1	0.2	7.6
		g's	1000		OOPS3.19	-35.0	31.5	1.5	49.2
		g's	180	Y	OOPS3.1	-0.62	98.70	0.73	54.30
		g's	180		OOPS3.2	-0.74	74.40	0.63	14.30
		g's	180		OOPS3.3	-0.48	84.40	0.73	35.00
		g's	180		OOPS3.4	-0.71	99.50	0.87	57.30
		g's	180		OOPS3.5	-0.87	21.30	0.93	41.00
		g's	180		OOPS3.6	-0.83	14.20	0.90	16.20
		g's	180		OOPS3.7	-1.4	32.0	0.4	51.5
		g's	180		OOPS3.8	-2.6	21.0	0.6	44.9
		g's	180		OOPS3.9	-1.5	32.9	1.5	26.0
		g's	180		OOPS3.10	-1.3	28.4	0.1	11.3
		g's	180		OOPS3.11	-1.7	27.5	1.2	37.0
		g's	180		OOPS3.12	-0.9	91.2	0.3	52.1
		g's	180		OOPS3.13	-1.6	14.3	2.9	21.1
		g's	180		OOPS3.14	-1.4	13.8	3.6	26.5
		g's	1000		OOPS3.15	-2.4	14.6	5.7	21.1

TABLE 3.2.3: SENSOR DATA SUMMARY

Measurement	Sensor Location	Unit	Filter Class	Axis ①	Test②	Minimum④		Maximum④	
						Value	Time	Value	Time
		g's	1000		OOPS3.16	-2.4	15.1	7.9	21.1
		g's	1000		OOPS3.17	-1.8	22.7	0.7	29.0
		g's	1000		OOPS3.18	-1.6	18.5	1.7	25.9
		g's	1000		OOPS3.19	-2.5	31.9	1.2	48.3
		g's	180	Z	OOPS3.1	-11.07	11.80	4.41	22.00
		g's	180		OOPS3.2	-14.57	12.70	6.64	19.90
		g's	180		OOPS3.3	-12.10	11.50	4.48	20.40
		g's	180		OOPS3.4	-12.93	11.80	6.40	19.70
		g's	180		OOPS3.5	-12.66	11.40	3.60	61.30
		g's	180		OOPS3.6	-13.27	11.30	4.83	18.70
		g's	180		OOPS3.7	-18.9	15.5	12.9	25.2
		g's	180		OOPS3.8	-19.0	14.6	15.7	20.4
		g's	180		OOPS3.9	-24.2	14.5	8.8	25.0
		g's	180		OOPS3.10	-22.6	15.4	14.9	19.5
		g's	180		OOPS3.11	-30.9	14.0	3.7	62.7
		g's	180		OOPS3.12	-27.0	14.1	8.0	22.3
		g's	180		OOPS3.13	-10.8	11.5	8.5	23.9
		g's	180		OOPS3.14	-9.7	10.9	6.4	29.1
		g's	1000		OOPS3.15	-12.8	13.0	11.9	23.8
		g's	1000		OOPS3.16	-14.0	12.4	14.8	24.4
		g's	1000		OOPS3.17	-40.0	14.3	13.3	22.4
		g's	1000		OOPS3.18	-39.2	14.2	15.2	21.9
		g's	1000		OOPS3.19	-33.9	14.8	26.9	25.6
	Head, Back, External	g's	180	1	OOPS3.1	-0.91	18.50	1.28	45.60
		g's	180		OOPS3.2	-2.93	14.70	1.50	21.30
		g's	180		OOPS3.3	-1.67	15.40	1.88	44.50
		g's	180		OOPS3.4	-1.75	25.90	1.84	53.60
		g's	180		OOPS3.5	-1.78	14.50	1.77	63.20
		g's	180		OOPS3.6	-1.76	21.10	1.59	66.00
		g's	180		OOPS3.7	-2.0	43.7	3.2	31.5
		g's	180		OOPS3.8	-2.0	29.3	2.2	21.2
		g's	180		OOPS3.9	-3.1	29.4	2.1	39.3
		g's	180		OOPS3.10	-2.8	21.5	0.8	16.2
		g's	180		OOPS3.11	-5.5	44.2	7.7	27.8
		g's	180		OOPS3.12	-1.2	62.7	1.9	28.3
		g's	180		OOPS3.13	-5.5	32.6	6.7	45.0
		g's	180		OOPS3.14	-6.1	26.3	6.8	40.6
		g's	180		OOPS3.15	-5.2	29.5	8.6	19.7
		g's	180		OOPS3.16	-3.9	22.6	7.2	20.0
		g's	180		OOPS3.17	-2.7	30.6	2.5	23.1
		g's	180		OOPS3.18	-1.9	55.5	3.5	23.0
		g's	180		OOPS3.19	-5.9	29.3	4.1	22.2
		g's	180	2	OOPS3.1	-14.83	18.70	15.80	36.20
		g's	180		OOPS3.2	-23.78	20.10	16.27	36.50

TABLE 3.2.3: SENSOR DATA SUMMARY

Measurement	Sensor Location	Unit	Filter Class	Axis ①	Test②	Minimum④		Maximum④	
						Value	Time	Value	Time
		g's	180		OOPS3.3	-18.10	20.40	18.13	37.50
		g's	180		OOPS3.4	-22.32	19.80	16.67	36.10
		g's	180		OOPS3.5	-15.39	19.90	15.54	41.30
		g's	180		OOPS3.6	-16.47	19.00	11.88	38.10
		g's	180		OOPS3.7	-34.8	25.1	41.0	31.1
		g's	180		OOPS3.8	-44.2	24.0	29.2	16.8
		g's	180		OOPS3.9	-19.9	24.4	23.0	30.2
		g's	180		OOPS3.10	-20.2	24.4	16.4	41.3
		g's	180		OOPS3.11	-12.9	20.0	33.0	14.0
		g's	180		OOPS3.12	-12.9	20.3	28.0	14.1
		g's	180		OOPS3.13	-28.6	42.7	22.7	31.5
		g's	180		OOPS3.14	-13.5	19.8	14.5	16.4
		g's	180		OOPS3.15	-10.9	34.3	11.9	42.5
		g's	180		OOPS3.16	-14.2	26.0	9.4	45.0
		g's	180		OOPS3.17	-20.4	24.9	30.5	14.2
		g's	180		OOPS3.18	-22.8	24.8	31.4	13.9
		g's	180		OOPS3.19	-24.0	25.4	23.5	14.8
		g's	180	3	OOPS3.1	-2.30	99.40	13.50	20.50
		g's	180		OOPS3.2	-2.45	99.40	16.17	21.00
		g's	180		OOPS3.3	-2.55	99.40	16.16	17.80
		g's	180		OOPS3.4	-2.68	99.40	12.97	17.40
		g's	180		OOPS3.5	-4.03	99.40	13.77	22.20
		g's	180		OOPS3.6	-3.82	99.40	12.22	22.70
		g's	180		OOPS3.7	-3.0	99.4	25.7	31.9
		g's	180		OOPS3.8	-3.4	99.5	27.5	27.9
		g's	180		OOPS3.9	-2.3	99.4	22.4	30.6
		g's	180		OOPS3.10	-1.1	99.4	20.7	22.0
		g's	180		OOPS3.11	-3.9	99.4	21.1	30.2
		g's	180		OOPS3.12	-3.1	99.4	19.1	33.7
		g's	180		OOPS3.13	-1.4	99.4	17.1	31.7
		g's	180		OOPS3.14	-1.3	99.4	15.4	26.9
		g's	180		OOPS3.15	-2.8	99.4	21.3	24.9
		g's	180		OOPS3.16	-3.1	99.4	19.6	21.1
		g's	180		OOPS3.17	-1.2	99.4	21.8	31.4
		g's	180		OOPS3.18	-1.9	99.4	16.6	19.9
		g's	180		OOPS3.19	-2.0	99.4	34.7	31.5
Chest									
Chest Acceleration	Chest, Center of Gravity	g's	180	X	OOPS3.1	-31.17	13.10	4.92	72.10
		g's	180		OOPS3.2	-32.36	13.50	4.76	72.90
		g's	180		OOPS3.3	-26.75	13.60	4.05	66.50
		g's	180		OOPS3.4	-27.22	13.70	4.77	67.90
		g's	180		OOPS3.5	-22.22	11.00	4.69	58.10
		g's	180		OOPS3.6	-22.34	11.30	4.69	77.70
		g's	180		OOPS3.7	-49.1	13.3	10.3	19.7

TABLE 3.2.3: SENSOR DATA SUMMARY

Measurement	Sensor Location	Unit	Filter Class	Axis ①	Test②	Minimum④		Maximum④	
						Value	Time	Value	Time
		g's	180		OOPS3.8	-52.2	13.3	9.0	18.6
		g's	180		OOPS3.9	-56.6	13.5	4.3	63.1
		g's	180		OOPS3.10	-58.2	13.9	8.1	20.2
		g's	180		OOPS3.11	-37.2	12.8	4.6	68.3
		g's	180		OOPS3.12	-37.5	12.9	4.9	66.0
		g's	180		OOPS3.13	-23.0	13.1	5.8	21.6
		g's	180		OOPS3.14	-17.5	12.4	2.7	77.2
		g's	180		OOPS3.15	-31.3	12.3	3.6	73.2
		g's	180		OOPS3.16	-29.7	12.6	5.6	25.4
		g's	180		OOPS3.17	-50.0	12.7	4.0	24.5
		g's	180		OOPS3.18	-52.0	12.3	6.9	18.5
		g's	180		OOPS3.19	-46.6	13.5	4.4	66.7
		g's	180	Y	OOPS3.1	-1.14	13.00	1.24	9.50
		g's	180		OOPS3.2	-1.80	12.80	1.20	18.60
		g's	180		OOPS3.3	-0.96	95.80	1.12	9.30
		g's	180		OOPS3.4	-0.97	8.20	1.62	25.70
		g's	180		OOPS3.5	-2.18	13.30	2.48	9.60
		g's	180		OOPS3.6	-1.09	28.40	4.42	9.30
		g's	180		OOPS3.7	-1.5	24.0	9.3	13.2
		g's	180		OOPS3.8	-1.9	28.2	30.5	13.5
		g's	180		OOPS3.9	-2.2	28.2	14.3	13.3
		g's	180		OOPS3.10	-2.7	15.4	20.5	13.6
		g's	180		OOPS3.11	-1.7	21.8	20.2	8.5
		g's	180		OOPS3.12	-2.0	14.5	24.9	8.5
		g's	180		OOPS3.13	-1.5	25.2	4.6	13.4
		g's	180		OOPS3.14	-0.8	74.0	4.9	12.9
		g's	180		OOPS3.15	-0.6	63.2	4.7	16.8
		g's	180		OOPS3.16	-0.4	89.9	4.9	11.7
		g's	180		OOPS3.17	-2.5	16.6	4.1	13.3
		g's	180		OOPS3.18	-2.5	16.7	2.0	19.4
		g's	180		OOPS3.19	-1.6	16.0	4.7	14.2
		g's	180	Z	OOPS3.1	-7.95	14.10	2.33	68.40
		g's	180		OOPS3.2	-9.14	13.30	1.52	64.60
		g's	180		OOPS3.3	-8.58	13.60	1.37	79.20
		g's	180		OOPS3.4	-8.96	14.80	1.94	69.00
		g's	180		OOPS3.5	-6.67	9.50	2.25	69.70
		g's	180		OOPS3.6	-6.46	37.10	1.63	70.90
		g's	180		OOPS3.7	-15.2	14.2	7.5	22.9
		g's	180		OOPS3.8	-12.3	14.1	13.2	27.8
		g's	180		OOPS3.9	-16.3	13.7	3.7	22.5
		g's	180		OOPS3.10	-15.7	14.9	5.6	21.3
		g's	180		OOPS3.11	-14.8	12.8	2.4	60.5
		g's	180		OOPS3.12	-12.0	15.1	5.6	9.0
		g's	180		OOPS3.13	-9.0	13.3	3.1	50.8

TABLE 3.2.3: SENSOR DATA SUMMARY

Measurement	Sensor Location	Unit	Filter Class	Axis ①	Test②	Minimum④		Maximum④	
						Value	Time	Value	Time
		g's	180		OOPS3.14	-6.2	12.7	3.3	8.0
		g's	180		OOPS3.15	-8.0	14.1	0.5	68.4
		g's	180		OOPS3.16	-10.7	14.1	4.1	20.5
		g's	180		OOPS3.17	-8.8	13.0	14.7	20.2
		g's	180		OOPS3.18	-21.5	12.4	7.4	9.5
		g's	180		OOPS3.19	-20.4	13.6	9.9	23.1
Sternum									
Sternal Acceleration	Sternum, Upper	g's	1000	X	OOPS3.1	-262.20	6.40	115.34	15.00
		g's	1000		OOPS3.2	-309.19	6.20	162.24	13.00
		g's	1000		OOPS3.3	-316.94	6.00	108.52	11.20
		g's	1000		OOPS3.4	-276.69	6.00	190.17	12.70
		g's	1000		OOPS3.5	-187.87	5.80	153.05	12.20
		g's	1000		OOPS3.6	-258.71	5.90	141.63	11.60
		g's	1000		OOPS3.7	-415.8⑤	6.2	172.2⑤	14.9
		g's	1000		OOPS3.8	-336.5⑤	6.1	306.7⑤	14.2
		g's	1000		OOPS3.9	-270.8⑤	5.9	286.4⑤	13.9
		g's	1000		OOPS3.10	-249.8⑤	6.3	416.1⑤	14.5
		g's	1000		OOPS3.11	-286.7⑤	6.1	168.5⑤	14.4
		g's	1000		OOPS3.12	-321.0⑤	6.0	166.0⑤	14.4
		g's	1000		OOPS3.13	-127.2⑤	6.2	148.4⑤	11.7
		g's	1000		OOPS3.14	-108.7⑤	6.0	215.8⑤	11.2
		g's	1000		OOPS3.15	-484.6	5.8	178.9	11.7
		g's	1000		OOPS3.16	-477.4	6.0	187.2	11.8
		g's	1000		OOPS3.17	-541.4	5.4	282.3	13.3
		g's	1000		OOPS3.18	-710.7	5.6	289.3	12.8
		g's	1000		OOPS3.19	-586.9	6.2	308.5	14.2
	Sternum, Lower	g's	1000	X	OOPS3.1	-205.19	6.50	142.45	14.50
		g's	1000		OOPS3.2	-219.66	6.40	151.03	13.40
		g's	1000		OOPS3.3	-214.41	6.20	128.50	12.10
		g's	1000		OOPS3.4	-217.46	6.30	161.79	13.00
		g's	1000		OOPS3.5	-189.93	6.10	98.16	12.40
		g's	1000		OOPS3.6	-201.48	6.10	119.12	12.60
		g's	1000		OOPS3.7	-263.1	8.8	224.2	13.7
		g's	1000		OOPS3.8	-235.1	6.1	274.8	13.3
		g's	1000		OOPS3.9	-244.1	5.7	239.2	12.7
		g's	1000		OOPS3.10	-208.9	6.2	274.1	14.6
		g's	1000		OOPS3.11	-331.2	6.0	299.4	12.8
		g's	1000		OOPS3.12	-308.2	6.0	286.3	13.1
		g's	1000		OOPS3.13	-213.8⑤	9.1	156.5⑤	15.1
		g's	1000		OOPS3.14	-182.6⑤	8.9	157.6⑤	11.5
		g's	1000		OOPS3.15	-311.3	5.7	161.2	12.6
		g's	1000		OOPS3.16	-284.5	5.8	159.4	12.3
		g's	1000		OOPS3.17	-541.8	5.6	304.7	12.2
		g's	1000		OOPS3.18	-604.4	5.7	334.4	12.1

TABLE 3.2.3: SENSOR DATA SUMMARY

Measurement	Sensor Location	Unit	Filter Class	Axis ①	Test②	Minimum④		Maximum④	
						Value	Time	Value	Time
		g's	1000		OOPS3.19	-572.1	6.3	251.4	12.8
Spine									
Spinal	Spine, Upper,	g's	180	1	OOPS3.1	-19.54	13.90	1.63	68.80
Acceleration	External	g's	180		OOPS3.2	-22.68	13.50	0.99	87.50
		g's	180		OOPS3.3	-16.26	14.10	1.47	95.70
		g's	180		OOPS3.4	-16.07	15.00	1.55	22.00
		g's	180		OOPS3.5	-11.81	13.10	2.16	70.30
		g's	180		OOPS3.6	-11.72	11.60	0.66	68.00
		g's	180		OOPS3.7	-28.3	16.4	11.5	23.0
		g's	180		OOPS3.8	-24.9	13.4	8.6	21.7
		g's	180		OOPS3.9	-28.3	14.0	6.9	22.9
		g's	180		OOPS3.10	-26.1	13.9	8.1	23.1
		g's	180		OOPS3.11	-29.5	15.7	4.1	11.7
		g's	180		OOPS3.12	-27.2	15.2	4.1	11.8
		g's	180		OOPS3.13	-14.5	16.1	4.2	22.4
		g's	180		OOPS3.14	-10.3	13.1	1.9	27.0
		g's	180		OOPS3.15	-16.1	13.6	1.8	24.6
		g's	180		OOPS3.16	-16.7	15.4	4.8	22.6
		g's	180		OOPS3.17	-47.1	16.2	8.1	20.1
		g's	180		OOPS3.18	-46.1	15.3	7.4	20.0
		g's	180		OOPS3.19	-33.0	16.7	13.1	23.3
		g's	180	2	OOPS3.1	-2.81	8.00	5.49	9.30
		g's	180		OOPS3.2	-7.09	17.90	7.15	9.40
		g's	180		OOPS3.3	-8.84	12.50	9.71	9.20
		g's	180		OOPS3.4	-7.60	12.20	15.43	16.50
		g's	180		OOPS3.5	-6.98	10.80	7.99	9.40
		g's	180		OOPS3.6	-7.03	22.10	3.13	35.30
		g's	180		OOPS3.7	-6.9	26.7	7.4	11.3
		g's	180		OOPS3.8	-6.6	16.9	10.8	13.8
		g's	180		OOPS3.9	-27.5	16.3	16.0	13.4
		g's	180		OOPS3.10	-28.4	16.9	16.9	14.3
		g's	180		OOPS3.11	-14.6	15.8	12.9	8.7
		g's	180		OOPS3.12	-18.6	16.3	11.4	8.4
		g's	180		OOPS3.13	-23.0	11.1	15.1	15.0
		g's	180		OOPS3.14	-23.2	10.9	25.2	14.7
		g's	180		OOPS3.15	-31.6	10.9	22.1	14.4
		g's	180		OOPS3.16	-34.2	11.0	26.1	14.3
		g's	180		OOPS3.17	-7.3	22.1	8.9	11.9
		g's	180		OOPS3.18	-9.8	22.0	16.1	16.5
		g's	180		OOPS3.19	-8.9	20.7	8.0	17.5
		g's	180	3	OOPS3.1	-13.54	13.40	1.74	70.10
		g's	180		OOPS3.2	-24.05	13.70	286.99	16.20
		g's	180		OOPS3.3	-17.29	11.30	310.12	14.10
		g's	180		OOPS3.4	-24.17	11.50	494.60	14.30

TABLE 3.2.3: SENSOR DATA SUMMARY

Measurement	Sensor Location	Unit	Filter Class	Axis ①	Test②	Minimum④		Maximum④	
						Value	Time	Value	Time
		g's	180		OOPS3.5	-10.03	11.90	1.97	58.10
		g's	180		OOPS3.6	-10.10	11.40	1.91	77.20
		g's	180		OOPS3.7	-22.0	13.2	4.3	22.0
		g's	180		OOPS3.8	-22.8	13.1	3.0	21.4
		g's	180		OOPS3.9	-24.7	13.6	2.9	22.2
		g's	180		OOPS3.10	-23.9	13.7	3.7	22.6
		g's	180		OOPS3.11	-10.0	13.9	1.8	68.6
		g's	180		OOPS3.12	-10.0	13.7	2.1	72.5
		g's	180		OOPS3.13	-8.6	13.5	2.7	22.9
		g's	180		OOPS3.14	-7.3	12.6	1.4	85.7
		g's	180		OOPS3.15	-12.5	12.7	1.9	73.2
		g's	180		OOPS3.16	-10.9	12.7	3.3	24.2
		g's	180		OOPS3.17	-16.5	15.4	1.7	76.3
		g's	180		OOPS3.18	-20.7	14.7	2.3	22.4
		g's	180		OOPS3.19	-12.6	15.5	1.9	61.9
Neck									
Neck Load	Neck, Upper	N	600	X	OOPS3.1	-15.36	4.10	370.92	19.70
		N	600		OOPS3.2	-41.56	9.50	440.66	17.80
		N	600		OOPS3.3	-43.24	9.50	505.36	18.20
		N	600		OOPS3.4	-28.40	9.20	387.82	17.60
		N	600		OOPS3.5	-25.48	9.00	397.54	23.60
		N	600		OOPS3.6	-36.01	8.40	351.28	38.10
		N	600		OOPS3.7	-1064.7⑤	10.7	795.3⑤	22.6
		N	600		OOPS3.8	-3708.6⑤	9.6	1084.4⑤	19.9
		N	600		OOPS3.9	-39.1	7.9	734.5	30.6
		N	600		OOPS3.10	-3798.8⑤	10.7	720.0⑤	21.7
		N	600		OOPS3.11	-19.6	7.3	405.3	29.0
		N	600		OOPS3.12	-3272.8⑤	8.9	483.2⑤	26.6
		N	600		OOPS3.13	-4164.7⑤	9.4	761.9⑤	35.4
		N	600		OOPS3.14	-4249.5⑤	8.0	626.2⑤	27.1
		N	600		OOPS3.15	-5.3	3.9	868.7	25.2
		N	600		OOPS3.16	-2506.9⑤	9.8	821.0⑤	21.7
		N	600		OOPS3.17	-4578.1⑤	10.1	684.7⑤	21.5
		N	600		OOPS3.18	-5122.7⑤	9.6	649.2⑤	20.2
		N	600		OOPS3.19	-15.7⑤	49.3	1086.6⑤	31.6
		N	600	Y	OOPS3.1	-22.88	55.80	105.91	8.90
		N	600		OOPS3.2	-22.85	4.00	33.44	15.20
		N	600		OOPS3.3	-39.39	9.60	456.59	8.70
		N	600		OOPS3.4	-22.87	6.60	39.25	15.70
		N	600		OOPS3.5	-22.67	5.40	30.66	15.10
		N	600		OOPS3.6	-26.01	5.60	40.99	16.60
		N	600		OOPS3.7	-18.7⑤	24.5	285.7⑤	10.7
		N	600		OOPS3.8	-47.4⑤	8.7	869.0⑤	20.8
		N	600		OOPS3.9	-20.4	43.0	44.4	29.4

TABLE 3.2.3: SENSOR DATA SUMMARY

Measurement	Sensor Location	Unit	Filter Class	Axis ①	Test②	Minimum④		Maximum④	
						Value	Time	Value	Time
		N	600		OOPS3.10	-12.1⑤	4.2	878.2⑤	13.8
		N	600		OOPS3.11	-67.8	28.3	38.7	43.8
		N	600		OOPS3.12	-39.9⑤	8.2	873.8⑤	9.0
		N	600		OOPS3.13	-71.8⑤	82.1	889.3⑤	8.5
		N	600		OOPS3.14	-61.9⑤	82.3	871.1⑤	8.0
		N	600		OOPS3.15	-46.4	85.0	107.7	30.4
		N	600		OOPS3.16	-59.8⑤	99.2	524.6⑤	9.8
		N	600		OOPS3.17	-40.2⑤	26.3	875.9⑤	27.1
		N	600		OOPS3.18	-43.8⑤	8.6	894.4⑤	9.6
		N	600		OOPS3.19	-28.0⑤	21.4	59.6⑤	21.9
		N	600	Z	OOPS3.1	-311.03	60.90	533.26	14.20
		N	600		OOPS3.2	-294.62	66.30	696.78	17.00
		N	600		OOPS3.3	-303.31	61.30	709.14	17.40
		N	600		OOPS3.4	-329.59	64.50	668.67	17.10
		N	600		OOPS3.5	-161.53	61.70	474.00	23.40
		N	600		OOPS3.6	-115.04	67.60	611.80	37.70
		N	600		OOPS3.7	-301.6⑤	25.3	1179.0⑤	31.6
		N	600		OOPS3.8	-1746.4⑤	9.6	1223.5⑤	18.3
		N	600		OOPS3.9	-158.4	66.5	999.6	30.7
		N	600		OOPS3.10	-1368.9⑤	10.6	812.8⑤	15.5
		N	600		OOPS3.11	-221.5	62.4	1055.0	14.1
		N	600		OOPS3.12	-687.9⑤	8.9	929.0⑤	14.3
		N	600		OOPS3.13	-2112.6⑤	8.4	905.0⑤	31.4
		N	600		OOPS3.14	-2026.2⑤	8.3	693.0⑤	27.0
		N	600		OOPS3.15	-65.6	71.4	851.4	25.3
		N	600		OOPS3.16	-818.3⑤	9.8	788.5⑤	29.9
		N	600		OOPS3.17	-1134.8⑤	10.0	854.4⑤	31.9
		N	600		OOPS3.18	-2335.1⑤	9.5	1212.9⑤	14.3
		N	600		OOPS3.19	-143.9	66.1	1415.9	31.6
	Neck, Lower	N	600	X	OOPS3.1	-17.00	7.50	369.30	21.10
		N	600		OOPS3.2	-18.90	7.40	443.41	21.10
		N	600		OOPS3.3	-24.04	7.20	499.81	22.00
		N	600		OOPS3.4	-27.08	7.30	367.09	21.80
		N	600		OOPS3.5	-34.03	7.30	245.65	56.80
		N	600		OOPS3.6	-35.41	7.30	269.03	47.70
		N	600		OOPS3.7	-504.0	10.7	691.1⑤	34.7
		N	600		OOPS3.8	-1970.5	9.6	714.2⑤	19.9
		N	600		OOPS3.9	-7.5	5.9	587.1	30.5
		N	600		OOPS3.10	-2074.7⑤	10.7	551.7⑤	25.3
		N	600		OOPS3.11	-12.9	99.6	506.2	30.7
		N	600		OOPS3.12	-2186.8⑤	8.9	579.8⑤	34.6
		N	600		OOPS3.13	-2170.5⑤	8.4	579.3⑤	35.6
		N	600		OOPS3.14	-2292.9⑤	8.0	341.3⑤	20.8
		N	600		OOPS3.15	-33.6	99.6	574.6	25.5

TABLE 3.2.3: SENSOR DATA SUMMARY

Measurement	Sensor Location	Unit	Filter Class	Axis ①	Test②	Minimum④		Maximum④	
						Value	Time	Value	Time
		N	600		OOPS3.16	-1248.4⑤	9.8	573.6⑤	25.7
		N	600		OOPS3.17	-2494.3⑤	10.1	632.7⑤	26.2
		N	600		OOPS3.18	-2562.3⑤	9.5	558.5⑤	24.9
		N	600		OOPS3.19	-55.4	48.3	842.0	31.5
		N	600	Y	OOPS3.1	-43.00	44.00	36.57	8.80
		N	600		OOPS3.2	-96.72	26.30	31.23	17.20
		N	600		OOPS3.3	-58.48	14.00	127.28	8.70
		N	600		OOPS3.4	-41.56	32.60	46.93	8.70
		N	600		OOPS3.5	-60.20	27.40	41.37	11.50
		N	600		OOPS3.6	-31.55	14.20	37.37	21.40
		N	600		OOPS3.7	-342.3⑤	10.7	76.9⑤	11.2
		N	600		OOPS3.8	-1442.6⑤	9.6	204.3⑤	15.2
		N	600		OOPS3.9	-77.0	40.2	79.4	16.6
		N	600		OOPS3.10	-1521.1⑤	10.7	141.6⑤	14.6
		N	600		OOPS3.11	-154.7	32.7	51.1	43.8
		N	600		OOPS3.12	-1550.2⑤	8.9	80.4⑤	9.7
		N	600		OOPS3.13	-1536.8⑤	8.4	375.7⑤	31.0
		N	600		OOPS3.14	-1602.2⑤	8.0	270.7⑤	30.8
		N	600		OOPS3.15	-65.6	99.3	215.6	28.9
		N	600		OOPS3.16	-820.6⑤	9.8	236.8⑤	29.9
		N	600		OOPS3.17	-1608.2⑤	10.1	51.9⑤	87.1
		N	600		OOPS3.18	-1662.8⑤	9.5	160.9⑤	10.4
		N	600		OOPS3.19	-200.5⑤	21.5	47.6	32.7
		N	600	Z	OOPS3.1	-780.38	13.40	525.35	64.50
		N	600		OOPS3.2	-1067.60	17.20	454.74	66.10
		N	600		OOPS3.3	-988.59	17.40	466.53	61.00
		N	600		OOPS3.4	-911.24	17.00	536.53	65.00
		N	600		OOPS3.5	-676.57	11.60	349.62	61.60
		N	600		OOPS3.6	-773.37	37.40	268.71	68.40
		N	600		OOPS3.7	-1382.2⑤	31.5	1792.9⑤	10.7
		N	600		OOPS3.8	-1817.6⑤	18.3	7000.2⑤	9.6
		N	600		OOPS3.9	-1255.3	13.9	318.7	65.6
		N	600		OOPS3.10	-1413.1⑤	14.6	6752.3⑤	10.7
		N	600		OOPS3.11	-1516.0	14.0	408.8	59.6
		N	600		OOPS3.12	-1317.8⑤	14.2	4280.8⑤	8.9
		N	600		OOPS3.13	-1116.3⑤	31.3	7960.0⑤	9.4
		N	600		OOPS3.14	-877.9⑤	27.1	7930.4⑤	8.0
		N	600		OOPS3.15	-960.6	25.4	171.0	71.8
		N	600		OOPS3.16	-921.1⑤	29.9	4378.9⑤	9.8
		N	600		OOPS3.17	-1406.4⑤	31.9	6388.1⑤	10.0
		N	600		OOPS3.18	-1870.2⑤	14.1	10371.0⑤	9.6
		N	600		OOPS3.19	-1770.7⑤	31.7	308.1⑤	66.2
Neck	Neck, Upper	Nm	600	X	OOPS3.1	-0.78	79.20	2.85	35.20
Moment		Nm	600		OOPS3.2	-2.68	81.70	2.14	31.30

TABLE 3.2.3: SENSOR DATA SUMMARY

Measurement	Sensor Location	Unit	Filter Class	Axis ①	Test②	Minimum④		Maximum④	
						Value	Time	Value	Time
		Nm	600		OOPS3.3	-2.18	88.70	4.50	8.80
		Nm	600		OOPS3.4	-1.17	82.60	2.91	26.20
		Nm	600		OOPS3.5	-1.48	81.20	3.37	36.20
		Nm	600		OOPS3.6	-0.45	5.60	3.91	34.50
		Nm	600		OOPS3.7	-1.9⑤	27.4	21.5⑤	10.7
		Nm	600		OOPS3.8	-2.8⑤	8.7	61.8⑤	20.8
		Nm	600		OOPS3.9	-2.2	88.2	5.2	31.3
		Nm	600		OOPS3.10	-1.7⑤	76.4	62.7⑤	13.8
		Nm	600		OOPS3.11	-6.4	31.5	6.0	43.8
		Nm	600		OOPS3.12	-2.8⑤	8.2	61.9⑤	8.9
		Nm	600		OOPS3.13	-7.3⑤	21.1	62.4⑤	8.5
		Nm	600		OOPS3.14	-6.0⑤	21.6	62.8⑤	8.0
		Nm	600		OOPS3.15	-10.1	20.1	8.6	29.9
		Nm	600		OOPS3.16	-10.6⑤	20.6	37.6⑤	9.8
		Nm	600		OOPS3.17	-3.0⑤	26.3	62.5⑤	27.1
		Nm	600		OOPS3.18	-4.6⑤	23.6	64.6⑤	9.6
		Nm	600		OOPS3.19	-3.4⑤	21.5	6.8⑤	31.4
		Nm	600	Y	OOPS3.1	-29.39	19.50	11.62	65.20
		Nm	600		OOPS3.2	-32.55	18.20	12.40	69.00
		Nm	600		OOPS3.3	-36.33	18.80	14.91	39.60
		Nm	600		OOPS3.4	-28.19	18.20	13.14	66.50
		Nm	600		OOPS3.5	-27.58	21.70	13.40	44.00
		Nm	600		OOPS3.6	-22.96	17.90	14.24	87.70
		Nm	600		OOPS3.7	-71.7⑤	10.7	20.2⑤	50.1
		Nm	600		OOPS3.8	-251.3⑤	20.7	21.9⑤	47.5
		Nm	600		OOPS3.9	-44.7	22.5	18.3	48.9
		Nm	600		OOPS3.10	-219.5⑤	13.4	16.6⑤	43.9
		Nm	600		OOPS3.11	-25.5	28.9	8.5	67.7
		Nm	600		OOPS3.12	-103.0⑤	8.9	12.1⑤	75.1
		Nm	600		OOPS3.13	-246.8⑤	8.4	14.7⑤	59.6
		Nm	600		OOPS3.14	-239.7⑤	8.3	13.2⑤	52.9
		Nm	600		OOPS3.15	-55.0	25.3	11.4	70.2
		Nm	600		OOPS3.16	-151.6⑤	9.8	13.2⑤	73.6
		Nm	600		OOPS3.17	-164.7⑤	10.0	15.1⑤	45.2
		Nm	600		OOPS3.18	-314.8⑤	9.6	16.7⑤	41.0
		Nm	600		OOPS3.19	-60.4⑤	31.6	19.9⑤	49.3
		Nm	600	Z	OOPS3.1	-0.85	60.80	0.32	14.40
		Nm	600		OOPS3.2	-0.60	28.90	0.28	49.90
		Nm	600		OOPS3.3	-1.63	66.00	0.43	15.40
		Nm	600		OOPS3.4	-0.99	87.50	0.54	15.80
		Nm	600		OOPS3.5	-0.44	34.70	0.93	70.80
		Nm	600		OOPS3.6	-0.39	18.90	0.52	55.70
		Nm	600		OOPS3.7	-9.1⑤	10.7	1.1⑤	91.1
		Nm	600		OOPS3.8	-29.5⑤	20.8	1.7⑤	15.3

TABLE 3.2.3: SENSOR DATA SUMMARY

Measurement	Sensor Location	Unit	Filter Class	Axis ①	Test②	Minimum④		Maximum④	
						Value	Time	Value	Time
		Nm	600		OOPS3.9	-1.2	18.0	0.2	12.2
		Nm	600		OOPS3.10	-30.7⑤	13.7	1.2⑤	9.9
		Nm	600		OOPS3.11	-5.1	44.1	1.9	93.3
		Nm	600		OOPS3.12	-25.7⑤	8.9	1.1⑤	8.2
		Nm	600		OOPS3.13	-32.4⑤	8.4	7.8⑤	40.0
		Nm	600		OOPS3.14	-33.7⑤	8.0	7.0⑤	43.3
		Nm	600		OOPS3.15	-2.5	94.7	7.1	42.9
		Nm	600		OOPS3.16	-19.6⑤	9.8	7.0⑤	42.6
		Nm	600		OOPS3.17	-37.0⑤	10.1	1.3⑤	9.2
		Nm	600		OOPS3.18	-38.6⑤	9.6	1.2⑤	8.6
		Nm	600		OOPS3.19	-0.8⑤	21.6	0.5⑤	14.9
	Neck, Lower	Nm	600	X	OOPS3.1	-4.73	99.60	4.12	44.60
		Nm	600		OOPS3.2	-6.27	74.50	2.79	26.40
		Nm	600		OOPS3.3	-4.10	82.20	3.77	39.00
		Nm	600		OOPS3.4	-3.52	94.20	3.77	32.80
		Nm	600		OOPS3.5	-4.81	73.10	4.73	40.80
		Nm	600		OOPS3.6	-3.18	21.50	2.91	61.50
		Nm	600		OOPS3.7	-6.5⑤	10.5	5.9⑤	37.8
		Nm	600		OOPS3.8	-63.3⑤	9.7	61.7⑤	24.9
		Nm	600		OOPS3.9	-7.6	79.2	4.4	41.1
		Nm	600		OOPS3.10	-62.9⑤	10.7	9.2⑤	14.6
		Nm	600		OOPS3.11	-6.5	91.4	13.8	32.7
		Nm	600		OOPS3.12	-52.8⑤	9.0	4.8⑤	8.5
		Nm	600		OOPS3.13	-62.7⑤	8.5	11.9⑤	79.9
		Nm	600		OOPS3.14	-60.9⑤	8.9	14.1⑤	98.1
		Nm	600		OOPS3.15	-23.0	29.4	12.3	99.7
		Nm	600		OOPS3.16	-35.9⑤	9.8	16.8⑤	99.6
		Nm	600		OOPS3.17	-63.7⑤	15.7	52.2⑤	28.4
		Nm	600		OOPS3.18	-62.6⑤	9.6	8.7⑤	21.1
		Nm	600		OOPS3.19	-3.6⑤	31.9	10.9⑤	21.9
		Nm	600	Y	OOPS3.1	-20.31	12.50	68.15	58.70
		Nm	600		OOPS3.2	-24.30	12.60	60.82	57.20
		Nm	600		OOPS3.3	-18.53	16.70	67.93	54.70
		Nm	600		OOPS3.4	-22.08	11.90	67.12	61.60
		Nm	600		OOPS3.5	-25.25	11.40	65.01	57.10
		Nm	600		OOPS3.6	-21.70	11.10	53.66	59.70
		Nm	600		OOPS3.7	-75.7⑤	10.7	70.5⑤	25.3
		Nm	600		OOPS3.8	-229.0⑤	9.6	55.3⑤	62.6
		Nm	600		OOPS3.9	-32.3	13.9	51.7	64.2
		Nm	600		OOPS3.10	-245.8⑤	13.8	52.4⑤	60.2
		Nm	600		OOPS3.11	-48.0	14.0	58.1	59.5
		Nm	600		OOPS3.12	-191.2⑤	8.9	57.8⑤	67.5
		Nm	600		OOPS3.13	-263.3⑤	9.4	36.0⑤	42.5
		Nm	600		OOPS3.14	-257.0⑤	8.0	28.9⑤	71.2

TABLE 3.2.3: SENSOR DATA SUMMARY									
Measurement	Sensor Location	Unit	Filter Class	Axis ①	Test②	Minimum④		Maximum④	
						Value	Time	Value	Time
		Nm	600		OOPS3.15	-15.1	10.6	34.8	67.2
		Nm	600		OOPS3.16	-164.7⑤	9.8	45.1⑤	24.3
		Nm	600		OOPS3.17	-312.0⑤	10.1	73.6⑤	28.6
		Nm	600		OOPS3.18	-308.1⑤	9.6	66.0⑤	58.4
		Nm	600		OOPS3.19	-56.1	14.9	57.0	25.8

NOTES:

NA = Not Applicable

① Frame of reference is local to the part on which the sensor is mounted, unless otherwise specified. See Appendix A.2 for definitions.

NA = Not Applicable: Frame of reference was undefined or unrelated to defined frames of reference.

1, 2, 3=Local frame of reference with respect to sensor, Axes undefined without further processing.

② See Table 1.2. for other details about the configurations of the tests.

③ Air bag used was depowered 1998 Ford Taurus driver side air bag.

④ The minimum and maximum values of the data, filtered to the appropriate SAE J-211Channel Frequency Class, occurred at the times shown, in milliseconds after T_0.

⑤ Questionable data, electronic noise spikes.

3.3: THORACIC DATA

The primary goal of the OOPS3 test series was to investigate out-of-position thoracic response of a 5th Percentile Female Hybrid III dummy under air bag deployment. As repeatable dummy response is crucial in the usefulness of such research, a preliminary investigation was performed to determine the repeatability of response of the dummy ribs under quasistatic deformation under various conditions. For these tests, a 2.54-cm diameter pin was screwed into the steering column load cell, temporarily replacing the steering wheel and air bag module. The pin was pressed into the horizontal and vertical center of the dummy sternum using the hydraulic cylinders supporting the test fixture. Displacements of the pin were measured using the Faro arm measurement device at the steering wheel fixture reference location. Results for selected tests are plotted in *Figure 12*.

The tests with skin performed before OOPS3.2 – OOPS3.4 showed very similar slopes for all cases. The thickness of the chestbands and associated tape resulted in an approximately 10 mm offset before OOPS3.2 and OOPS3.4. Testing delays between the three tests with skin were approximately an hour and approximately 24 hours. In addition, the deformations performed without skin both before testing started and after tests OOPS3.1, OOPS3.5, and OOPS3.6 all show similar force/deflection slopes. The delay between the earliest and latest tests was approximately 36 hours. Subsequent tests resulted in negligible variation of slope from those seen below. This indicates a negligible change in occupant rib stiffness over the quasistatic conditions tested and suggests that subject rib repeatability is acceptable under the test conditions used.

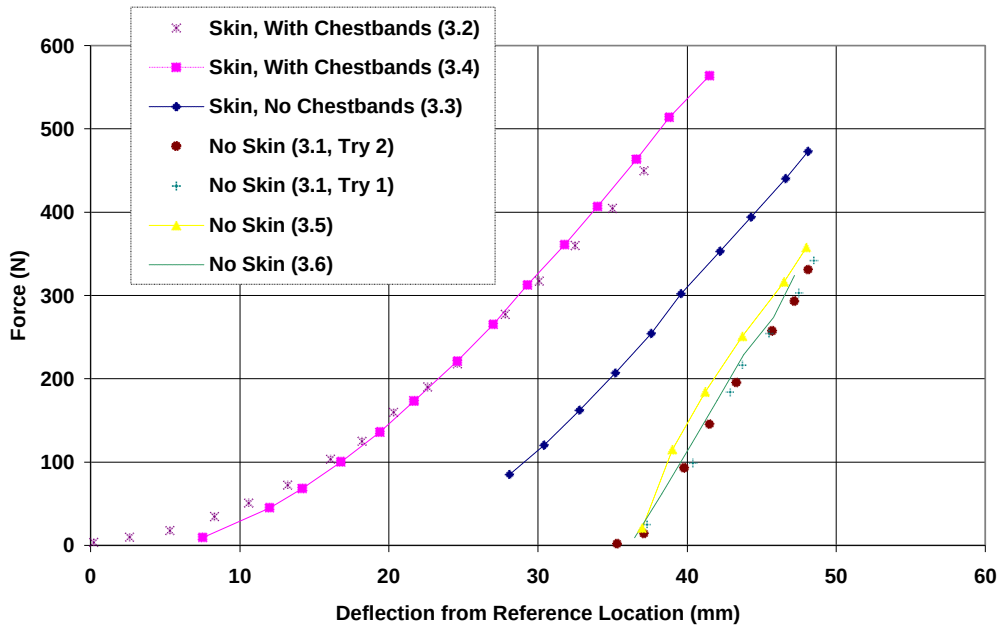

Figure 12: *Force/Deflection Profiles for Mid-Thorax Quasistatic Compression with 2.54 cm Diameter Pin*

The maximum calculated values of chest and sternal deflection, sternal viscous response, sternal velocity, and change in chestband curvature are summarized in Table 3.3.1. Thoracic displacement data are discussed in Section 3.3.1 and tabulated for accelerometers, chestbands, and CRUX units in Table 3.3.1.1. This discussion includes a brief exposition on CRUX unit performance. In Section 3.3.2, the dynamic viscous response of the dummy thorax is investigated using V*C data from each thoracic instrumentation.

TABLE 3.3.1: CHESTBAND DATA SUMMARY

Measurement	Unit	Test ②	Airbag Stage ③	Occupant Position⑥	Upper Chestband ⑤			Lower Chestband ⑤		
					Value	Dist.④	Time	Value	Dist.④	Time
Maximum Chest Deflection	mm	oops3.1	1998 Ford Taurus	ISO-2, CC	63.3	-29.0	14.3	44.0	-8.5	15.6
		oops3.2	1998 Ford Taurus	ISO-2, CC	66.1	-29.0	14.9	51.1	-13.5	15.3
		oops3.3	1998 Ford Taurus	ISO-2, CC	49.3	-10.2	14.9	41.5	-8.8	16.2
		oops3.4	1998 Ford Taurus	ISO-2, CC	52.5	-10.2	13.7	42.3	-8.8	12.5
		oops3.5	1998 Ford Taurus	ISO-2, CC	33.4	-10.2	12.7	24.9	-4.8	13.4
		oops3.6	1998 Ford Taurus	ISO-2, CC	31.4	0.4	5.9	27.4	-4.7	13.7
		oops3.8	1998 Ford Taurus	ISO-2, CC	74.9	-13.2	14.2	60.5	-13.9	14.8
		oops3.9	1998 Ford Taurus	ISO-2, CC	57.2	-24.7	14.6	55.5	-1.5	14.3
		oops3.10	1998 Ford Taurus	ISO-2, CC	63.2	-19.6	15.3	56.7	-11.7	16.3
		oops3.11	1998 Ford Taurus	ISO-2, CU4	50.3	-28.9	15.9	73.5	-13.9	12.3
		oops3.12	1998 Ford Taurus	ISO-2, CU4	49.6	-28.9	14.3	74.4	-13.9	12.1
		oops3.13	1998 Ford Taurus	ISO-2, CU4	75.2	1.6	14.8	53.2	16.5	15.3
		oops3.14	1998 Ford Taurus	ISO-2, L4C	39.3	11.8	14.4	37.1	21.6	13.8
		oops3.15	1998 Ford Taurus	ISO-2, L4C	45.3	10.6	16.7	46.6	16.3	16.3
		oops3.16	1998 Ford Taurus	ISO-2, L4C	30.7	-4.7	16.9	40.9	16.3	15.3
		oops3.17	1998 Ford Taurus	ISO-2, CU2	61.3	-46.1	14.8	80.4	-13.6	12.6
		oops3.18	1998 Ford Taurus	ISO-2, CU2	64.6	--46.1	13.9	78.3	-8.4	12.8
		oops3.19	1998 Ford Taurus	ISO-2, CU2	68.0	-35.9	13.9	74.7	-13.6	13.7

TABLE 3.3.1: CHESTBAND DATA SUMMARY (CONTINUED)

Measurement	Unit	Test ②	Airbag Stage ③	Occupant Position⑥	Upper Chestband ⑤			Lower Chestband ⑤		
					Value	Dist.④	Time	Value	Dist.④	Time
Maximum Sternum Deflection	mm	oops3.1	1998 Ford Taurus	ISO-2, CC	59.3	0	14.2	43.5	0	15.3
		oops3.2	1998 Ford Taurus	ISO-2, CC	60.1	0	14.6	50.3	0	15.3
		oops3.3	1998 Ford Taurus	ISO-2, CC	48.5	0	15.0	40.9	0	16.0
		oops3.4	1998 Ford Taurus	ISO-2, CC	51.7	0	13.6	41.8	0	12.9
		oops3.5	1998 Ford Taurus	ISO-2, CC	33.1	0	13.2	24.8	0	13.5
		oops3.6	1998 Ford Taurus	ISO-2, CC	27.5	0	12.7	26.9	0	13.9
		oops3.8	1998 Ford Taurus	ISO-2, CC	74.1	0	14.3	59.4	0	15.0
		oops3.9	1998 Ford Taurus	ISO-2, CC	54.9	0	14.5	55.4	0	14.2
		oops3.10	1998 Ford Taurus	ISO-2, CC	59.4	0	15.6	56.0	0	15.7
		oops3.11	1998 Ford Taurus	ISO-2, CU4	44.5	0	15.9	71.9	0	12.4
		oops3.12	1998 Ford Taurus	ISO-2, CU4	46.3	0	19.7	72.7	0	12.2
		oops3.13	1998 Ford Taurus	ISO-2, CU4	74.8	0	14.7	51.3	0	15.4
		oops3.14	1998 Ford Taurus	ISO-2, L4C	38.3	0	14.0	34.2	0	14.3
		oops3.15	1998 Ford Taurus	ISO-2, L4C	44.4	0	16.4	45.4	0	16.1
		oops3.16	1998 Ford Taurus	ISO-2, L4C	30.1	0	17.0	38.9	0	15.6
		oops3.17	1998 Ford Taurus	ISO-2, CU2	52.3	0	14.9	79.0	0	12.7
		oops3.18	1998 Ford Taurus	ISO-2, CU2	56.6	0	12.4	77.6	0	12.6
		oops3.19	1998 Ford Taurus	ISO-2, CU2	60.8	0	13.7	73.8	0	13.7

TABLE 3.3.1: CHESTBAND DATA SUMMARY (CONTINUED)

Measurement	Unit	Test ②	Airbag Stage ③	Occupant Position⑥	Upper Chestband ⑤		Lower Chestband ⑤	
					Value	Time	Value	Time
Sternal V*C	m/s	oops3.1	1998 Ford Taurus	ISO-2, CC	1.3	10.7	0.8	9.9
		oops3.2	1998 Ford Taurus	ISO-2, CC	1.1	9.0	1.0	13.0
		oops3.3	1998 Ford Taurus	ISO-2, CC	1.0	8.7	0.8	8.9
		oops3.4	1998 Ford Taurus	ISO-2, CC	1.3	9.9	0.9	9.0
		oops3.5	1998 Ford Taurus	ISO-2, CC	1.3	5.9	0.4	7.5
		oops3.6	1998 Ford Taurus	ISO-2, CC	1.2	5.7	1.0	7.3
		oops3.8	1998 Ford Taurus	ISO-2, CC	3.5	9.3	2.4	10.6
		oops3.9	1998 Ford Taurus	ISO-2, CC	2.7	8.6	1.6	12.0
		oops3.10	1998 Ford Taurus	ISO-2, CC	1.8	8.9	2.1	13.1
		oops3.11	1998 Ford Taurus	ISO-2, CU4	1.3	11.1	4.1	11.2
		oops3.12	1998 Ford Taurus	ISO-2, CU4	1.9	12.7	4.6	10.8
		oops3.13	1998 Ford Taurus	ISO-2, CU4	3.3	11.5	1.2	11.8
		oops3.14	1998 Ford Taurus	ISO-2, L4C	1.0	9.9	0.7	10.8
		oops3.15	1998 Ford Taurus	ISO-2, L4C	1.5	8.1	1.7	9.4
		oops3.16	1998 Ford Taurus	ISO-2, L4C	0.7	8.1	1.5	14.2
		oops3.17	1998 Ford Taurus	ISO-2, CU2	1.5	11.1	5.2	10.9
		oops3.18	1998 Ford Taurus	ISO-2, CU2	1.8	11.0	4.6	10.9
		oops3.19	1998 Ford Taurus	ISO-2, CU2	2.4	12.3	3.8	11.5

TABLE 3.3.1: CHESTBAND DATA SUMMARY (CONTINUED)

Measurement	Unit	Test ②	Airbag Stage ③	Occupant Position⑥	Upper Chestband ⑤		Lower Chestband ⑤	
					Value	Time	Value	Time
Maximum Sternum Velocity	m/s	oops3.1	1998 Ford Taurus	ISO-2, CC	14.9	6.0	9.7	8.4
		oops3.2	1998 Ford Taurus	ISO-2, CC	15.4	5.7	9.3	8.5
		oops3.3	1998 Ford Taurus	ISO-2, CC	11.0	5.8	11.0	7.7
		oops3.4	1998 Ford Taurus	ISO-2, CC	10.7	5.7	11.6	7.6
		oops3.5	1998 Ford Taurus	ISO-2, CC	19.5	5.7	9.6	7.2
		oops3.6	1998 Ford Taurus	ISO-2, CC	18.9	5.5	15.9	7.1
		oops3.8	1998 Ford Taurus	ISO-2, CC	20.2	9.0	19.8	9.9
		oops3.9	1998 Ford Taurus	ISO-2, CC	18.5	8.4	11.6	8.4
		oops3.10	1998 Ford Taurus	ISO-2, CC	14.4	8.8	12.0	12.9
		oops3.11	1998 Ford Taurus	ISO-2, CU4	14.6	10.9	15.5	10.9
		oops3.12	1998 Ford Taurus	ISO-2, CU4	12.9	12.5	18.1	10.6
		oops3.13	1998 Ford Taurus	ISO-2, CU4	23.2	6.1	12.1	9.7
		oops3.14	1998 Ford Taurus	ISO-2, L4C	11.6	4.9	8.6	9.7
		oops3.15	1998 Ford Taurus	ISO-2, L4C	12.4	5.3	15.9	9.1
		oops3.16	1998 Ford Taurus	ISO-2, L4C	8.9	12.2	10.8	14.0
		oops3.17	1998 Ford Taurus	ISO-2, CU2	10.2	4.6	18.7	10.7
		oops3.18	1998 Ford Taurus	ISO-2, CU2	12.0	5.3	16.5	10.6
		oops3.19	1998 Ford Taurus	ISO-2, CU2	11.8	5.7	15.2	11.2

TABLE 3.3.1: CHESTBAND DATA SUMMARY (CONTINUED)

Measurement	Unit	Test ②	Airbag Stage ③	Occupant Position⑥	Upper Chestband ⑤			Lower Chestband ⑤		
					Value	Dist.④	Time	Value	Dist.④	Time
Maximum Chestband Curvature	1/mm	oops3.1	1998 Ford Taurus	ISO-2, CC	0.038	91.2	8.7	0.028	-84.6	9.3
		oops3..2	1998 Ford Taurus	ISO-2, CC	0.040	-162.8	13.2	0.028	-84.6	9.2
		oops3.3	1998 Ford Taurus	ISO-2, CC	0.042	-101.6	7.6	0.028	-87.6	8.1
		oops3.4	1998 Ford Taurus	ISO-2, CC	0.040	152.4	14.2	0.029	-87.6	8.3
		oops3.5	1998 Ford Taurus	ISO-2, CC	0.027	-127.0	10.4	0.024	130.0	10.5
		oops3.6	1998 Ford Taurus	ISO-2, CC	0.027	131.0	10.8	0.024	131.0	9.9
		oops3.8	1998 Ford Taurus	ISO-2, CC	0.044	-157.8	15.2	0.023	63.8	11.1
		oops3.9	1998 Ford Taurus	ISO-2, CC	0.043	-170.8	11.6	0.023	-162.8	11.5
		oops3.10	1998 Ford Taurus	ISO-2, CC	0.041	-145.4	10.1	0.022	-162.8	12.9
		oops3.11	1998 Ford Taurus	ISO-2, CU4	0.034	-187.2	16.4	0.035	-190.2	12.1
		oops3.12	1998 Ford Taurus	ISO-2, CU4	0.031	-161.8	16.3	0.034	-190.2	11.9
		oops3.13	1998 Ford Taurus	ISO-2, CU4	0.048	-212.6	6.6	0.023	114.6	11.1
		oops3.14	1998 Ford Taurus	ISO-2, L4C	0.041	143.0	11.0	0.021	114.6	10.9
		oops3.15	1998 Ford Taurus	ISO-2, L4C	0.047	156.4	10.1	0.021	87.2	11.2
		oops3.16	1998 Ford Taurus	ISO-2, L4C	0.047	156.4	9.7	0.025	61.8	11.0
		oops3.17	1998 Ford Taurus	ISO-2, CU2	0.047	-130.8	11.4	0.034	-134.4	11.2
		oops3.18	1998 Ford Taurus	ISO-2, CU2	0.047	148.6	14.8	0.033	-134.4	11.1
		oops3.19	1998 Ford Taurus	ISO-2, CU2	0.041	-130.8	11.6	0.029	-134.4	11.7

TABLE 3.3.1: CHESTBAND DATA SUMMARY (CONTINUED)

Measurement	Unit	Test ②	Airbag Stage ③	Occupant Position⑥	Upper Chestband ⑤			Lower Chestband ⑤		
					Value	Dist.④	Time	Value	Dist.④	Time
Maximum Change in Chestband Curvature	1/mm	oops3.1	1998 Ford Taurus	ISO-2, CC	0.027	-13.7	9.7	0.018	-8.5	9.3
		oops3.2	1998 Ford Taurus	ISO-2, CC	0.032	-16.3	13.2	0.019	-8.5	9.2
		oops3.3	1998 Ford Taurus	ISO-2, CC	0.024	-10.2	7.6	0.020	-8.8	8.1
		oops3.4	1998 Ford Taurus	ISO-2, CC	0.027	15.2	14.2	0.019	-8.8	8.3
		oops3.5	1998 Ford Taurus	ISO-2, CC	0.032	0.0	6.0	0.014	0.3	7.6
		oops3.6	1998 Ford Taurus	ISO-2, CC	0.032	0.4	5.8	0.014	0.4	7.3
		oops3.8	1998 Ford Taurus	ISO-2, CC	0.031	-15.8	15.2	0.022	-3.8	13.2
		oops3.9	1998 Ford Taurus	ISO-2, CC	0.034	-17.1	11.6	0.017	-13.7	10.7
		oops3.10	1998 Ford Taurus	ISO-2, CC	0.028	-14.5	10.1	0.019	-11.7	14.5
		oops3.11	1998 Ford Taurus	ISO-2, CU4	0.025	-18.7	16.4	0.023	-19.0	12.1
		oops3.12	1998 Ford Taurus	ISO-2, CU4	0.024	-16.2	16.3	0.024	-13.9	10.6
		oops3.13	1998 Ford Taurus	ISO-2, CU4	0.040	-21.3	6.6	0.018	1.3	13.7
		oops3.14	1998 Ford Taurus	ISO-2, L4C	0.033	14.3	11.0	0.014	1.3	13.5
		oops3.15	1998 Ford Taurus	ISO-2, L4C	0.036	15.6	10.1	0.016	1.1	14.4
		oops3.16	1998 Ford Taurus	ISO-2, L4C	0.035	18.2	12.3	0.019	1.1	13.5
		oops3.17	1998 Ford Taurus	ISO-2, CU2	0.036	-13.1	11.4	0.024	-13.4	11.2
		oops3.18	1998 Ford Taurus	ISO-2, CU2	0.038	14.9	14.8	0.023	-10.9	9.8
		oops3.19	1998 Ford Taurus	ISO-2, CU2	0.031	14.9	15.9	0.040	-168.0	11.0

NOTES:

NA = Not Applicable

① Frame of reference is local to the part on which the sensor is mounted, unless otherwise specified. See Appendix A.2 for definitions.

NA = Not Applicable: Frame of reference was undefined or unrelated to defined frames of reference.

RES = Resultant: See Appendix I.3 for an explanation of the generation of resultants.

② See Table 1.2. for other details about the configurations of the tests.

③ Air bag used was depowered 1998 Ford Taurus driver-side air bag.

④ Distance counterclockwise from the sternum.

⑤ Upper chestband was located at the first rib, lower chestband was located at the sixth rib. The minimum and maximum values of the data, filtered to the appropriate SAE J-211Channel Frequency Class, occurred at the times shown, in milliseconds after T_0.

⑥ Occupant positioning of the dummy thorax relative to the steering wheel center is:

CC = Center, Center

CU4 = Center, Up 4 cm

CU2 = Center, Up 2 cm

L4C = Left 4 cm, Center.

3.3.1: CHEST DISPLACEMENT DATA

TABLE 3.3.1.1: CHEST DISPLACEMENT DATA COMPARISON

OOPS TEST	Position Vert., Horiz., Chest	Skin	Upper Sternum Displacement (mm @ ms)			Lower Sternum Displacement (mm @ ms)	
			Chestband	Crux	Accel.	Chestband	Accel.
3.1	Center, Center, Nom ISO-2	On	59.3@14.2	44.9@14.4	31.1@15.4	43.5@15.3	36.8@15.4
3.2	Center, Center, Nom ISO-2	On	60.1@14.6	47.5@14.2	27.5@13.3	50.3@15.3	41.7@15.5
3.3	Center, Center, Nom ISO-2	On/no breasts	48.5@15.0	42.8@14.6	40.0@13.0	40.9@16.0	34.9@15.5
3.4	Center, Center, Nom ISO-2	On/no breasts	51.7@13.6	43.9@14.8	29.1@13.2	41.8@12.9	36.5@14.7
3.5	Center, Center, Nom ISO-2	Off	33.1@13.2	31.7@14.1	19.5@12.5	24.8@13.5	22.8@14.3
3.6	Center, Center, Nom ISO-2	Off	27.5@12.7	29.5@13.6	26.0@12.9	26.9@13.9	22.4@13.8
3.7	Center, Center, Chest on Module	On	NA	59.2@14.6	NA	NA	54.8@15.6
3.8	Center, Center, Chest on Module	On	74.1@14.3	58.6@14.6	39.1@14.1	59.4@15.0	47.6@14.7
3.9	Center, Center, Chest on Module	On	52.9@14.5	57.6@14.3	35.2@13.8	55.4@14.2	47.5@14.5
3.10	Center, Center, Chest on Module	On	59.4@15.6	59.4@14.9	NA	56.0@15.7	49.0@15.3
3.11	Up 4 cm, Center, Chest on Module	On	44.5@15.9	38.9@32.2	39.7@15.0	71.9@12.4	47.5@13.9
3.12	Up 4 cm, Center, Chest on Module	On	46.3@19.7	39.0@21.2	50.0@16.4	72.7@12.2	48.6@14.1
3.13	Center,Left 4 cm, Chest on Module	On	74.8@14.7	36.9@16.1	NA	51.3@15.4	35.8@15.2
3.14	Center,Left 4 cm, Chest on Module	On	38.3@14.0	24.7@15.1	NA	34.2@14.3	24.1@13.5
3.15	Center,Left 4 cm, Chest on Module	On	44.4@16.4	37.0@15.8	41.0@14.5	45.4@16.1	37.0@14.9
3.16	Center,Left 4 cm, Chest on Module	On	30.1@17.0	36.4@16.1	40.0@14.4	38.9@15.6	33.9@14.7
3.17	Up 2 cm, Center, Chest on Module	On	52.3@14.9	49.5@14.3	51.7@15.2	79.0@12.7	49.0@14.2
3.18	Up 2 cm, Center, Chest on Module	On	56.6@12.4	52.0@14.3	54.8@14.6	77.6@12.6	50.7@13.7
3.19	Up 2 cm, Center, Chest on Module	On	60.8@13.7	48.9@15.1	49.2@15.7	73.8@13.7	47.8@14.7

All of the sensors used for thoracic displacement, chestbands, CRUX units and accelerometers, were mounted at approximately the first and the sixth ribs in the dummy thorax.

These sternal displacements are shown in *Table 3.3.1.1*. For most tests with skin/with breasts (OOPS3.1-3.2, OOPS3.8, OOPS3.11-OOPS3.12, OOPS3.17, OOPS3.19); the upper chestband data shows much larger deflections than the crux or accelerometer data. This is attributable to thickness and compliance of the external breast forms. The tests with skin with no breasts (OOPS3.3, OOPS3.4) showed chestband deflection maximum values that were also higher than the crux or the accelerometer data. This is attributable to the deformation of the dummy skin.

The tests with no skin (OOPS3.5, OOPS3.6) show crux and chestband data that were consistent for upper sternal positions. In addition, the upper crux data is consistent for all groups of tests excepting the tests with air bag tears. All groups but one show a variation of less than a millisecond between peaks and a variation of less than 10% from high to low values. Where available, the upper sternum accelerometer data is at variance with the crux and chestband data. This is likely the effect of an accelerometer sensor failure in OOPS3.1-OOPS3.14. In those tests, the accelerometer showed substantial post-test offsets. This may invalidate integration of upper sternum accelerometer data for those tests.

The tests with the dummy thorax offset 4 cm left of the air bag module are very sensitive to details of the air bag deployment. In OOPS3.16, the exterior chestband shows smaller sternum deformation than the internal crux as the result of significant lateral deformation of the dummy ribs. Electrical noise in the first millisecond of deployment causes a sharp peak in upper chestband data, in OOPS3.5 and 3.6. As discussed above, similar electrical phenomena are seen frequently in load cell and MHD angular rate sensor channels using this air bag system.

The upper sternum crux deformation shows significant variation between tests in the center position and tests with the dummy thorax moved up 2 cm and 4 cm as shown in *Figure 13*. There is a 15% decrease in upper sternum deformation for a position 2 cm above center and a 33% decrease for a position 4 cm above center. In addition, there is over a 37% difference in dummy upper sternum deformation between the dummy in the center position and 4 cm to the left of center. Similar variations are seen in the chestband data, though variations are exacerbated by the non-biofidelic compliance in the dummy breasts.

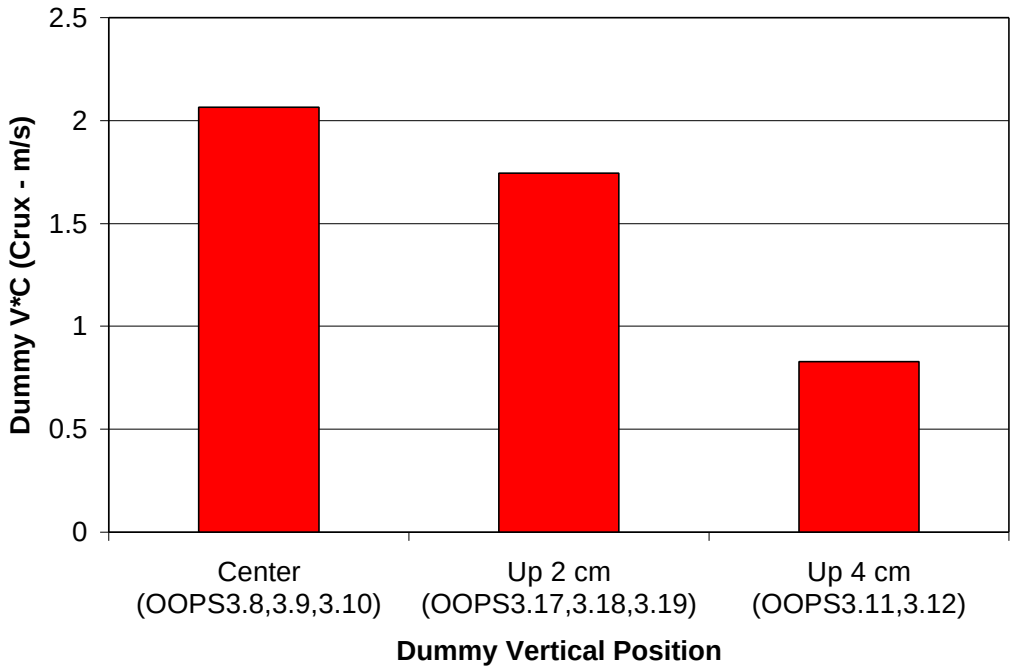

Figure 13: *Vertical Position Sensitivity of Upper Sternum Deflection*

3.3.1.1: CRUX PERFORMANCE

Two CRUX units were initially installed in the dummy used in this testing. However, the lower crux data in all tests was unrecoverable as the result of cross wiring in the original cabling and a malfunctioning (loose) potentiometer in the CRUX housing of the lower CRUX unit. The upper CRUX unit performed well, however, especially considering the limited volume available for its articulated arms in the 5th Percentile Female Hybrid III thorax. The upper CRUX unit measured displacements of nearly 60 mm without evidence of binding or bottoming. The upper CRUX unit demonstrated generally repeatable results as shown in both thorax displacements in *Table 3.3.1.1* and sternal V*C in *Table 3.3.2.1*. There was a maximum of 6% difference in thorax displacement in repeated tests. This variation was well within the expected 10% variation owing to manufacturing differences in the air bag inflators.

A comparison of the dynamic sternal deformations measured using the upper chestband and using the upper CRUX unit is shown in ***Figure 14*** and ***Figure 15*****.** In ***Figure 14***, the effect of the compliance of the dummy skin is apparent in the 'Nominal ISO-2' position (OOPS3.1). Since the chestband is an external thoracic measuring device and the CRUX unit measures internal rib deformation, the deformation of the chestband occurs earlier and with a greater slope than the deformation of the upper CRUX unit. This provides evidence that the difference between the chestband and the CRUX unit is the result of dynamic deformation of the skin. Thereafter, when the rib cage begins deformation, the slopes of the deformations of the chestband and the upper CRUX unit are similar. In addition, peak deformations in the chestband and the upper CRUX unit occur at similar times. Similarly, in ***Figure 15,*** the proximity of the air bag to the chest in the 'Chest on Module' position in OOPS3.8 results in a more rapid deformation of

the compliant dummy skin into the ribs. Again, the upper CRUX unit and the chestband show similar behavior and peak deformations. So, the upper CRUX unit demonstrated dynamic performance that is consistent with chestband measurements in tests where the chestband measurement accuracy is not compromised by conditions that do not affect the upper CRUX unit.

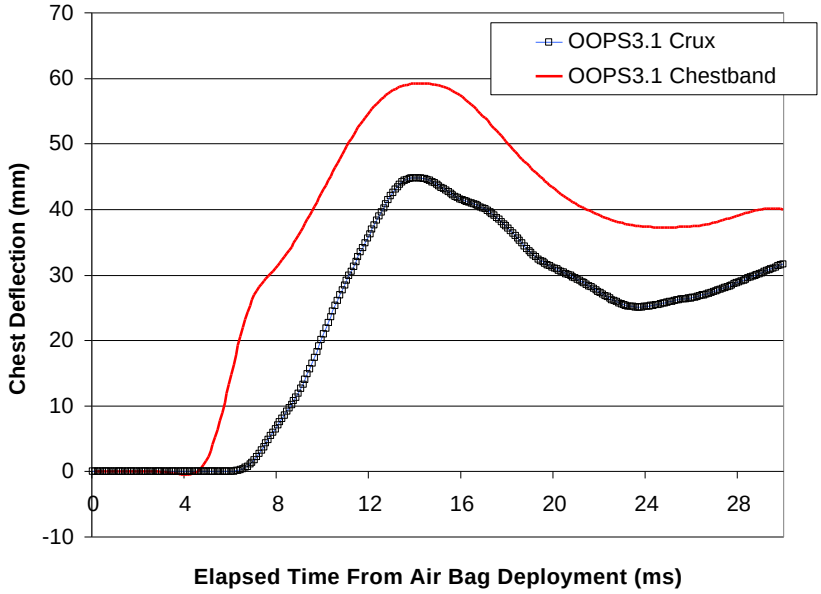

Figure 14: *CRUX Thoracic Deformation vs. Chestband Sternal Deformation – OOPS3.1 - 'Nominal ISO-2' Position*

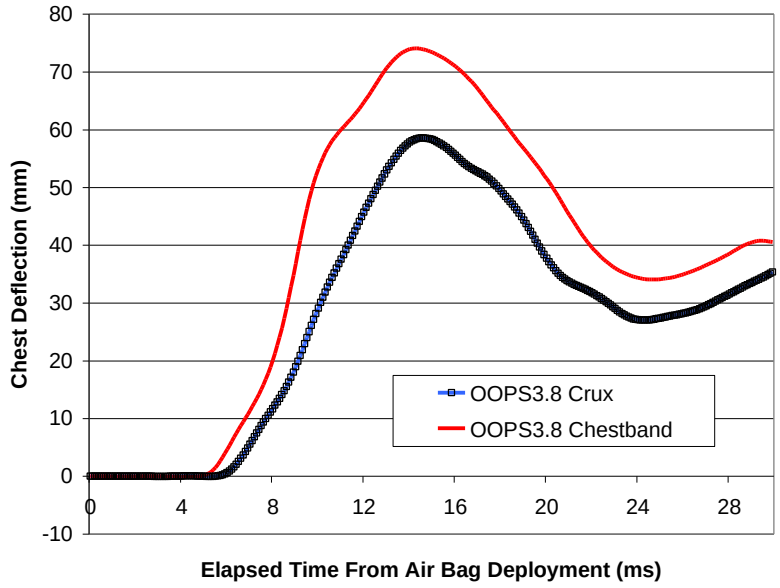

Figure 15: *CRUX Thoracic Deformation vs. Chestband Sternal Deformation – OOPS3.8 – 'Chest on Module' Position*

In addition to the CRUX unit sternal deformations in the local X direction discussed above, the CRUX units are capable of measuring deflections in the local Y and local Z directions at the attachment point. The maximum displacements in all translational axes measured using the upper CRUX unit are shown in Table 3.3.1.1.1. In the tests with the dummy centered on the air bag module (OOPS3.1-3.12, OOPS3.17-3.19), the local Y displacement measured by the upper CRUX unit is less than 6 mm. In contrast, the tests with the dummy offset to the left of the steering wheel (OOPS3.13-3.16) show significantly larger deformations of greater than 11 mm. The timing of the maximum displacement in Y is consistent for similar test conditions for all runs. These local Y deformations, as expected, are still far smaller than the X deformations for all tests.

The local Z deformation measured by the upper CRUX unit is consistent for all tests with dummy centered on the air bag module (OOPS3.1-OOPS3.10). In addition, the tests with the dummy sternum offset 4 cm to the left of the air bag module (OOPS3.13-OOPS3.16) and those with the dummy sternum offset 2 cm up the air bag (OOPS3.17-OOPS3.19) showed similar Z displacements owing to similar Z location of air bag contact with the dummy thorax except OOPS3.14. In OOPS3.14, a rupture of the air bag led to an anomalous deployment that affected the upper CRUX measurement. In contrast, the tests with the dummy sternum center offset 4 cm relative to the air bag showed much smaller displacements as a consequence of the substantially decreased interaction of the upper thorax with the deploying air bag.

TABLE 3.3.1.1.1: UPPER STERNUM CRUX DATA COMPARISON					
OOPS TEST	Position Vert., Horiz., Chest	Skin	Maximum Displacement (mm @ ms) ① Crux X	Crux Y	Crux Z.
3.1	Center, Center, Nom ISO-2	On	44.9@14.0	2.3@23.6	8.5@16.0
3.2	Center, Center, Nom ISO-2	On	47.5@13.9	-2.5@12.9	10.0@15.4
3.3	Center, Center, Nom ISO-2	On/no breasts	42.8@14.2	2.5@22.5	7.1@23.3
3.4	Center, Center, Nom ISO-2	On/no breasts	43.9@14.6	3.3@23.3	6.3@11.2
3.5	Center, Center, Nom ISO-2	Off	31.7@13.8	-4.2@14.4	10.3@22.6
3.6	Center, Center, Nom ISO-2	Off	29.5@13.6	-4.3@14.9	12.2@42.1
3.7	Center, Center, Chest on Module	On	59.2@14.6	5.0@18.2	11.2@14.4
3.8	Center, Center, Chest on Module	On	58.6@14.6	5.2@18.4	12.6@14.2
3.9	Center, Center, Chest on Module	On	57.6@14.3	3.9@18.3	11.6@13.4
3.10	Center, Center, Chest on Module	On	59.4@14.9	5.7@18.7	11.93@14
3.11	Up 4 cm, Center, Chest on Module	On	38.9@32.2	5.0@13.2	4.9@15.5
3.12	Up 4 cm, Center, Chest on Module	On	39.0@21.2	5.3@13.2	3.9@9.0
3.13	Center,Left 4 cm, Chest on Module	On	36.9@16.1	13.7@27.9	10.2@15.7
3.14	Center,Left 4 cm, Chest on Module	On	24.7@15.1	13.6@30.3	4.7@14.5
3.15	Center,Left 4 cm, Chest on Module	On	37.0@15.8	11.1@14.9	13.3@15.5
3.16	Center,Left 4 cm, Chest on Module	On	36.4@16.1	11.3@13.2	12.2@15.7
3.17	Up 2 cm, Center, Chest on Module	On	49.5@14.3	-3.4@12	11.7@17.1
3.18	Up 2 cm, Center, Chest on Module	On	52.0@14.3	-2.9@11.7	13.5@17.0
3.19	Up 2 cm, Center, Chest on Module	On	48.9@15.1	-3.4@12.8	9.8@30.2

NOTES:

① Frame of reference: X = Positive Inward at Sternum, Y = Positive to Dummy Right, Z = Positive Upward.

3.3.1.2: CHESTBAND PERFORMANCE

Two chestbands were used in all tests except OOPS3.7. Chestbands are designed to measure external thoracic contours. So, the response of the chestbands generally includes the compliance and stiffness of both the skin and the ribs. The CRUX units, in contrast, measure the local deformation of the internal ribs. So, the chestband deformations are expected to be generally larger than the crux deformations. Also, since the chestband contours are calculated using all the chestband gauge curvature information, the deformation contours are sensitive to the loss of chestband gauge and gauge distribution.

Generally, the chestbands performed repeatably among similar test conditions in this study as seen in ***Table 3.3.1.1***. Normalized by a chest deformation of 7.6 cm, the maximum sternal deformation taken from chestband contours shows approximately 1% variation among similar test conditions in OOPS3.1-3.2. There was approximately 4% difference between chestband maximum sternal deformations in OOPS3.3-OOPS3.4, and less than 5% variation among OOPS3.5-OOPS3.6. Further, there was less than 3% difference between chestband maximum sternal deformations in tests OOPS3.11 and OOPS3.12. Finally, there was approximately 11% variation in maximum sternal deformation inferred from chestbands among OOPS3.17-OOPS3.19.

However, maximum upper CRUX unit deformations were larger than chestband sternal deformations in tests OOPS3.6, OOPS3.9, and OOPS3.16. In addition, the maximum CRUX unit deformations in test OOPS3.10 was similar to that calculated from the chestband contours. For test OOPS3.6 with no dummy skin, the crux maximum sternal deformations are expected to be similar to the chestband deformations. There is less than 6% difference between the two measurements, normalized by upper CRUX unit maximum deformation. This is within the combined accuracy of the chestband and CRUX units. In addition, the upper crux was located approximately 20 mm from the centerline of the dummy sternum. The maximum sternal deformation calculated using the chestband in this region was 30.4 mm. This value is less than 4% different from the maximum sternal deformation measured by the upper crux.

In the centered ‘Chest on Module’ tests, OOPS3.9 and OOPS3.10, the upper chestband maximum sternal deformation seen in *Table 3.3.1.1* was commensurate with deformation measured by the upper CRUX unit though compliance in the dummy skin would suggest that the chestband deformations would be larger. However, during these tests chestband gauges were lost in regions of high curvature leaving gaps that significantly decrease the accuracy of the sternum position.

In the off-center test, OOPS3.16, there was evidence of the upper chestband sliding with the skin. The calculated chestband contour deflected sharply at the lateral chest and bulged near the sternum at the time of maximum deformation measured by the upper CRUX unit. This apparent sliding made the chestband sternal calculations unreliable as the computed position of the sternum may not maintain a fixed relationship with the physical sternum.

So, the chestband measurements were generally repeatable within known caveats in the use of chestbands as a contour measuring device. Among these are loss of accuracy with loss of chestband gauges in regions of high local curvature and the potential for compliance of overlying tissue to complicate the interpretation of chestband measurements when used for underlying rib structure.

3.3.2: DYNAMIC CHEST V*C DATA

TABLE 3.3.2.1: CHEST V*C DATA

OOPS	Position	Upper Sternum V*C (m/s @ ms)			Lower Sternum V*C (m/s @ ms)	
TEST	Vert., Horiz.	Chestband	Crux	Accel.	Chestband	Accel.
3.1	Center, Center	1.3@10.7	1.36@12.4	0.50@11.4	0.8@9.9	0.77@11.8
3.2	Center, Center	1.1@9.0	1.67@11.8	0.49@10.4	1.0@13.0	0.98@11.8
3.3	Center, Center	1.0@8.7	1.11@12.2	0.91@10.8	0.8@8.9	0.68@11.1
3.4	Center, Center	1.3@9.9	1.08@12.2	0.56@10.6	0.9@9.0	0.81@11.2
3.5	Center, Center	1.3@5.9	0.62@12.1	0.29@10.1	0.4@7.5	0.32@10.8
3.6	Center, Center	1.2@5.7	0.58@9.9	0.47@10.2	1.0@7.3	0.31@10.9
3.7	Center, Center	NA	2.01@12.1	2.9@12.4	NA	1.76@11.9
3.8	Center, Center	3.5@9.3	1.96@11.9	1.02@11.5	2.4@10.6	1.5@11.9
3.9	Center, Center	2.7@8.6	2.03@11.8	0.8@11.1	1.6@12.0	1.47@11.5
3.10	Center, Center	1.8@8.9	2.20@13.4	NA	2.1@13.1	1.49@12.6
3.11	Up 4 cm, Center	1.3@11.1	0.82@12.2	0.83@11.8	4.1@11.2	1.51@11.1
3.12	Up 4 cm, Center	1.9@12.7	0.84@12.4	1.2@11.9	4.6@10.8	1.52@11.1
3.13	Center,Left 4 cm	3.3@11.5	0.69@10.5	NA	1.2@11.8	0.75@11.2
3.14	Center,Left 4 cm	1.0@9.9	0.54@10.4	NA	0.7@10.8	0.45@10.6
3.15	Center,Left 4 cm	1.5@8.1	0.65@10.1	0.98@11.0	1.7@9.4	0.82@11.2
3.16	Center,Left 4 cm	0.7@8.1	0.67@10.3	0.95@11.1	1.5@14.2	0.71@11.4
3.17	Up 2 cm, Center	1.5@11.1	1.77@12.4	1.38@11.5	5.2@10.9	1.58@11.1
3.18	Up 2 cm, Center	1.8@11.0	1.92@12.0	1.62@11.4	4.6@10.9	1.76@10.8
3.19	Up 2 cm, Center	2.4@12.3	1.54@13.3	1.22@11.7	3.8@11.5	1.47@11.6

There is a significant variation between V*C calculated using crux data and chestband data owing to the compliance of the dummy skin. However, upper crux V*C data shows very good repeatability within test conditions. The variation in V*C among test conditions is shown in *Figure 16*. The variation is substantial, with over 15% variation from the center position to 2 cm up and over 60% variation in upper sternum V*C from the center position to 4 cm up.

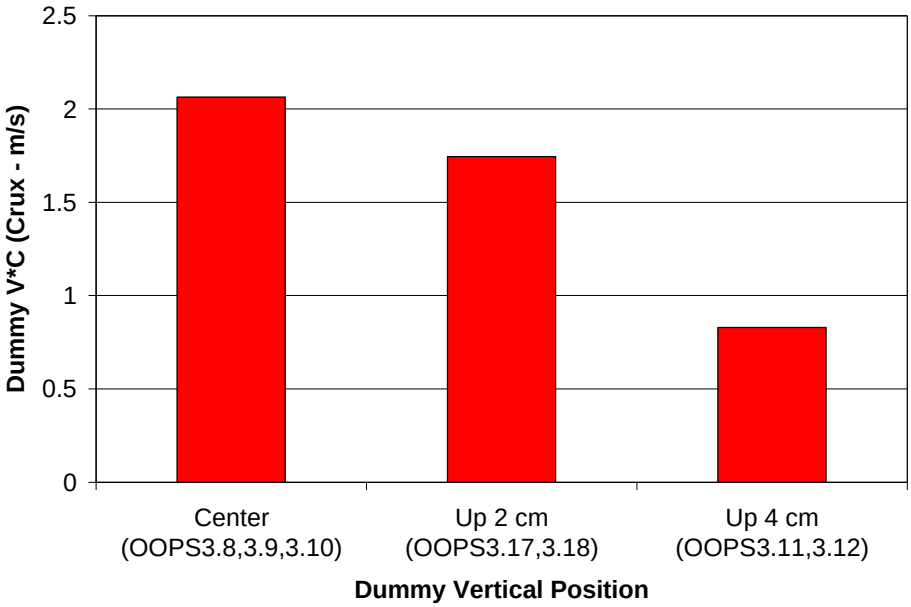

Figure 16: *Vertical Position Sensitivity of V*C*

3.4: PHOTOGRAPHIC RESULTS

Motion analysis was performed on the high-speed motion picture images of the tests, as recorded by the offboard driver's side film camera. The motions of the photo targets on the occupant's head center, shoulder, elbow, and hip, as well as the head rear and upper spine external MHD angular rate sensors, were tracked relative to the test fixture, as described in Appendix I.7.

Analysis of the high-speed motion pictures identified several qualitative and quantitative differences between the air bag deployments under different conditions. A generic deployment begins with airbag squib activation. After activation, the air bag was first observed breaking through the seam of the module at approximately 4 ms.

During deployments with the dummy sternum centered on the air bag module (OOPS3.1-3.10), the air bag expanded into the occupant's chest until contacting the dummy chin at approximately 13 ms, and the occupant pelvis at 18 ms. The dummy thorax began rotating at approximately 12 ms. The dummy head began rotating downward at approximately 17 ms, and began translating rearward at approximately 24 ms. The dummy continued a rotational motion essentially centered at the pelvis for the rest of the air bag deployment. Owing to the proximity of the dummy thorax and the air bag module, the air bag was forced away from the occupant through the upper opening of the steering wheel (the space between the air bag module and the upper steering wheel rim) between approximately 14 and 75 ms. In OOPS3.7-3.10, a portion of the air bag does not escape the upper rim of the steering wheel before 100 ms after air bag initiation. Viewed from the top, the air bag symmetrically deploys outside the shoulders at approximately 17 ms.

For the air bag deployments with the occupant sternum center moved upward relative to the steering wheel (OOPS3.11-3.12, OOPS17-OOPS3.19), the air bag deploys towards the

dummy abdomen and initially proceeds downward. The air bag reaches the pelvis at approximately 15 ms and reaches the chin at approximately 25 ms, later than that seen in the centered tests. Thorax rotation occurs at approximately 13 ms. Head rotation downward occurs at approximately 15 ms with head motion rearward at approximately 25 ms. This behavior is similar to that seen in the centered tests. These tests, however, have qualitatively more pelvis translation than those with the sternum centered on the air bag module as the result of lower center of pressure of air bag contact. From the top, the air bag deploys symmetrically as in the centered tests.

For the air bag deployments with the occupant sternum center moved laterally relative to the steering wheel (OOPS3.13-OOPS3.16), we see a substantially different deployment. The air bag begins deploying to the right of the dummy at approximately 8 ms. Subsequently, the air bag deploys toward the occupant chin and into the upper right side steering wheel opening at approximately 12 ms. By 18 ms, the air bag is deployed only to the right of the dummy centerline. The succeeding deployment moves the dummy thorax to the left, while the head rotates towards the right as the result of steering wheel deformation. After approximately 50 ms, the occupant head begins rotation to the left under the influence of the air bag deployment. The air bag fully inflates at approximately 60 ms with the dummy moved to the dummy left.

Differences in occupant loading and kinematics can be attributed to the differences in deployment patterns between occupant positions.

3.5: SENSOR AND TEST FAILURES

For the test series, there were several tests with generic multiple sensor failures of load cell sensors and magnetohydrodynamic angular rate sensors. These were initially attributed to local static discharge resulting from inadequate grounding of the sensors and data acquisition system. Before the test series, the dummy head, spine box, front of the ribs, and sternum were individually grounded. In addition, the main body of each section of the test fixture was grounded, as was a mesh shielding vest around the dummy thorax. In succeeding tests, the bolt connecting the airbag to the steering wheel and individual sections of the test fixture were grounded. These ground wires were connected to the electrical service ground. In a later test series (see OOPS4 Test Report), these ground wires were connected to a local ground rod installed less than 20 feet from the test fixture. In several tests, liquid “Static Guard” was sprayed on the occupant thorax. None of these steps recommended by the load cell manufacturer were successful in completely eliminating noise and spikes in sensor channels. After the OOPS4 test series, additional investigation of the airbag squib firing circuit indicated that unintended oscillations might have occurred in the circuit output that might have been dynamically transmitted into the sensors though the system ground. Subsequently, the circuit was redesigned as a capacitive discharge device to avoid such behavior. This new airbag squib firing circuit was tested using an out-of-position test similar to those of the OOPS3 series and no further problems were seen. These problems and the subsequent solution are detailed in ASL document *Noise Spike Interference in OOPS Test Data*.

Of these generic failures, severe failures occurred in load cell and MHD channels in OOPS3.8 and OOPS3.17. Multiple spikes in numerous load cell channels characterized these severe failures. Isolated spikes in multiple channels occurred in OOPS3.10, OOPS3.12, OOPS3.13, OOPS3.14, and OOPS3.18. These isolated spikes occurred during air bag deployment at approximately 9 ms. These electrical phenomena occurred in both the dummy

load cells and the steering column load cell. In addition, channels 2 and 3 of the dummy magnetohydrodynamic angular rate sensors were often affected. These phenomena occurred at the same time in all affected channels and is not likely the result of a failure in the data acquisition system. These failures did not apparently affect the subsequent operating order of the sensors involved. Also, these failures did not generally affect accelerometers, CRUX units or chestband sensors.

In addition, the upper sternum accelerometer suffered post-test offsets of up to 100 g's after OOPS3.7-3.14, and sternum accelerometers clipped briefly in OOPS3.5. Chestband gauge failures occurred in chestband sensor CB125.22 and CB125.33 in test OOPS3.1. In addition to these failures, the sudden loading of the chest by the air bag caused the sternum slider to dislodge from the slot on the sternum in the initial dummy test. As this was noted in previous out-of-position tests, the sternum slider was not used in subsequent tests. In test OOPS3.7, the dummy thigh was scarred from contact with the steering wheel fixture. In OOPS3.11, the air bag break sensor failed and chestband channel CB133.25 failed. The chestband sensor CB133.18 clipped during tests OOPS3.12 and OOPS3.14. In addition, chestband sensors CB125.4, and CB125.19 failed during test OOPS3.15.

Air bag tears were seen during OOPS3.13, and OOPS3.14, tests in which the occupant was displaced 4 cm left of the center position. These were small tears, approximately 3 cm in diameter. There were three in OOPS3.13 and one in OOPS3.14. The effects of these tears are seen in decreased occupant response when compared to tests without such tears, implying a decrease in air bag forcing of the occupant thorax. No tears were seen in subsequent tests OOPS3.15 and OOPS3.16 in the same position.

3.6: DISCUSSION OF RESULTS

This section presents the results of several substudies including the effect of skin and distance from module in Section 3.6.1. This substudy also investigates the effect of chestbands on thoracic response. Vertical and horizontal position sensitivity are discussed in Section 3.6.2. Tests were performed with the occupant 2 cm and 4 cm vertically up from the center of the dummy sternum, and 2 cm left of the dummy sternum. Finally, the dummy response seen in the current OOPS tests is compared with dummy response in previous tests performed at ASL in Section 3.6.3.

3.6.1: SKIN/DISTANCE FROM MODULE STUDY

As the result of the consistent "Nominal ISO-2" positioning, the study of skin conditions effectively became a study of the effect of distance from the thorax to the air bag module. In the "Nominal ISO-2" condition, the dummy skin with breasts rested on the module with the breasts undeformed. Maintaining the same chin and spine positions meant that the dummy thorax effectively moved away from the air bag module when the breasts were removed from the 5th Percentile Female Hybrid III skin. The effective distance from module to thorax was further increased in the tests with no dummy skin. Effective skin thickness for the conditions tested are shown below. The distance to the air bag module is defined as zero for the skin with breasts deformed by the air bag module ("Skin on Module" case). It was further observed that the compliance of the dummy breasts is significantly variable among dummy skins, as the breasts are simply conical forms glued onto the dummy skin. Two dummy skins with breasts were available for examination. The four individual breasts have qualitatively different stiffnesses.

TABLE 3.6.1.1: EFFECTIVE DISTANCE FROM AIR BAG MODULE		
Skin	**Skin Thickness (mm)**	**Effective Distance from Module (mm)**
Skin with breasts – Nominal ISO-2 (undeformed)	53	18
Skin with breasts – Chest on Module (deformed by module)	35	0
Skin without breasts – Nominal ISO-2	24	29
No Skin – Nominal ISO-2	0	53

The variation of peak chest resultant acceleration with effective distance from the air bag module is shown in *Figure 17*. There is over a 60% decrease in peak acceleration as the effective distance from the air bag module increases from zero (skin with breasts – Chest on Module) to 53 mm (no skin – Nominal ISO-2). The variation in peak chest CG resultant is approximately exponential in effective thorax distance to air bag module. Similar results are seen in the dummy sensor time histories. As an example, the upper sternum acceleration time histories for the four cases are plotted in *Figure 18*. They are qualitatively similar for all cases. However, the acceleration peaks are largest for the skin with breasts in the "Chest on Module" position, with the thorax effectively closer to the module.

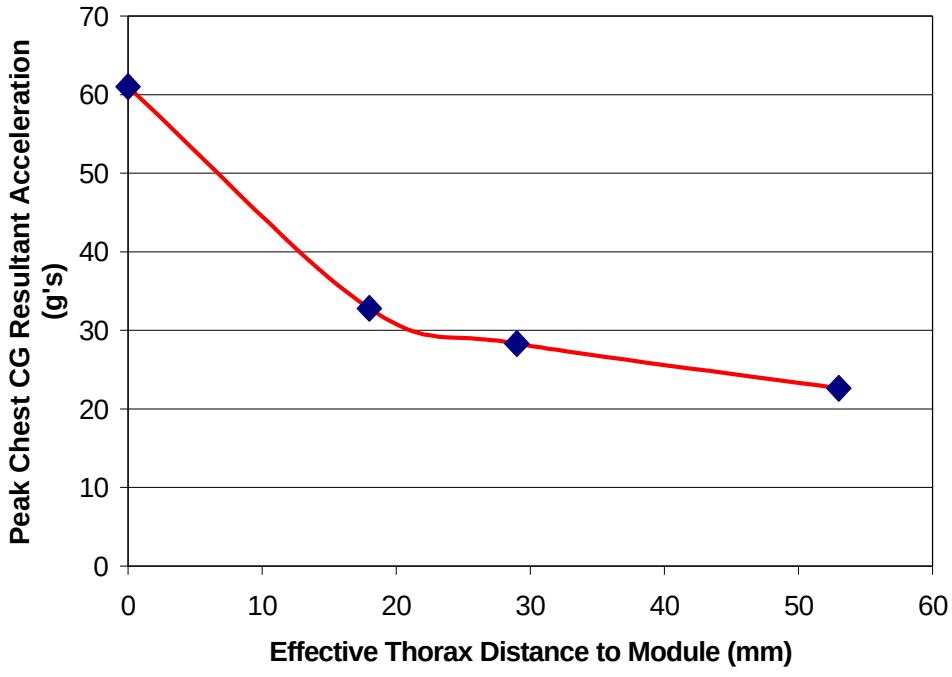

***Figure 17**: Peak Chest CG Resultant vs. Effective Distance from Sternum to Module*

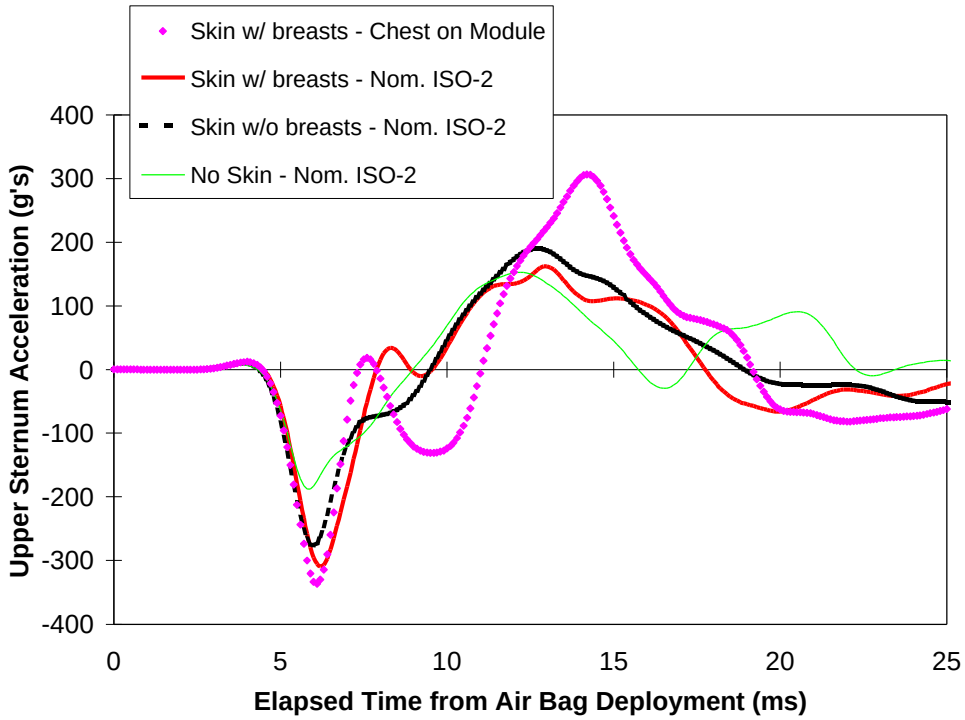

Figure 18: *Time History of Upper Sternal Accelerometer - Different Skin Conditions*

3.6.2: POSITIONING STUDY

The chest accelerometer data shows substantial differences in response when the occupant is moved 4 cm up or 4 cm to the left as shown in *Figure 19*. An intermediate level of response is seen in the 2 cm up case. It is clear the chest center-of-gravity acceleration resultant peaks group well within a test condition, and that OOPS3.13 and OOPS3.14 did not inflate properly owing to the air bag tears. Differences in peak chest center-of-gravity acceleration from the tests in the center position to the tests with the dummy offset 4 cm left are substantial, nearly 50% in peak acceleration.

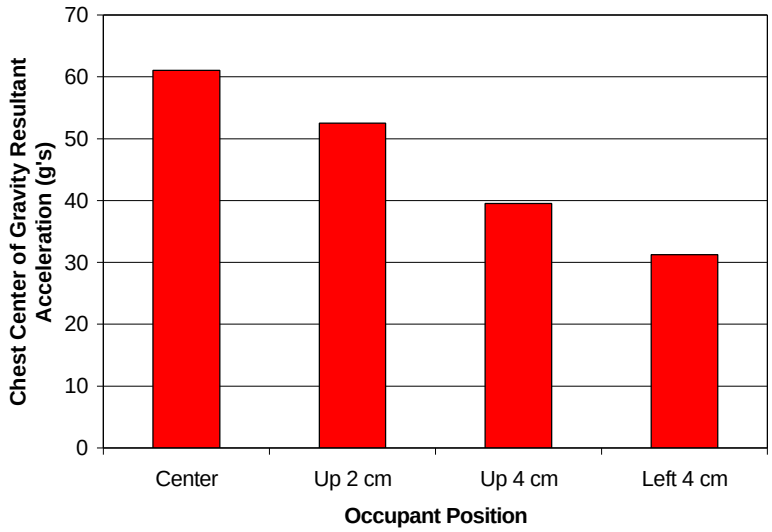

Figure 19: *Acceleration Response Position Sensitivity*

Typical sensitivity of chest CG resultant for tests under the same conditions is graphed in *Figure 20*. For the dummy thorax positioned 4 cm up from the center position, the two available time histories show qualitatively and quantitatively similar behavior with a variation of less than 4% in peak acceleration. This is well within the expected air bag deployment variation of 10% as suggested by the manufacturer.

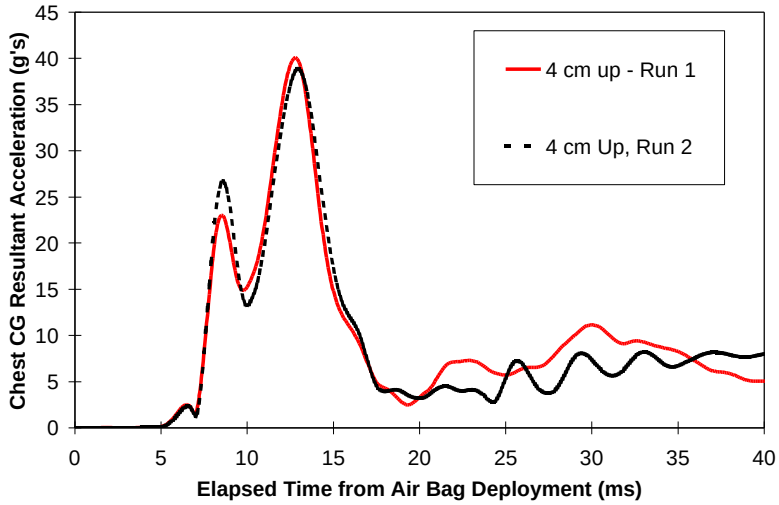

Figure 20*: Chest CG Resultant Acceleration Sensitivity to Repeated Tests*

Position behavior similar to the chest center-of-gravity peak acceleration is seen in the thoracic viscous response. As shown in *Figure 21*, the chest V*C decreases 13% at 2 cm up from the dummy sternum centered on the airbag module. In addition, the chest V*C decreases 61% at 4 cm up, and 69% at 4 cm left.

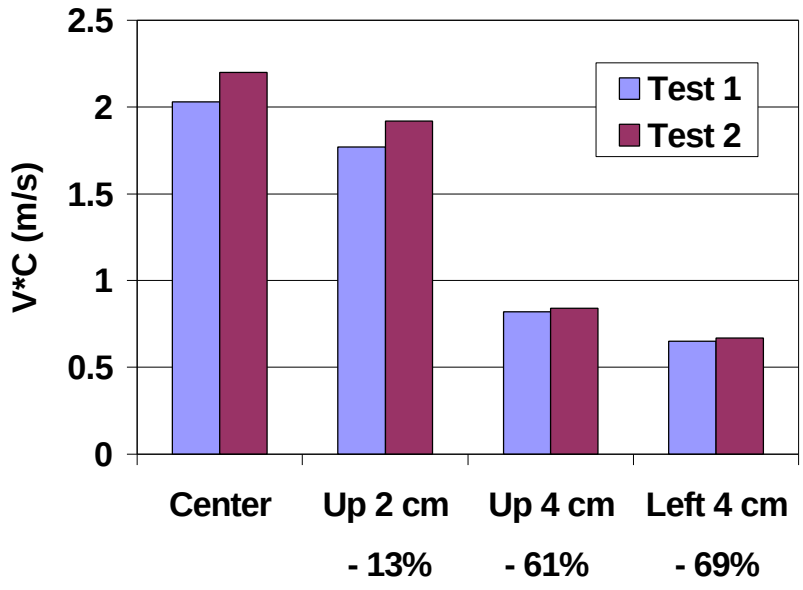

Figure 21: *Position Sensitivity of V*C for Repeated Tests*

As seen in the chest acceleration and V*C peaks, chest center-of-gravity resultant acceleration time history shows quantitatively different peaks while showing qualitatively similar behavior. In *Figure 22*, the peaks vary over 30% while the timing of the peaks varies less than 3 ms. The initial peak in the 4 cm up case is exacerbated by enhanced initial acceleration caused by details of the air bag/thorax interaction in that position. In the 4 cm up case, the air bag deploys into the lower thorax/abdominal region of the dummy compared with the upper thorax in the centered case. This allows the air bag room for earlier deployment and forces the top of the steering wheel into the upper thorax at approximately 8 ms, causing the early peak.

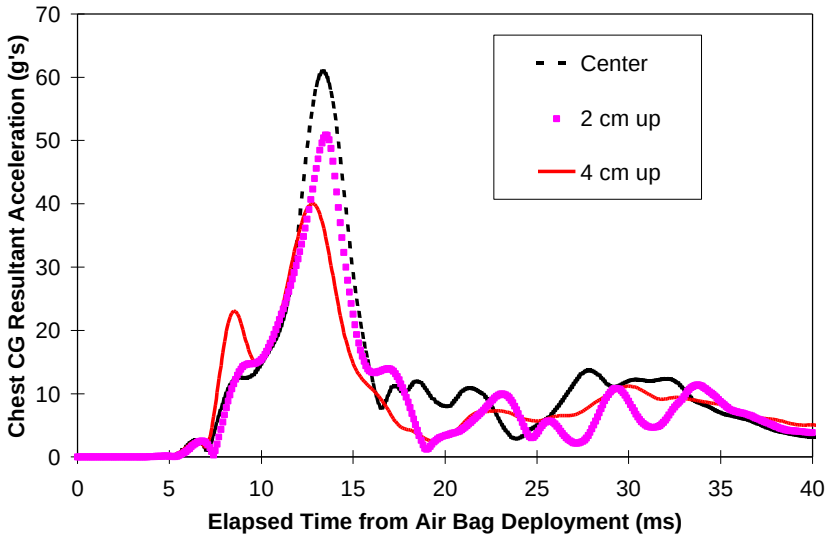

Figure 22: *Chest CG Resultant Acceleration Vertical Position Sensitivity*

3.6.3: COMPARISON WITH PREVIOUS ISO-2 TESTS AT ASL

Shown in *Table 3.6.3.1* below are several representative out-of-position occupant tests from the current test series and previous out-of-position test series with a 5th Percentile Female Hybrid III dummy. All tests were performed using an out-of-vehicle positioning fixture with the dummy sternum centered on the air bag module center.

The air bags used range from the relatively aggressive 1991 Mercury Grand Marquis air bag to the relatively nonaggressive 1992 Honda Accord air bag. The response of the dummy under the depowered 1998 Ford Taurus in the Nominal ISO-2 position was qualitatively similar in most respects to the dummy response found in previous tests under 1992 Honda Accord air bag deployment. The two tests had similar levels of upper sternum deflection measured using the chestbands, and similar levels of thoracic viscous response. Differences between the lower sternum deflection and the upper spine acceleration resultant of OOPS3.1 using the depowered 1998 Ford Taurus airbag and ATD.47A.381 using the 1992 Honda Accord air bag suggest that the Honda air bag deployed generally higher on the occupant than the Taurus air bag. This result was confirmed by video analysis.

In contrast, the 1991 Mercury Grand Marquis showed much greater levels of lower sternum deflection as the result of both greater inflator gas generation and a very low module tear seam. In addition, the upper spine resultant acceleration for the Grand Marquis air bag was over four times that seen with either the Taurus or the Accord air bags, suggesting that the Grand Marquis air bag is a substantially more aggressive air bag.

It is interesting to note again that there is a significant increase in occupant viscous response between the Nominal ISO-2 position in OOPS3.1 and the Chest On Module position in OOPS3.8. This difference in response results from the dummy sternum in the Chest on Module position being approximately 18 mm closer to the center of the steering wheel than in the Nominal ISO-2 position as discussed above. This suggests that substantial increases in the occupant response from Grand Marquis air bag deployment may be seen with the occupant forced against the steering wheel module in the Chest On Module position.

TABLE 3.6.3.1: OOPS TEST COMPARISON

Parameter	Oops3.8	Oops3.1	ATD.47A.381	ATD.47C.383
Air Bag	1998 Ford Taurus	1998 Ford Taurus	1992 Honda Accord	1991 Mercury Grand Marquis
Occupant Position	Chest On Module	Nominal ISO-2	Nominal ISO-2	Nominal ISO-2
Maximum Steering Column Axial Load (N @ ms)	9815 @ 10.0	6716 @ 9.2	7470 @ 9.5	12,100 @ 10.0
Maximum Upper Spine Acceleration Resultant (g @ ms)	60.8 @ 13.3	32.0 @ 13.1	50.6 @ 13.9	228 @ 12.4
Maximum Sternum Deflection – Upper Chestband (mm @ ms)	74.1 @ 14.3	59.3 @ 14.2	68.0 @ 16.0	65.0 @ 16.6
Maximum Sternum Deflection – Lower Chestband (mm @ ms)	59.4@ 15.0	43.5 @ 15.3	44.0 @ 17.4	106.0 @ 12.6
Maximum V*C – Upper Sternum (m/s @ ms)	3.5 @ 9.3	1.3 @ 10.7	1.8 @ 10.7	1.9 @ 15.3
Maximum V*C – Lower Sternum (m/s @ ms)	2.4 @ 10.6	0.8 @ 9.9	0.7 @ 13.0	7.8 @ 9.7
Tank Peak Pressure (60 Liter tank @ 21 C – kPa)	142	142	151	185
Tank Peak Pressure Rise (60 Liter tank – @ 21 C - kPa)	4.7	4.7	5.0	10.6

4: CONCLUSIONS

An out-of-vehicle occupant fixture for out-of-position tests was developed that allows accurate positioning – within 0.5 cm in all axes for fixed structural points on the dummy. This fixture permits the detailed investigation of the effect of positioning on out-of-position occupants under air bag deployment into the occupant thorax. Positioning repeatability was within the dimensional variation of approximately 1 cm between the spines of two 5th Percentile Female dummies available for testing at ASL. The dummy used in this study was received by ASL in July of 1996. Since that time, the dummy has undergone a number of revisions which may influence the results and conclusions presented in this report.

As expected, head and neck injury tolerance values were not generally exceeded for this testing as the ISO-2 position involves predominantly air bag/thorax interactions. In addition, though the current study used a depowered air bag from the current automobile fleet, the use of a worst-case positioning (Chest on Module position) resulted in sternal deflection, chest CG acceleration, and viscous criterion values that generally exceeded accepted and proposed injury tolerances.

The thoracic response under out-of-position air bag deployment was not found to be sensitive to the presence of chestbands used to measure thoracic contours. Upper sternal displacement varied less than 1% between tests with chestbands off and chestbands on the dummy. Peak chest CG resultant acceleration varied approximately 10% among the tests. In addition, two CRUX units were installed within the 5th Percentile Female Hybrid III dummy to measure upper and lower thoracic deformations. Though the lower CRUX unit malfunctioned, the upper CRUX performed well giving repeatable and accurate results that compared well with other thoracic instrumentation.

Sensitivity to distance from the air bag module was found to be substantial. There was over a 60% decrease in peak acceleration as the effective distance from the air bag module increases from zero (skin with breasts – Chest on Module) to 53 mm (no skin – Nominal ISO-2). The variation in peak chest CG resultant was approximately exponential in effective thorax distance to air bag module. Similar results were seen in the dummy sensor time histories. It was further observed that the compliance of the dummy breasts was significantly variable among dummy skins, as the breasts are simply conical forms glued onto the dummy skin. Two dummy skins with breasts were available for examination. The four individual breasts had qualitatively different stiffnesses.

Also, a large variation in occupant response was found when moving a 5th Percentile Female Hybrid III dummy thorax from a center position to +2 and +4 cm up the steering wheel. Variation in response of up to 30% was seen in chest CG acceleration. In addition, there was a variation of up to 34% in upper sternum deflection between the three positions and up to 60% variation in upper sternal V*C among the positions tested.

Additional testing was performed with the occupant thorax centered vertically while offset 4 cm horizontally to the left of center. This occupant position resulted in a qualitatively different deployment of the air bag. In this deployment, the air bag opened asymmetrically to the right of the occupant producing large differences in occupant response relative to a centered occupant. Over 30% variation in peak chest CG resultant acceleration was seen. Also, there was over 35% difference in upper sternum deflection between the two cases and nearly 70% difference in upper sternal V*C.

This large variation in occupant response for small differences in position may have implications for sled and vehicle testing of out-of-position occupants. Variations of +/-2 cm in occupant center-of-gravity position are common in occupant positioning in sled testing at ASL. This is likely also the case for any positioning not using a dedicated positioning fixture.

In addition, use of different interpretations of 'ISO-2' positioning may cause large variations in occupant response under air bag deployment as a nearly 50% reduction in peak chest CG resultant acceleration is seen from positioning with dummy breasts deformed against the module to positioning with dummy breasts touching the module. This variation may be exacerbated by significant qualitative differences in the compliance of breast forms for the 5th Percentile Female Hybrid III dummy.

DESCRIPTIONS AND PROCEDURES MANUAL

An Appendix to Reports

prepared

FEBRUARY 1997

for

National Highway Traffic Safety Administration

Cooperative Agreement No. DTNH22-93-Y-07028

by

Automobile Safety Laboratory
of the
University of Virginia

Principal Investigator
Walter D. Pilkey
Morse Professor of Engineering

February 1, 1997

Table of Contents

APPENDIX A: STANDARDS AND CONVENTIONS 4

A.1: STANDARDS USED 4
A.2: SIGN (POLARITY) CONVENTIONS 5
A.2.1: VEHICLE AND OCCUPANT 5
A.2.2: KNEE BOLSTER SIMULATOR 6
A.2.3: OTHER RELEVANT DIAGRAMS 7

APPENDIX B: REFERENCES 10

APPENDIX C: MECHANICAL EQUIPMENT DESCRIPTIONS 12

C.1: CRASH SIMULATOR 12
C.1.1: SLED 12
C.1.2: DECELERATOR 12
C.2: TEST FIXTURE 13
C.3: SEAT 13
C.4: STEERING COLUMN 14
C.5: INTRUSION SIMULATOR 14
C.6: KNEE BOLSTER SIMULATOR 14
C.7: CARDIOVASCULAR AND PULMONARY PRESSURIZATION DEVICE 15
C.8: FORCE-LIMITING SEAT BELT RETRACTOR 15

APPENDIX D: PHOTOGRAPHY 16

D.1: HIGH SPEED MOTION PICTURE PHOTOGRAPHY 16
D.1.1: CAMERAS AND VIEWS 16
D.1.2: HIGH SPEED VIDEO 16
D.1.3: STROBES 16
D.1.4: TIMING MARKS 16
D.1.5: LIGHTS 17
D.2: STILL PHOTOGRAPHY 17

APPENDIX E: DATA ACQUISITION SYSTEM DESCRIPTIONS 18

E.1: SYSTEM 18
E.1.1: SYSTEM HARDWARE 18
E.1.2: DATA ACQUISITION SYSTEM HARDWARE SUMMARY 18
E.1.3: TRIGGER CIRCUIT 19
E.1.4: SYSTEM VERIFICATION 19
E.2: SOFTWARE 19
E.2.1: IMPAX 19
E.2.2: OTHER SOFTWARE 20

APPENDIX F: INSTRUMENTATION DESCRIPTIONS 21

F.1: GENERAL 21
F.2: DESCRIPTIONS OF SENSOR TYPES 21
F.3: VERIFICATION OF SENSORS 22
F.3.1: PRE-TEST 22
F.3.2: PRE-LAUNCH 22
F.4: CRASH SIMULATOR VELOCITY MEASUREMENT SYSTEM 23

APPENDIX G: CADAVER HANDLING AND PREPARATION 24

G.1: CADAVER ACCEPTANCE CRITERIA 24
G.2: CADAVER HANDLING PROTOCOLS 24
G.3: INFECTIOUS DISEASE SCREENING PROCEDURES 24

G.4: PRESERVATION PROCEDURES 25
G.4.1: EMBALMING PROCEDURES AND FLUIDS 25
G.4.2: REFRIGERATED STORAGE 26
G.4.3: FREEZING AND THAWING PROCEDURES 26
G.5: ANTHROPOMETRY PROCEDURES 26
G.6: IDENTIFICATION OF INSTRUMENTATION MOUNTING SITES 27
G.6.1: ACCELEROMETER MOUNTING SITES 27
G.6.2 STRAIN GAUGE MOUNTING SITE 29
G.7: PRE-TEST X-RAY PROCEDURES 29
G.8: INSTRUMENTATION MOUNTING PROCEDURES 30
G.8.1: ACCELEROMETERS 30
G.8.2: TIBIAL LOAD CELLS 32
G.8.2.1 : HUMERUS LOAD CELLS 33
G.8.3: MAGNETOHYDRODYNAMIC ANGULAR RATE SENSORS (MHD'S) 34
G.8.4: LIGAMENT STRAIN TRANSDUCERS 35
G.8.5 STAIN GAUGE APPLICATION 35
G.9: PRESSURIZATION PREPARATION 36
G.10: POST-TEST X-RAY 36
G.11: POST-TEST NECROPSY PROCEDURES 37
G.11.1: AUTOPSY PREPARATION 37
G.11.2 : AUTOPSY PROCEDURES 37
G.11.3: RIB FRACTURE DOCUMENTATION 38
G.11.4: LOWER EXTREMITY DISSECTION 38
G.12: EVALUATION OF SKELETAL QUALITY TEST PROCEDURES 39
G.12.1: RIB TESTING 39

APPENDIX H: PROCEDURES 40

H.1: OCCUPANT POSITIONING PROCEDURE 40
H.2: ANGULAR RATE SENSOR INITIAL POSITION MEASUREMENT PROCEDURE 41
H.3: CHESTBAND INSTALLATION AND VERIFICATION PROCEDURE 41
H.4: CARDIOVASCULAR AND PULMONARY PRESSURIZATION PROCEDURE 42
H.5: RESTRAINT BELT SPOOL-OUT MEASUREMENT PROCEDURE 42

APPENDIX I: DATA PROCESSING PROCEDURES 44

I.1: SENSOR DATA POST-PROCESSING 44
I.2: DATA TAPE GENERATION 44
I.3: GENERATION OF RESULTANTS 44
I.4: INERTIAL COMPENSATION OF LOAD CELL DATA 44
I.5: FOOTPLATE DATA PROCESSING 45
I.6: ANKLE ROTATION DATA PROCESSING 45
1.7 ELBOW FLEXION DATA PROCESSING 45
1.7.1 NECK FLEXION DATA PROCESSING 46
I.8: HEAD CENTER OF GRAVITY ACCELERATION CALCULATION 46
1.9: HIGH SPEED MOTION PICTURE ANALYSIS 47
I.10: DATA PLOTTING 47
I.11 STRAIN GAUGE PROCESSING 48

Appendix A: Standards and Conventions

A.1: Standards Used

A.1.1: "Dummy Positioning Procedures for Test Dummy Conforming to Subpart E of Part 572", in Appendix VIII of *Laboratory Indicant Test Procedure, New Car Assessment Program (NCAP)*, National Highway Traffic Safety Administration (NHTSA), Jan. 1, 1990.

A.1.2: "Instrumentation for Impact Test - SAE Recommended Practice SAE J211 JUN88", in *SAE Handbook*, Volume 4: On-Highway Vehicles and Off-Highway Machinery, Society of Automotive Engineers, June 1989.

A.1.3: Section 571.208 Standard No. 208; Occupant Crash Protection, in Volume 49 of *Code of Federal Regulations*, U.S. Government Printing Office, 1991.

A.1.4: "Road Vehicles - Test Procedures for Evaluating Out-of-Position Vehicle/Occupant Interactions with Deploying Airbags," Draft Document ISO DTR 10982, *International Standards Organization, November 21, 1995.*

A.2: Sign (Polarity) Conventions

A.2.1: Vehicle and Occupant

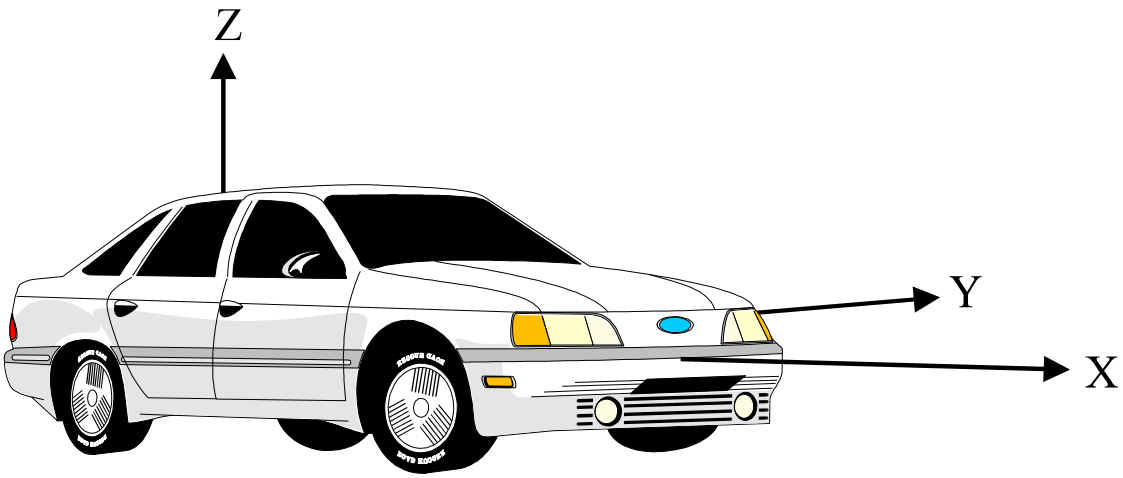

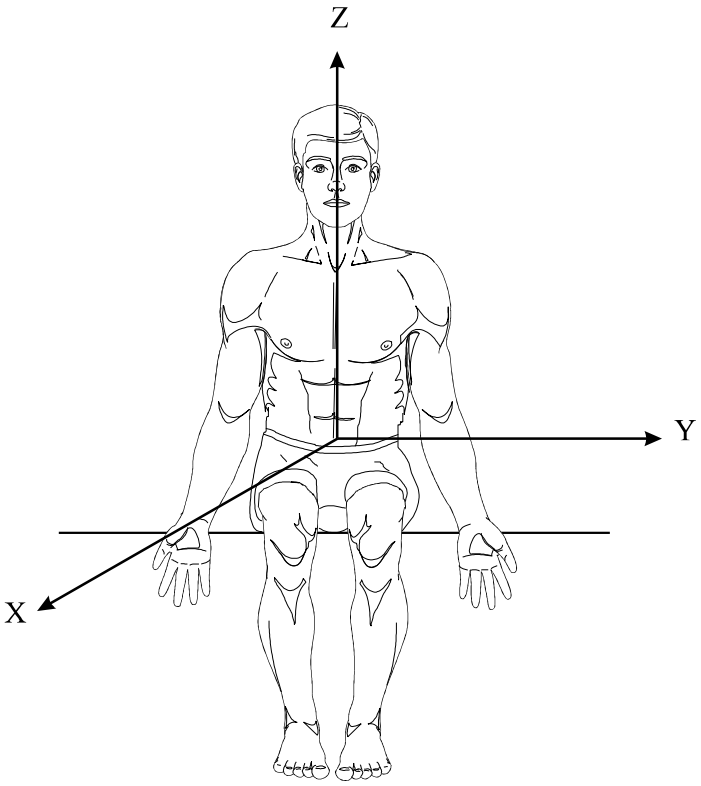

A.2.2: Knee Bolster Simulator

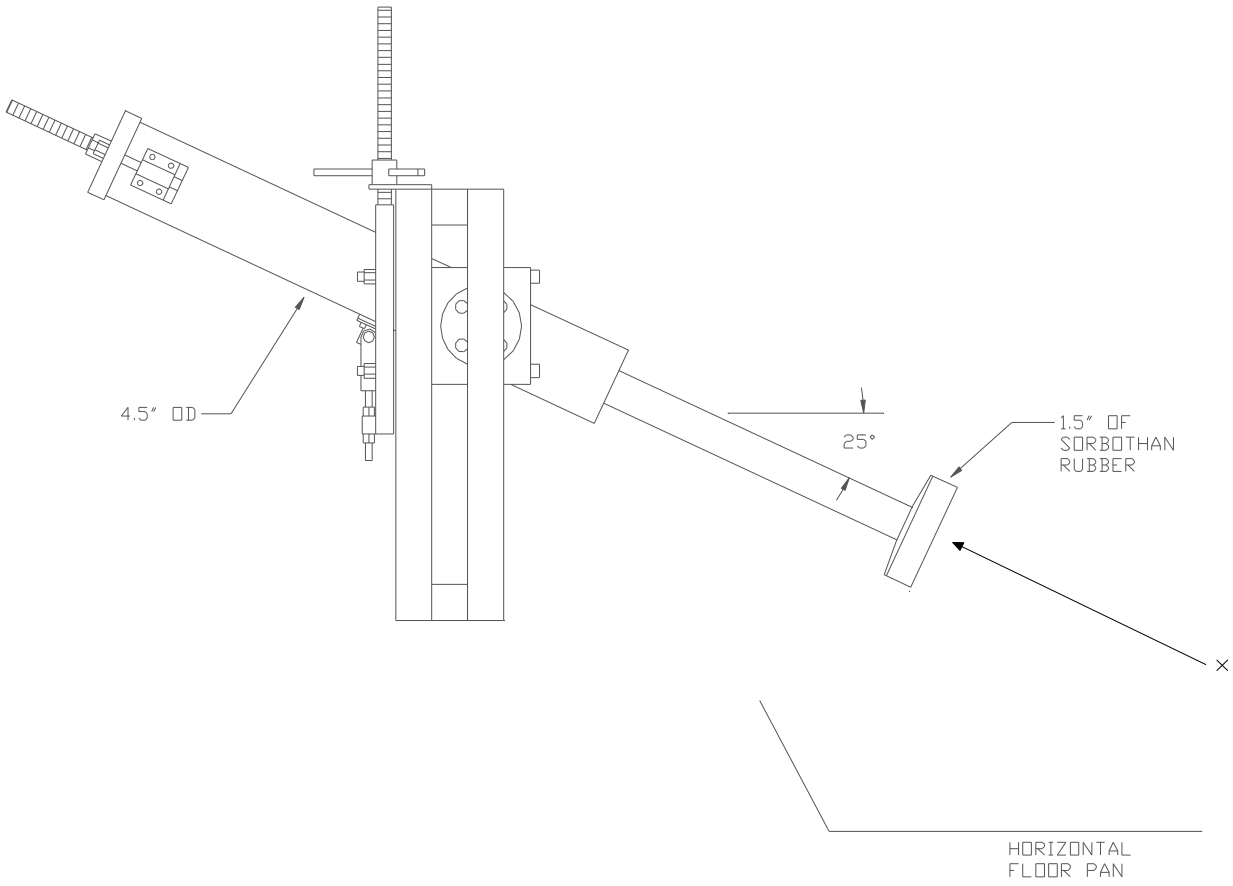

A.2.3: Other Relevant Diagrams

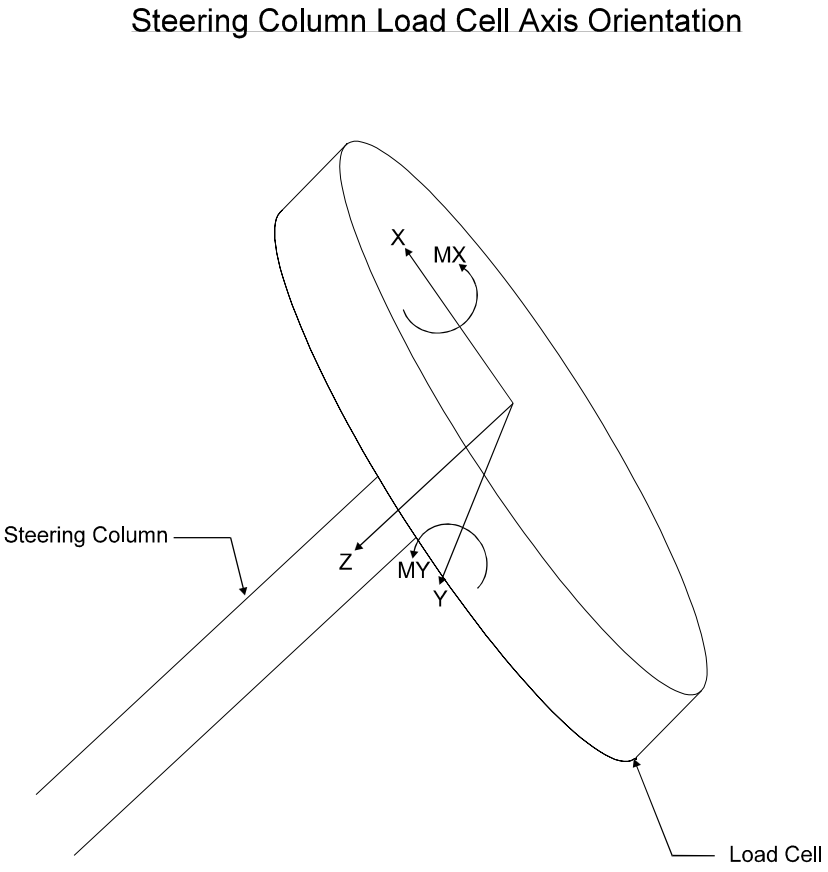

Tibia Load Cell Axis Orientation

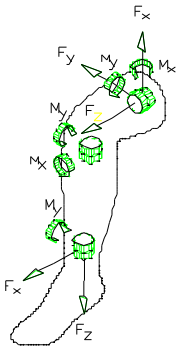

DUMMY
(HYBRID III)

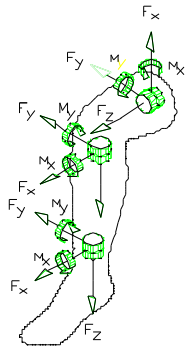

DUMMY
(ALEX)

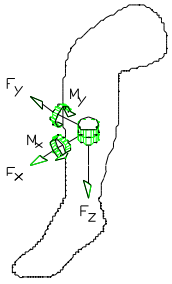

CADAVER

TOP VIEW

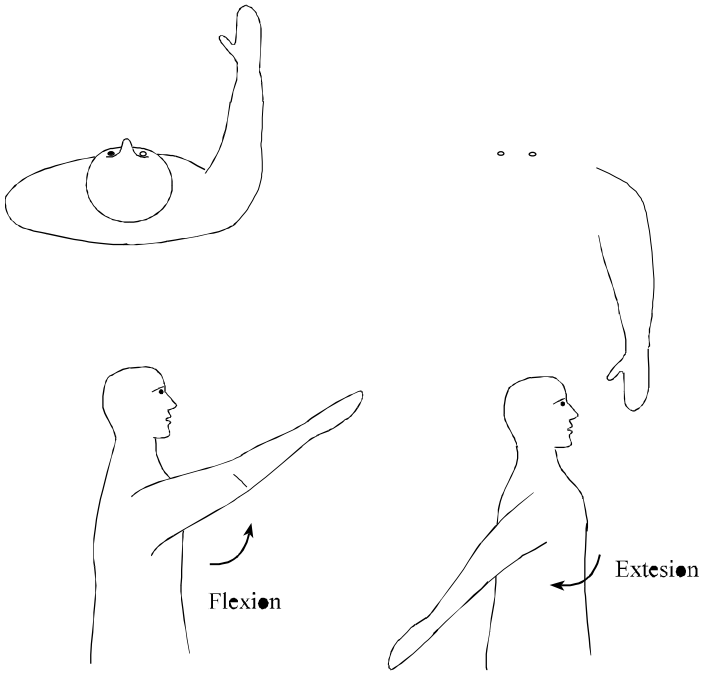

SIDE VIEW

TOP VIEW

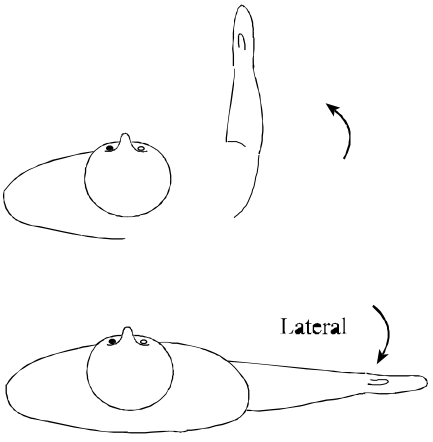

FRONT VIEW, ARM PRONATED

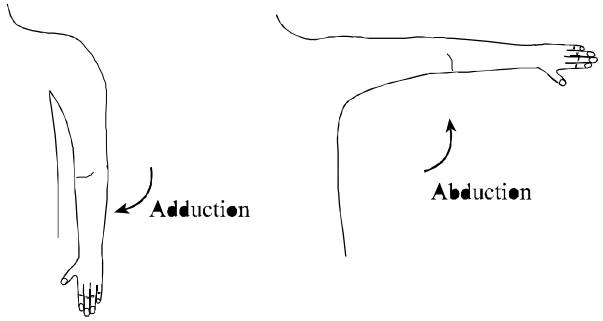

Appendix B: References

B.1: *H.I.T.S. Manual for 713 Sled System*, VIA Systems, Selinas, CA.

B.2: *Users' Manual for the 50th Percentile Hybrid III Test Dummy,* SAE Engineering Aid 23, Society of Automotive Engineers, Warrendale, PA, June 1986.
Calibration Procedures for the Hybrid III Small Female Test Dummy, SAE Engineering Aid 25, Society of Automotive Engineers, Warrendale, PA, November 1994.

B.3: *NHTSA Data Tape Reference Guide*, Volume II: Biomechanics Tests (B2), July 1992.

B.4: Radwan, R and J. Nickles "Performance Evaluation of Crash Test Data Acquisition Systems" *Proceedings of 13th ESV Conference*, 1991.

B.5: *The Abbreviated Injury Scale*, Association for the Advancement of Automotive Medicine, 1990.

B.6: Kennett, K, J. Crandall and W. Pilkey "Warming of Cadaveric Specimens" *Proceedings of 22nd International Workshop on Human Subjects for Biomechanical Research*, Sept. 1994.

B.7: Crandall, J. *Preservation of Human Surrogates for Impact Studies.* University of Virginia, Ph.D. Dissertation, Dec. 1993.

B.8: Granik, G and I. Stein. "Human Ribs: Static Testing as a Promising Medical Application." *Biomechanics*, 6:237-240, 1973.

B.9: Lau, I. and D. Viano. "The Viscous Criterion - Bases and Applications of the Injury Severity Index for Soft Tissues." *Proceedings of the 30th Stapp Car Crash Conference*. SAE No. 861882. Warrendale, PA. 1986. pp. 123-142.

B.10: Mertz, H. "Anthropomorphic Test Devices." In *Accidental Injury: Biomechanics and Prevention*. Edited by A. Nahum and J. Melvin. Springer-Verlag, 1993. p. 81.

B.11: *Road Vehicle - Test Procedures for Evaluating Out of Position Vehicle Occup[ant Interactions with Deploying Airbags.* International Standards Organization, Draft Technical Report 10982, November 21, 1995.

B.12: Carter, D R and Hayes, W C. "The Compressive Behavior of Bone as a Two-Phase Porous Structure". *Journal of Bone and Joint Surgery,* 1997. Vol. 59A, pp. 954-962.

B.13: Rho, J Y, Hobatho, M C and Ashman, R B. "Relations of Mechanical Properties to Density and CT Numbers in Human Bone". Medical and Engineering Physics, 1995. Vol. 17, pp. 347-355.

B.14: Carter, D R. "Anisotropic Analysis of Strain Rosette Information from Cortical Bone". *Journal of Biomechanics*, 1978. Vol. 11, pp. 199-202.

Appendix C: Mechanical Equipment Descriptions

C.1: Crash Simulator

C.1.1: Sled

Crash testing conducted at the Automobile Safety Laboratory is performed on a Via Systems Model 713 test sled which employs a pneumatic propulsion system to accelerate a track-mounted carriage to a pre-determined test velocity. The velocity achieved in any particular test is a function of the run-up distance, the air pressure supplied to the cylinder at launch, and the payload weight. The test sled has a maximum run-up distance of 18 meters and is capable of accelerating payloads of up to 680 kg to a maximum velocity of 80 km/h.

C.1.2: Decelerator

Once test velocity has been achieved, the sled carriage is decelerated through the action of a Via Systems Hydraulic Impact Device (HID), Model 931-4000 which is mounted to the front of the sled carriage and precedes it down the track during the acceleration phase. The HID is a hydraulic damping device consisting of a piston and cylinder assembly mounted horizontally inside a vessel filled with hydraulic fluid (a mixture of water and miscible oil). The cylinder is fitted with rows of threaded ports arranged along its full length into which either plugs or inserts containing orifices of various diameters may be installed. A diagram of the location of these ports is presented in Figure C-1.

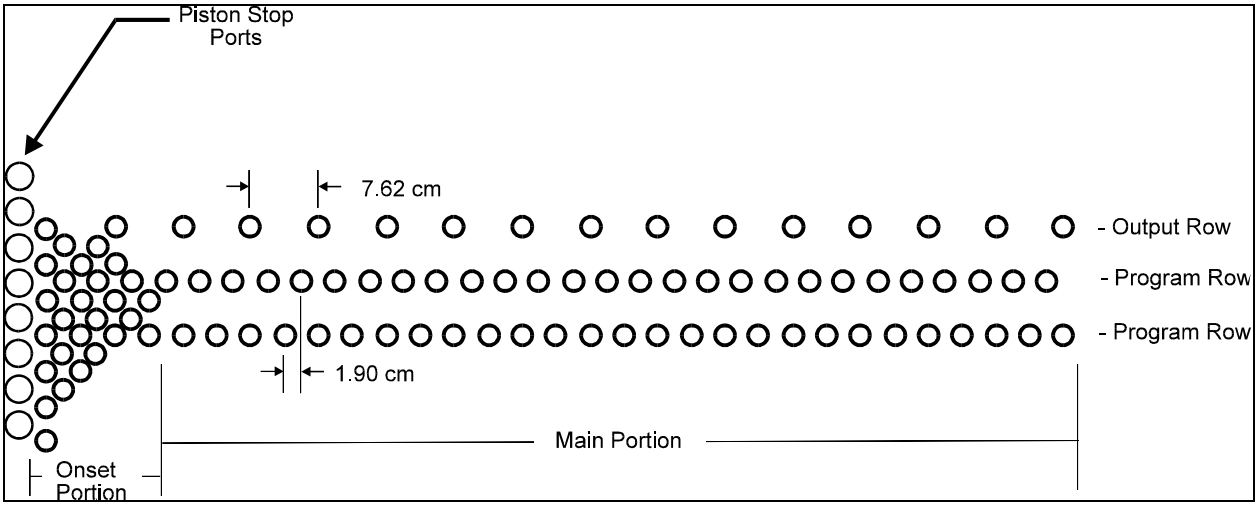

Figure C-1. Schematic of hydraulic decelerator orifice discharge and output ports

A push rod connected directly to the piston projects forward through the front of the vessel and contacts a stationary impact cushion assembly, fixed to the reaction mass at the impact end of the sled track, to initiate the deceleration phase of the test event. As the cylinder is forced forward around the now-stationary piston by the energy stored in the moving sled mass, the fluid contained therein becomes pressurized and is forced out into the vessel through the orifice array at a rate which is a function of both the square of the instantaneous sled velocity and the ratio of the piston area to the instantaneous total orifice area. The varying pressure generated in the cylinder functions

to decelerate the system in a controllable, predetermined, and non-destructive manner, commonly referred to as a deceleration pulse. By appropriately distributing the orifice array over the length of the stroke, the forces can be tailored to produce a variety of pulse shapes (see Appendix B.1). In addition, when the intrusion simulator is used (see Appendix C.5) fluid is forced through hydraulic lines connected to appropriate decelerator output ports to drive the intrusion slave cylinder.

C.2: Test Fixture

In order to accommodate various types of testing, the sled carriage has been designed to accept various fixtures or "bucks", which function as the basic platforms on which different tests may be set up. The test fixture, or "buck", utilized in this test was an approximation of the front seating area of the passenger compartment of a 1993 model year Ford Taurus, a configuration deemed typical of current automotive technology in terms of the spatial relationship between the occupant and the passenger compartment, restraint design, and occupant response during the crash event. The buck was constructed of rectangular steel tubing utilizing a "space frame" design which eliminates the sheet metal structure found in production automobiles and consequently affords fewer obstructions to the recording of photographic data, better accessibility during the set-up process, and a greater degree of ease and flexibility in the mounting of peripheral test equipment. The interior dimensions and spatial relationships of the production automobile (which are crucial to overall occupant response, as well as the realistic interaction of the occupant with the passenger compartment and the proper functioning of the restraint systems) were carefully maintained during the fabrication process. Areas subjected to high force loading (seat attachment points, seat belt anchorages, etc.) were reinforced with steel gussetting or additional tubing as necessary to increase rigidity and /or reduce the likelihood of structural failure. In order to ensure that any occurrences of interaction between the occupant's head and the windshield header "bow" be as realistic as possible, this section was removed from a production automobile and integrated into the buck framework in such a way as to allow for its replacement in the event of damage. The shoulder belt "dee" ring anchor was modified to include a stop to limit "dee" ring rotation.

C.3: Seat

The seat employed in the current series of tests is a production model Ford Tempo bucket seat (small pattern) equipped with a production anti-submarining pan integral with the bottom cushion frame. In order to insure consistency from test to test and to minimize the need to replace parts between tests, the stock mounting pedestal/adjustment rail assembly has been replaced with a rigid mounting frame designed to allow forward and rearward adjustment of the seat in 2.54 cm increments relative to the original center position. Reinforcement of the seat back is accomplished by the addition of an adjustable anchoring bar which is attached to the seat back and the buck frame in such a way that the seat back is supported both in impact (forward) and rebound (rearward) loading, while accommodating both seat position and seat back angle adjustment. In addition, the production seat cushion has been modified by the addition of a wedge-shaped piece of foam between the rear section of the cushion and the overlying upholstery in order to produce a cushion profile and resultant occupant seating position which more closely approximate those associated with the 1993 Taurus.

C.4: Steering Column

The test buck is outfitted with an energy-absorbing steering column based on a modification of a production design which employs a split plastic bushing (Delrin AF), fixed in a split collar and clamp assembly, through which the column tube may stroke. The resistance to the motion of the column tube is constant throughout its stroke and may be adjusted by varying the torque applied to the collar clamping screws, allowing a range of energy-absorbing characteristics and column strokes. Column stroke is recorded manually by measurements taken before and after the test, or, electronically, through the use of a displacement sensing device such as a string pot.

C.5: Intrusion Simulator

Not applicable.

C.6: Knee Bolster Simulator

The knee bolster simulator is a device designed by the Automobile Safety Laboratory to simulate the energy-absorbing characteristics of production knee bolster/dash assemblies while allowing a range of adjustment of position, angle, and energy-absorbing capability along with the ability to measure the forces involved. It consists of two piston and cylinder assemblies, one for each knee, mounted to the sled buck in the fire wall area. Each cylinder contains a column of aluminum honeycomb, manufactured by the Hexcel Corporation, which functions as the energy absorbing medium (see Section 2.1.1). A rigid push rod connects each piston to a knee contact plate to which is attached a rubber pad which functions to dampen the initial force spike which occurs when the knee first contacts the device. As the occupant's knees stroke the device, the columns of honeycomb are crushed, providing deformations at constant force levels. The force levels may be adjusted by utilizing honeycomb of different alloys and/or densities, or combinations thereof in varying configurations. Load cells located between the push rods and the pistons measure the forces along the axis of the bolster stroke and accelerometers mounted on the push rod assembly provide data which is utilized to compensate for the inertial effects of the push rod assembly mass on the measured force levels. Measurements of the length of the honeycomb columns before and after the test, and of the push rod travel, provide a record of the associated deformations (see Appendix A.2.2 for drawing).

The problem of selecting an appropriate initial knee bolster position which ensures direct, on-axis contact of the occupant’s knees while maintaining a knee-to-bolster spacing that is consistent with the 1993 Ford Taurus seating drawing is complicated by both the anthropometric variations from cadaver to cadaver and by the fact that the curved sectional profile of the knee bolster area of the production Taurus dash implies knee distances which vary considerably (and non-linearly) with variations in tibia length and corresponding knee height.

While the knee bolster simulator is capable of a wide range of adjustment of initial position and angle, it has been found that three distinct initial configurations of contact pad height and initial piston position (along the axis of stroke) not only accommodate the range of tibia lengths likely to be encountered among cadaveric specimens, but also closely approximate the corresponding knee distances which would be encountered in the production automobile. The coordinates representing the relationship between the buck reference target and the point at which the stroking axis intersects the contact pad centerline for each of the three positions (which, for the sake of convenience, may be

POSITION	X	Y
High	46.2 cm	35.5 cm
Mid	40.4 cm	33.0 cm
Low	35.0 cm	32.8 cm

referred to as “high”, “mid” and “low” respectively) may be summarized in the following table.

C.7: Cardiovascular and Pulmonary Pressurization Device

In order to approximate the conditions present in the living body, a device is employed to both fill the pulmonary system of the cadaver with air before the sled is launched, and to maintain a constant arterial and pulmonary pressure during the crash event. The apparatus, which is mounted on-board, consists of an air tank to supply pressurized air to both systems, a reservoir for the fluid which is introduced into the cardiovascular system, and pressure regulators and flow controls to allow adjustment of the supply pressure and flow rate in each system separately. In addition, because the pressure regulators employed are of the back-pressure relief type, any excess pressure generated during the test event is vented to the atmosphere, allowing, for example, air to be expelled from the lungs as the chest cavity is compressed by the restraint systems during the crash event. Gauges are connected to monitor the pressure in both systems during the pre-launch adjustment procedure, and are removed once the pressures have stabilized at the desired levels.

The preparation of cadavers for connection to the pressurization systems is described in Appendix G.9. The procedure for connecting cadavers to the system is described in Appendix H.4.

C.8: Force-Limiting Seat Belt Retractor

Not applicable.

Appendix D: Photography

D.1: High Speed Motion Picture Photography

D.1.1: Cameras and Views

High speed photographic data are recorded by servo-controlled 16mm high speed rotary prism movie cameras (either Photosonics 16mm-1B, or Hycam) arranged in stationary, off-board, or on-board positions as appropriate for any particular series of tests. One camera (conventionally Camera #1) is positioned so that it will record a side view of the crash event through the driver's side door opening and is oriented normal to the longitudinal axis of the sled track. The focal length of the lens fitted to this camera is chosen both to maximize image quality and to allow camera placement as far from the subject as possible, within the constraints of available space, thereby minimizing the detrimental effects of parallax on subsequent film analysis. Additional cameras are positioned as necessary to record views of areas of particular interest typically including views from the passenger side of the knee bolster and toe board areas. (See Section 2.1.2.2 for applicable diagram) Unless otherwise noted, the cameras are operated at a speed of 1,000 frames per second.

D.1.2: High Speed Video

In addition to the motion picture photography described above, each test event is recorded using a Kodak Ektapro EM Motion Analyzer (Model 1012), which captures visual information electronically and stores it digitally in random access memory which may be accessed for immediate replay and/or “downloaded” to either VHS tape or computer disc for subsequent viewing or analysis.

D.1.3: Strobes

In order to provide a marker on the film record to denote the beginning of the crash event, a strobe light is triggered at the moment (referred to as time zero, or T_0) that the decelerator push rod contacts the impact cushion assembly, initiating the deceleration phase of the test. Because the strobe light and the data acquisition system are triggered simultaneously, the flash appearing on the film record may be used as a reference for the temporal correlation of the data collected photographically with that collected electronically.

D.1.4: Timing Marks

Two sets of commonly generated, synchronous timing marks are recorded on the motion picture film to provide not only a common real-time reference for the events recorded by separate cameras, but also a means to synchronize the photographic and electronic data recorded, and a reference for the calculation of the "instantaneous" speed of any camera at any point in the event. One set, which is recorded on the right side of each frame as viewed, appears at a "background" frequency of 1000 Hz with a long pulse every ten counts until T_0, at which point it resets and continues counting. The appearance of the second set of timing marks, which is recorded on the left side, coincides with T_0 and continues at a frequency of 100 Hz, with a long pulse every ten counts, for the remainder of the event. It should be noted that because the film is not exposed to the timing mark pulses at the same physical location in the camera as it is exposed to the light entering through the shutter, there is an apparent offset, when viewing the film, between the timing marks and the

associated photographic image, or frame, recorded simultaneously in real time. In other words, the timing marks associated with a particular frame actually appear adjacent to a subsequent frame on the film. This offset, or lag, which is 4 frames in the case of the Photosonics cameras and 5 frames in the case of the Hycam, must be taken into account when attempting to correlate a particular frame with a particular time in the electronic data record and explains the apparent discrepancy, when the film is viewed, between the appearance of the left-hand timing mark and the simultaneous strobe flash which denotes T_0.

D.1.5: Lights

In order to provide sufficient light for adequate film exposure at the high frame rates (and, consequently short exposure times) involved, the event stage is lit with two lighting arrays, each consisting of thirty 1,000 Watt tungsten filament lamps, one on either side of the sled track. This lighting may be supplemented, as necessary, with 6,000 Watts each of auxiliary off-board and on-board lighting.

D.2: Still Photography

Still photographs are taken both before and after each test using a 35mm Nikon 6006AF single-lens reflex camera to document details of the pre-test set-up configuration and post-test resultant conditions.

Appendix E: Data Acquisition System Descriptions

E.1: System

E.1.1: System Hardware

Electronic data collection at the Automobile Safety Laboratory is performed with a DSP Technology Transient Acquisition and Processing System, model TRAQ P. The system is all electronic, and consists of amplifier, digitizer, controller and memory modules housed in CAMAC backplane crates. Sensor data is recorded by a process of real-time digitization of the sensor output signals and storage of the resulting digital data in semiconductor memory. The system operates under the control of software running on a 486 IBM PC-compatible computer, which controls and communicates with the modules through an IEEE 488 GPIB link. Table E.1.2 lists the various modules which comprise the system.

With the exception of the sensor, all data channels are identical. The signals from the sensors travel from the test sled to the data acquisition system through cables approximately 28 meters long, that are pulled behind the test sled. These "umbilical" cables are grouped into two bundles, and terminate in two sled-mounted breakout boxes. Each data channel consists of, in addition to the sensor, a connector on one of the two breakout boxes, an umbilical cable, an amplifier module, a digitizer and a portion of the data memory. Digital data from the digitizers is read by one of the controller modules and stored in the data memory. After all the data samples have been recorded, the contents of the data memory is down-loaded to the hard disc of the control computer. After each test, all data is archived on diskettes or tape cartridges.

Each amplifier module contains a programmable direct-current sensor power supply, a sensor bridge balancing and calibration system, a programmable low-pass filter and a programmable-gain multi-stage amplifier. The various parameters within each amplifier module are programmed directly by the controlling software. The sensor power supplies automatically compensate for voltage drop in the umbilical cables. The low-pass filters are used as anti-aliasing filters only. (The frequency content of the processed data, as presented on the data tape, is determined by post-test software filtering. See Appendix I.1 and I.2) The calibration system uses current injection to simulate resistor shunting of one sensor bridge arm and is used only as a means of sensor integrity verification.

E.1.2: DATA ACQUISITION SYSTEM HARDWARE SUMMARY

NUMBER OF CHANNELS		128
MODULES		
Amplifier	Model	1501UL
	Number in system	128
8-Channel Digitizer	Model	2812
	Number in system	16
System Controller	Model	4012A
	Number in system	2
Data Memory	Model	5004A
	Number in system	2
	Total capacity	2,048,000 samples
CAMAC CRATES		
Crate model		MAXIMA 885
Number in system		8
Crate Controller Model		CC-488

Each digitizer module contains eight identical 12-bit digitizers. The rate at which the digitizers operate and the total number of samples collected are programmable within the controller modules. All digitizers in the system sample at the same time, in response to a clock

signal from one of the two controller modules. The controller modules are each directly connected to digitizer modules and to a memory module.

E.1.3: Trigger Circuit

Triggering of the data acquisition system is controlled by external circuitry. The circuit is activated when the end of the crash simulator decelerator piston rod contacts either of two pairs of expendable brass strips affixed to the reaction mass at the end of the test sled track. This contact takes place just as the deceleration of the test sled begins. As a backup, the circuit also responds to a proximity sensor, mounted on the sled track, which is activated by the velocity sensor blade on the test sled. A "time zero" (T_0) signal is generated by the trigger circuit, in response to these inputs and is connected to the trigger inputs of both system controller modules. When triggered, the controllers collect the pre-programmed number of data samples and then stop the digitizers. A small number of pre-trigger samples also remain in the data memory, and these, combined with the post-trigger samples, constitute the full record of the impact data.

The T_0 signal also triggers the time zero marker strobe and is coupled to the photographic timing mark generator. See Appendix D.1.3 and D.1.4.

When a restraint airbag or a squib-activated restraint belt retractor pre-tensioning device is used, the deployment of the squib is controlled by the trigger circuit. Crystal-controlled delays, adjustable in 100 ms. increments, can be introduced between T_0 and the firing of either squib. The squib firing circuit is powered by a pair of small lead-acid storage batteries and is isolated from the trigger circuit and all data channels.

E.1.4: System Verification

The system hardware and the procedures used meet the provisions of the Society of Automotive Engineers Recommended Instrumentation Practice, SAE J211 JUN88, Part 1 (Referenced in Appendix A.1.2). In addition, the system hardware and the post-processing procedures normally used are tested approximately yearly with a NHTSA-furnished and certified Signal Waveform Generator (SWG). The test results evaluated and reported by NHTSA. See Appendix B.4 for reference to a description of the SWG testing procedure.

Individual sensors are recalibrated periodically and are tested for proper operation before and during each test. The procedures used are described in Appendix F.3.

E.2: Software

E.2.1: IMPAX

The software which controls the data acquisition system hardware is DSP Technology IMPAX. In addition to configuring and controlling the modules in the system, this program allows the user to configure and monitor the test instrumentation environment, monitor and analyze the signals from sensors, collect test data, post-process data and save and retrieve data. A database of all available sensors and the various necessary parameters associated with them is also maintained.

Some examples of IMPAX capabilities include: Test description information can be entered, saved and linked to test data. Sensors can be chosen and assigned to specific system channels. Names can be assigned to various parameters associated with sensors, sensor output

signals and data channels. A display of all the sensors used and the various parameters associated with them can be viewed and printed. Sensors and data channels can be tested and the results displayed for analysis. Signals from sensors can be monitored in real time and the results displayed in several formats for analysis. Sensor data is automatically scaled to engineering units and is presented for analysis and saved in engineering units. The process of recording and saving data can be configured and monitored. Once recorded and saved, data can be processed various ways, viewed, plotted and reported various ways.

E.2.2: Other Software

Automobile Safety Laboratory software is used for general post-processing of data and for creation of the data tape. Other in-house, commercial or NHTSA-furnished software packages are used for specialized data processing, as necessary. Descriptions of the procedures used are in Appendix I.

Appendix F: Instrumentation Descriptions

F.1: General

Most sensors used are of the direct-current-powered Whetstone bridge type, with either two or four active strain-gauge bridge arms. An appropriate supply voltage is generated and regulated by the data channel amplifier module. Power and signal conductors are generally grouped in a single 3.5- to 5-meter long shielded cable, terminated with a standard connector, which connects the sensor to the breakout box on the test sled. Bridge completion resistors, when not inside the sensor itself, are housed in the connector.

The mounting of sensors on cadavers is described in detail in Appendix G.6 and G.8.

F.2: Descriptions of Sensor Types

Accelerometers for general use are industry-standard miniature undamped piezo-resistive two-arm strain-gauge bridge types. For cadaver external spinal and pelvic applications, larger triaxial cubes are used. Because hydraulic shock waves within the crash simulator decelerator create high-frequency, high energy vibrations, accelerometers mounted directly on the test sled or the test fixture must be internally damped or use a damped mounting.

Load cells and pressure transducers are of the piezo-resistive strain-gauge bridge type. Belt webbing tension load cells used on restraint belts are instruments specifically designed for this purpose.

Magnetohydrodynamic (MHD) angular rate sensors are used to determine the flexion of anatomical joints, such as the ankle and neck. MHD sensors quantify the change in electric field across a conductive fluid (mercury) annulus while an applied magnetic field changes with sensor motion. This is an application of the equation $\mathbf{E} = \mathbf{U} \times \mathbf{B}$; where **E** is the electric field vector, **U** is the relative velocity of the fluid, and **B** is the magnetic field vector. The sensors have an operating bandwidth of 0.5 to 2650 Hz and are not affected by linear accelerations. Angular rates about a single axis are obtained with an MHD ARS-04E (ATA, Albuquerque, NM), with a mass of 6 grams. For three-dimensional rotational information, an orthogonal set of three sensors is required. These sensors are mounted in an aluminum housing, approximately 3 cm square by 4 cm tall, with a total mass of 86 grams (MHD ARS-04E Triaxial Cube). MHD angular rate sensors are rigidly mounted to either side of a joint in order to determine the joint flexion response.

Five-axis implantable tibia load cells were developed jointly by the Automobile Safety Laboratory and Robert A. Denton, Inc., specifically for cadaver use. Forces are measured along three orthogonal axes and moments about two axes. The forces measured are inferior/superior axial load, medial/lateral shear load and anterior/posterior shear load. Bending moments are measured about medial/lateral and anterior/posterior axes. Each load cell weighs 327 grams and is 6.35 cm long. One cell is mounted in each tibia, after a section of the bone has been removed.

Instrumented footplates are used to measure the forces applied to the lower extremities of the occupant by the intruding toepan of the test fixture. Each footplate consists of a rectangular unit, approximately 18 cm by 36 cm and 3.5 cm thick, mounted on the angled portion of the crash simulator toepan. The footplates are located so that each of the occupant's feet, when correctly positioned, is approximately centered on a footplate. A small horizontal platform supports each heel. Each footplate contains a load cell at each corner and a single miniature

accelerometer, with a damped mounting, at the center of the bottom surface. The active axis of the footplate, perpendicular to the top surface, is defined as the local Z-axis of the device. (See drawing in Appendix C.5; Figure 5.)

Chestbands are thin flexible steel bands, used to monitor the shape of closed spaces by measuring the curvature at many points along the circumference. Each chestband contains 40 piezo-resistive bridge strain gauges mounted at 2.5 cm intervals and encased in plastic potting. The unpotted ends of the steel bands extend beyond the area containing the strain-gauges, to facilitate installation. Connections to the strain-gauge bridges are made through unshielded ribbon cables terminated in standard sensor connectors. Not all of the 40 strain gauges are always used, but, for average-sized human chests, configurations with less than 25 active gauges do not always yield acceptable results.

The string pot chest is a series of string potentiometers incorporated into the Hybrid III dummy chest which are designed to measure local thoracic deformation. Within the chest are eight string potentiometers connected to four locations within the dummy chest such that each location has a ‘straight’ potentiometer originating directly from the dummy back and a ‘cross’ potentiometer originating from the dummy back across the chest. During the dynamic test event, the strings retract or extend in response to chest deformation.

F.3: Verification of Sensors

F.3.1: Pre-Test

Sensors are recalibrated to standards traceable to National Institute of Standards and Technology (NIST), at approximately 1-year intervals, by the manufacturers or by independent calibration laboratories. The calibrated sensor sensitivity information is stored in a database maintained by the IMPAX software, which automatically notifies the operator when a sensor is due for calibration.

Before each test, the instrumentation is checked to reduce the possibility of failure during the test. Sensors which have given satisfactory results in recent tests are checked for electrical integrity with an ohmmeter. If there is any doubt about a sensor, further testing is done by applying an approximate known input to the sensor and confirming the output. For an accelerometer, this testing would consist of mounting the unit on a small portable shaker and exciting it with approximately 10 g’s at 100 Hz. For load cells and the String Pot Chest the Tinius Olsen testing machine would be used. Belt webbing tension load cells can be checked by installing them on a piece of webbing and hanging a known weight with the webbing. A set of precision mandrils is available for the verification of chestbands. Note that these procedures are not intended as calibrations of the sensors, but only as integrity checks.

F.3.2: Pre-Launch

During a test, the integrity of the sensors and the data channels is checked several times before the launch. An automatic procedure, initiated by the IMPAX software, adjusts each amplifier module to minimize the direct-current offset at the output and then checks each amplifier output. Another automatic procedure balances each appropriate bridge-type sensor, by injecting a small current into one leg of the bridge. Each amplifier output is then automatically checked. IMPAX also performs an automatic integrity check on each data channel. For most

bridge-type sensors, this consists of a current-injection "shunt emulation" of the sensor bridge, followed by an evaluation of the resulting output signal. For other sensors, a known voltage is connected to the amplifier input, instead of the sensor, and the amplifier output is monitored, verifying the integrity of the data channel, except for the sensor itself. These automatic procedures notify the data acquisition system operator in the case of any failures, and appropriate action is taken to repair or replace the malfunctioning part.

In addition to the automatic integrity checks described above, the data acquisition system operator verifies the output of all sensors periodically during the pre-launch phase of each test, using the real-time monitoring capability of the IMPAX software. Some sensors require special verification procedures to insure that they are installed properly.

With sensors in the zero or unloaded position, a small sample of data is recorded on the appropriate channels and saved as a zero reference. Immediately before the launch, all data channels are monitored one last time, and another small sample of data is recorded on all channels. This data is saved as a final record of the state of the sensors before the test sled was placed in motion.

F.4: Crash Simulator Velocity Measurement System

This system consists of a steel blade, mounted on the test sled, which passes in front of a proximity sensor mounted on the sled track. The sensor is located so that the blade passes just before the impact deceleration begins. The shape of the blade is such that 2 leading edges, 10” apart, pass the sensor. The signal from the sensor is recorded on a data channel, and the time which elapsed between the passing of the 2 edges is measured after the test, using the on-screen plotting capability of the IMPAX software. Because both ends of the interval represent the passing of leading edges, any difference in the response time of the sensor to leading and trailing edges does not affect the measurement. The measured time interval and the known distance between the blade edges are used to mathematically determine the test sled velocity just before impact.

The blade also passes through the sensor of a GHI Systems model VS 300R Optical Velocimeter, which provides a backup velocity measurement.

Appendix G: Cadaver Handling and Preparation

G.1: Cadaver Acceptance Criteria

Limits are placed on the range of acceptance criteria for the cadavers in order to standardize the test conditions as much as possible. These parameters ensure that accurate, valid, and reliable analysis of the cadaver test data can be performed.

AGE RANGE	18-70 years
MAXIMUM BODY MASS	100 kg
MAXIMUM STATURE	196 cm
GENDER	Male/ Female
CONVALESCENCE	
Subjects exhibiting an extended period of convalescence prior to death may have severe muscle atrophy and poor bone quality making them inappropriate for the research. Decisions on the appropriateness of these cadavers is made on a case by case basis.	
PREVIOUS INJURIES/ DISEASES	
Cadavers exhibiting previous injuries that may potentially bias the test results (e.g., healed fractures with mounting hardware) are not included in the study. In general, cadavers with metastatic cancer or other diseases resulting in deterioration of the skeleton are rejected.	
COMMUNICABLE DISEASES	
The medical records of the cadavers are reviewed for the presence of infectious diseases. The diseases include, but are not limited to, tuberculosis, bubonic plague, hepatitis A, hepatitis B, hepatitis C, yellow fever, cholera, AIDS, typhoid fever, and dysentery.	

G.2: Cadaver Handling Protocols

Particular care is taken when handling, testing, and disposing of cadavers used in this program. Cadavers are obtained through the Virginia State Anatomical Board with explicit permission given by the family to conduct biomechanics research. All test procedures have been approved by the Human Use Review Panel (HURP) of the NHTSA. All personnel involved in cadaveric testing have read and signed Ethical Treatment of Human Surrogate Forms supplied by the HURP. In addition, an institutional review board (oversight committee) has been established to review, evaluate, and approve all procedures involving cadavers. The procedures followed in order to allow the ethical and dignified use of all cadaveric material include:

NHTSA Order 700-2 (April 24, 1979)

NHTSA Order 700-4 (April 24, 1979)

G.3: Infectious Disease Screening Procedures

Screening of blood for Hepatitis A, B, C, and HIV is conducted with each cadaver prior to acceptance into the research program. A venous cut down is performed at either the jugular or femoral vein. Approximately 5 cc of blood is drawn with a syringe and transferred to a pressure-sealed test tube (vacutainer). Extreme care is taken when poking the needle through the cap of the vacutainer since this procedure runs a high risk of needlestick injury. If it is difficult to obtain

blood via the jugular or femoral artery, a large gauge needle is inserted into the heart through the left fourth intercostal space. If the biomechanical test to be performed requires a perfused heart, however, this last approach should be avoided.

Two 5 cc vacutainers are collected and submitted for testing. Because of hemolysis, separation of serums is difficult and false positives are known to occur during testing. Therefore, the second vacutainer of blood is used to confirm any positive test results using alternative testing methods.

The blood samples are transported to the immunopathology department where they are centrifuged and the serum is separated. An assay of antigen and antibody tests are conducted with the serum. The presence of HIV or Hepatitis C infection in the host subject is determined by testing for the antibody rather than the virus itself. The antibody is produced by a person's immune system in response to the virus and is not part of the virus. The tests for Hepatitis A and Hepatitis B are antigen tests, which test for a part of the virus directly. Any positive test results are discussed with the testing laboratory personnel. If a test is considered a true positive for any of the infectious diseases, the cadaver is rejected for biomechanical studies.

G.4: Preservation Procedures

Depending on the length of storage, cadavers are preserved using one of three methods:

1. Refrigeration (short term storage)
2. Freezing (long term storage)
3. Embalming (long term storage)

Whereas a brief description of these procedures is provided below, detailed information on the storage techniques can be found in Appendix B.7.

G.4.1: Embalming Procedures and Fluids

Embalming involves the injection, distribution, diffusion, and drainage of a preserving solution through the arteries of the circulatory system. Tissue preservation using the embalming process is accomplished through a chemical "fixation" or coagulation of the proteins within the tissue cells. After entering the arterial system, the embalming fluid flows through the venous and capillary systems while simultaneously draining the body of blood and other tissue fluids. Through several active and passive transport processes, the solution then passes from the capillaries into the extravascular tissue beds.

The embalming fluids and techniques, developed at UVA, are used to maximize cadaver biofidelity and preservation. These embalming methods require that an extremely slow flow rate and a low pressure are maintained. These cadavers are embalmed during two six-hour stages in order to supersaturate the body's tissues and to promote equal parity of fluid in the tissue.

The custom embalming fluid, herein referred to as the Biofidelity Fluid, contains the following agents:

Water (H2O)	9 l
Phenol (C6H5OH)	100 g
Alcohol (C2H5OH)	500 cc
10% Formalin (HCOH)	1500 cc
Glycerin (CH2OHCHOHCH2OH)	250 cc
Sodium Sulfate (Na2SO4)	125 g
Magnesium Sulfate (MgSO4.7H2O)	125 g
Potassium Nitrate (KNO3)	250 g
Water Conditioning Agents	(Case Specific)

Following the embalming of the cadaver, the body is placed in a shroud pouch (i.e., body bag), which maintains high humidity levels. The cadaver is then stored in a +2°C to +4°C cooler until needed for testing

G.4.2: Refrigerated Storage

Decomposition of the cadavers is minimized by storing bodies at low temperatures. Refrigeration conditions at the ASL maintain the cadavers at +2°C to +4°C. Fresh cadavers are stored in the cooler for post-mortal periods of less than one week. To prevent dehydration, cadavers are kept in sealed shroud pouches. If storage intervals longer than one week are required, embalming of the cadavers is performed prior to refrigeration.

G.4.3: Freezing and Thawing Procedures

The freezing process significantly slows tissue decomposition by altering the state of the body's fluids. At the ASL, cadavers are placed in shroud packs and stored at -70°C. Particular attention is given to maintaining the neck and extremities in anthropometric positions. Since the freezing and thawing process involves contraction and expansion of tissues, anomalous ranges of motion can be introduced if the body is stored in an abnormal position.

Several days prior to testing, the cadavers are removed from the freezer and allowed to thaw to room temperature. Thawing periods have been developed based on the cadaver's size and mass, (see Reference B.6).

G.5: Anthropometry Procedures

Anthropometry procedures are standardized by NHTSA in order to assure that the measurements made by different test laboratories are for the same reference points. A list of the anthropometry measurements as well as the data are provided in Section 2.1.5.1. More detailed information, such as anthropometry figures and definitions, can be found in the NHTSA Data Tape Reference Guide (see Appendix B.3).

G.6: Identification of Instrumentation Mounting Sites

G.6.1: Accelerometer Mounting Sites

Prior to x-rays, potential accelerometer locations are marked using lead targets, paper clips, i.e., alligator clips. After x-rays, exact mounting locations are determined such that incision sizes are minimized. With the subject initially in a supine position, the x-ray target sites are determined in the following manners:

Fourth Rib:

By palpating the upper thorax, the jugular notch at the superior region of the sternum is located. Sliding down the manubrium sterni (past the juncture of the sternum with the first rib), the sternal angle is identified. The sternal angle or sternomanubrial joint signifies the beginning of the second rib. Following the shaft of the second rib over the costal cartilage and along the body of the second rib, the most lateral segment of the rib is found. By palpating the chest, the third rib and the fourth rib can be located by moving inferiorly along the lateral rib cage. A target is placed at the lateral segment of the fourth rib.

Eighth Rib:

The xiphisternal joint is identified at the base of the sternum. From this juncture, the costal margin is found by palpation. Continuing down the costal margin, the seventh rib, also known as the last "true" rib, is the most inferior rib directly connected to the sternum. Following the body of the seventh rib along the rib's contour to where the next inferior rib, the first "false" rib (i.e., ribs indirectly connected to the sternum) is located. At the lateral most portion of this eighth rib, an x-ray target is placed.

Both of the aforementioned procedures are performed independently in order to verify the target locations by comparing their relative locations. In other words, the eighth rib is located relative to the fourth rib by moving vertically down four ribs on the side of the subject. The fourth rib is similarly located relative to the eighth rib location. Relative movement along the lateral aspect, however, is often difficult with obese patients and the procedure of locating one rib in relation to another is only used as a final verification.

Sternum:

By palpating the manubrium sterni, the center (horizontal and vertical) of the sternum is identified. This location is marked with an x-ray target and is referred to as the suprasternal upper mounting location. Approximately 3 cm above the xiphisternal joint (where the xiphoid process connects to the body of the sternum), another x-ray marker is placed at the substernal lower mounting location.

The cadaver is then placed in a prostrate position. Forward flexion of the body is necessary to accentuate the protrusion of the vertebrae. This is achieved by placing a rubber or wooden block underneath the thorax of the subject. The spinal and vertebral mounting location are then identified.

Vertebra T1:

The distinct posterior bony projection at the base of the neck is the spinous process of the seventh cervical. Because of its prominence and importance as a reference for locating other vertebrae, it is commonly referred to as the vertebra prominens. The first thoracic vertebra is located directly inferior to the vertebra prominens and is easily found by palpation.

Vertebra T12:

Beginning with the first thoracic vertebra and counting spinous processes while moving inferiorly along adjacent vertebrae, the twelfth vertebra can be identified. An x-ray target is placed directly over the spinous process.

Due to subcutaneous fatty tissue, it can be extremely difficult to follow the inferior vertebrae relative to T1 and to locate accurately the twelfth vertebra. An approximate technique is used for these instances. The first step is to locate the iliac crest of the hip bone at the most superior point. This position is projected medially to the mid-sagittal plane of the body. From this intersection with the spine, the mounting position is found by counting four vertebrae as one moves superiorly along the spine. Although this method appears crude, it quickly identifies an approximate mounting position which can later be verified and readjusted from the x-rays.

Vertebra L2:

The first step is to locate the iliac crest of the hip bone at the most superior point. This position is projected medially to the mid-sagittal plane of the body. From this intersection with the spine, the mounting position is found by counting two vertebrae while moving superiorly along the spine. Although this method appears crude, it quickly identifies an approximate mounting position which can later be verified and readjusted from the x-rays.

Pelvis:

The iliac crest is identified on the right side of the subject and traced to the external lip of the crest until reaching the posterior superior iliac spine. Proceeding laterally approximately 2 cm, an x-ray target is placed at this site. An identical procedure is performed on the left side.

Skull:

The X axis of the head is determined by marking a line that connects the tragion to the palpated location of the inferior-lateral corner of the orbital socket (Figure G-1). From this line, a perpendicular line is drawn from the tragion to the vertex of the skull. The distance from the tragion to the vertex in the Z direction is measured with calipers. A uniaxial accelerometer mount is placed in the Y direction, superior to the tragion, 17% of the distance from the tragion to the vertex in order. This locates the sensor at the same height as the skull center of gravity. A second uniaxial accelerometer, in the head Z direction, is fastened to the skull at the vertex of the skull. Head X accelerations are measured from the posterior skull by a sensor mounted on a MHD angular rate sensing cube.

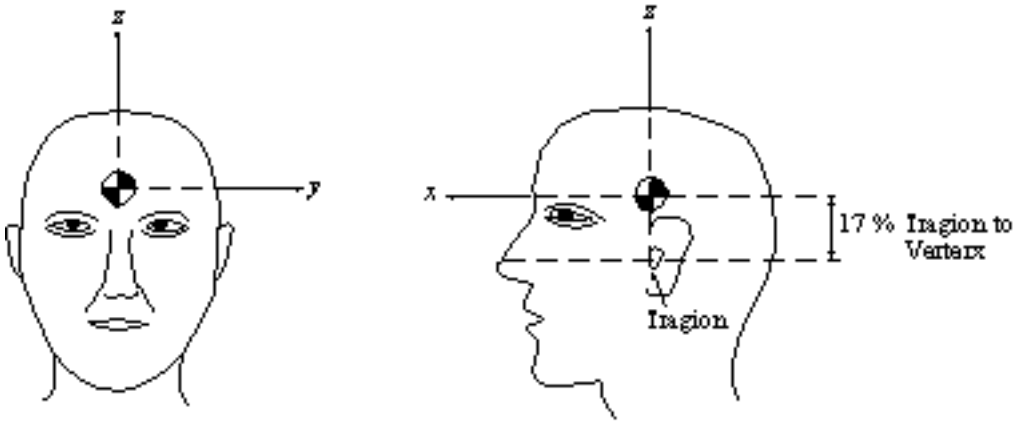

Figure G-1: Head coordinate system.

Radius:

The lateral surface of the distal radius is identified by palpation.

Ulna:

Accelerometers are located on the medial, posterior edge of the ulna, approximately 40% of the radiale-stylion length from the elbow joint. This location is near the center of mass of the forearm.

G.6.2 Strain Gauge Mounting Site

Two strain gauge rosettes are place on each of the radius and ulna. Since the forearm is positioned so that the flap of the airbag loads it at the distal third, the strain gauges are applied mid-shaft on the two bones. The posterior and anterior sides are used on the radius, while the posterior and medial sides of the ulna are used. These sites were selected to minimize damage to the surrounding tissues during the strain guage application

G.7: Pre-Test X-Ray Procedures

After placing the x-ray markers on the test subject, preliminary radiography is performed. Pre-test radiography is intended to identify any existing injuries or anomalies, to verify instrumentation mounting locations, and to provide a reference with which to compare post-test radiography. The pre-test radiographic examination consists of the following views:

Anterior-Posterior (A-P) Skull
A-P C-Spine
A-P Chest (thoracic spine and ribs)
Crosswise View of Upper Abdomen to Lower Ribs
A-P L-Spine
A-P Pelvis
A-P Femur, Left and Right
Lateral Femur, Left and Right
A-P Tibia/Fibula, Left and Right
Lateral Tibia/Fibula, Left and Right
A-P Ankle, Left and Right
Lateral Ankle, Left and Right
A-P Foot, Left and Right
Lateral Foot, Left and Right
Oblique Calcaneus View, Left and Right
A-P Humerus, Left and Right

Lateral C-Spine
Lateral Skull
Oblique Ribs Bilateral Left, Right
Lateral T-Spine
Lateral L-Spine
Lateral Chest
Swimmer's View

All films are interpreted by a radiologist and a formal report is written (see Section 2.1.5.3). Anatomical directions and planes are defined in Appendix A.2.3.

G.8: Instrumentation Mounting Procedures

Internally-mounted instrumentation can cause problems by producing artifactual injury and influencing response. Therefore, minimal tissue damage is essential in all procedures and surgical incisions are made as small as possible while still providing a suitable work area. Recommended incision sizes are provided below for all mounting locations and techniques but exact dimensions may differ due to anthropometric variability among subjects.

G.8.1: Accelerometers

Accelerometer mounts are securely mounted to the skeletal framework of the test subject. Various fastening techniques are employed to ensure a firm bond between the mount and the underlying bony structure. Combinations of stainless steel wire, self tapping screws, and orthopedic pins are used to affix the mounts.

Rib Mounts (Fourth and Eighth):

The procedures for the fourth and eighth ribs are nearly identical with the exception that the fourth rib mount positions the accelerometer principal direction normal to the body while the eighth rib is parallel to the body. Although the procedure is described in detail for the fourth rib mount, it is also applicable to the eight rib mount. On either side of the test subject at the fourth rib, a 5 cm incision is made along the direction of the rib. Using a retractor to hold open the incision, the rib is isolated from the surrounding tissue with a small blunt object. A liberal layer of the orthodontic resin is then applied to the rib in an area approximating that of the fourth rib accelerometer mount. The mount is pressed firmly against the rib and held for approximately five minutes.

The rib mounts are moored with aluminum wire wrapped through either side of the accelerometer mounting holes. Slots have been machined in the mounts to provide for proper wire placement on the fourth rib mount. On the eighth rib mount, there is sufficient space on either side of the accelerometer slot for the aluminum wire. For each side of the mount, two 25 cm pieces of aluminum wire are cut and threaded through a half-moon curved needle. The pieces of wire are brought together at the eye of the needle and all four ends are combined away from the point of the needle. Holding the ends of the wire, the needle with the aluminum wire is wrapped around the rib. Remaining as close as possible to the rib, the rib is circumscribed. A hemostat is used to grip the point of the needle and to complete circumnavigation of the rib. The process of wrapping the rib in wire is repeated several times. Next, the four strands of wire are

gathered and cut with wire cutters. The procedures are repeated for the opposite end of the accelerometer mount. Finally, the entire procedure is repeated on the opposite aspect of the cadaver's rib cage.

Sternum:

Two 5 cm incisions are made at the prescribed sternal locations identified with x-ray targets. The sternum is isolated from the surrounding tissue with a blunt object. If the surface of the sternum appears planar, it is not necessary to use orthodontic resin in the mounting process. If the surface is not planar, a flat surface must be created by attaching either double sided foam tape or a layer of dental acrylic. The mounts are placed on the sternum and visibly aligned with the body's mid-sagittal plane. After positioning the mounts, two 1/16" pilot holes are drilled into the sternum through the openings in the mounts. Since the screws are self-tapping, the depth of the incision is only 0.5 cm. Two #6 Pan Head Screws, one-half inch in length, are screwed into the bone and used to securely fasten the mounts.

T-1, T-12, L2 Vertebrae:

A single 0.5 cm cross-shaped incision is made through the superficial layer of skin approximately 1.0 cm lateral to the spinous process. The vertebral mounting bracket is placed over the vertebra with one of the lateral holes aligned with the incision. A 9/64" Steinmann (orthopedic) pin is then threaded into a variable speed hand-held drill. Using the pin as a screw, the transverse process is penetrated. Penetration of the spiral process is identified by increased resistance of the pin. Using either a straight needle or marker, the other two holes are marked on the skin while the mount is pressed firmly against the skin.

The mount is removed with the pin left in the spiral process. Cross-shaped incisions are made at the marked locations. The mount is again placed on the first pin while a second pin is screwed through the contralateral hole. The mount is removed again and a 6-32 nut is threaded onto each pin until it rests firmly again the skin. The mount is placed on the pins and a 3/32" pilot hole is drilled through the center mounting hole of the bracket into the spinous process. A #8 slotted wood screw, ranging in length from 2 cm to 7 cm depending on the osseous integrity of the subject, is screwed into the spinous process. This screw firmly presses the mount against the nuts on the Steinman pins. Finally, a nut is threaded over each Steinman to reinforce the secure attachment of the mount.

Skull:

Uniaxial accelerometers are placed on the skull in the head Y and head Z direction. The X axis of the head is determined by marking a line that connects the tragion to the palpated location of the inferior-lateral corner of the orbital socket. From this line, a perpendicular line is drawn from the tragion to the vertex of the skull. The distance from the tragion to the vertex in the Z direction is measured with calipers. A uniaxial accelerometer mount is placed superior to the tragion, 17% of the distance up to the vertex. A second uniaxial accelerometer mount is fastened to the skull at the vertex of the skull (Figure G-2).

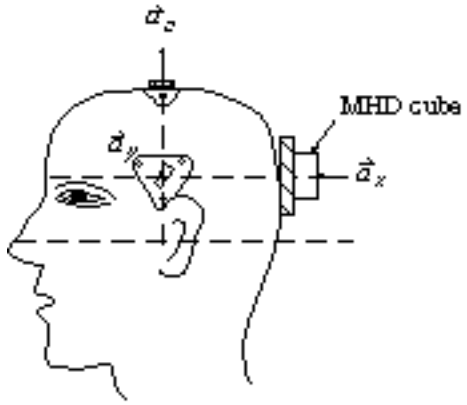

Figure G-2: Head accelerometer array.

The accelerometer mounts are triangular (3 cm length side) 3/16" thick aluminum with recessed #6 screw holes in each corner. Accelerometer mounts are fastened to the skull by tightening three #6 flat head, self-tapping wood screws into predrilled holes in the bone. Uniaxial accelerometers are fastened to the center of the accelerometer mounts via two #0-80 screws with fiber washers.

Radius:

The lateral surface of the distal radius is identified by palpation. An incision through the epidermis and subcutaneous tissues is made with a scalpel. Then, the incision is bluntly extended to the bone cortex with a pair of scissors. The bone cortex is cleaned with an osteotome along a 4 cm length of bone. Acrylic potting cement is mixed and placed on the surface of the bone, beneath the accelerometer mount to eliminate vibrations of the plate. The mount is secured to the bone with two nylon "tie-wraps".

Ulna:

An incision is made along the proximal, posterior edge of the ulna, approximately 40% of the radiale-stylion length from the elbow joint. This location is near the center of mass of the forearm. The muscle belly is lifted away to expose the medial ulna surface. The bone cortex is cleaned with an osteotome along a 5 cm length of bone. The mount is placed on the bone for a trial installation and four screws on the mount are adjusted to align the mount with the ulna coordinate frame. Acrylic potting cement is mixed and placed on the surface of the bone, beneath the accelerometer mount to eliminate vibrations of the plate. The mount is secured to the bone with two nylon "tie-wraps".

G.8.2: Tibial Load Cells

The limb to be implanted with the tibia load cell is positioned horizontally with the anterior apex of the tibia facing upwards. A supporting block positioned under the calf aids in holding the tibia in a working position without interference from the foot. An 18 cm long incision, centered around the tibia's mid-diaphysis, is made longitudinally along the anterior-medial face of the tibia. Two lateral incisions are made at the ends of the first incision to allow two flaps of skin to be reflected, revealing the anterior-medial face of the tibia. The tibialis anterior tendon and its muscle lie just lateral to the anterior apex of the tibia. Great care must be taken not to sever this tendon when making the initial incisions and when making further cuts.

Next, the surrounding musculature and connective tissues must be separated from a 16 cm section of the tibia to allow room for the mounts. On the medial, posterior side of the tibia, the tibialis posterior and its tendon are closest to the bone. Just posterior to this are the flexor digitorum longus and flexor hallucis longus muscles and tendons. All three of these muscle tendon groups must be separated from the tibia without severing them. The interosseous membrane must be separated from the posterior apex of the tibia in the region designated for the mounts. On the lateral side of the tibia, the extensor hallucis longus and the extensor digitorum longus and their tendons run along the lateral face of the tibia. These must also be carefully separated from the segment of tibia to be involved in the mounts.

Next, the section of tibia to be removed is marked. An 8.9 cm long section of tibia is removed. This section is centered in the region where the tissues have been separated from the tibia. The tibia is cut with an oscillating bone saw, which cuts bone but not the surrounding tissues. The cuts are made perpendicular to the long axis of the bone. Any cortical bone fragments that cannot be reached with the bone saw are cut with a close-space hacksaw. The periosteum is then scraped off the tibia ends for a length of 3 cm to allow for bonding of the epoxy-sand mixture directly to the cortical bone surface.

A small brush is used to clear the marrow from the medullary canal to a depth of approximately 2 cm. This small cavity can then be filled with the epoxy-sand mixture that will harden around the small screw protrusion through the mounting cups inside the bone. This provides more complete support for the cut bone end, as well as centering the cup on the bone.

After clearing the small spaces in the medullary canal, the epoxy-sand compound can be mixed. Epoxide resin and hardener are mixed in a five to one ratio by weight. After the resin and hardener are thoroughly blended, the sand can be added. Fine grit blasting sand is added in a two to one ratio by weight of the combined resin and hardener mixture. A small amount of the mixture is then placed into the spaces created in the medullary canal.

Next, the disposable cup mounts, with load cell cradles attached, are filled with the mixture. The mounts are then pressed onto the bone ends until the bone ends seat fully on the cup bottoms and the protruding screws are centered in the medullary canal. The load cell or dummy slug is now set in place. The caps are put in place on the load cell cradles and secured. Finally, the alignment of the mounting is checked. Viewing the leg medially, the mount must not sag posteriorly, rather it must be a straight continuation of the natural tibia shaft. The central #10 fasteners in the caps must be facing anteriorly, aligned with the anterior apex of the tibia. For proper polarities of the load cell channels, the cables of the load cell must exit proximally.

G.8.2.1 : Humerus Load Cells

The 5 degrees of freedom load cell that is used *in situ* in the tibia is also used for upper extremity experiments. The only difference is that while one side of the load cell is attached to the humerus, the other side is rigidly mounted to the universal joint and support structure.

G.8.3: Magnetohydrodynamic Angular Rate Sensors (MHD's)

MHD angular rate sensor cubes are rigidly mounted to bone on both sides of a joint to be studied. For the ankle joint, MHD cubes are mounted on the medial aspect of the shin and heel. During subject preparation, a portion of the medial calcaneus is exposed in order to drill two 3/32" holes for the MHD mounting plate. The holes are oriented on a line that bisects the long axis of the calcaneus, one hole superior and one hole inferior to the long axis of the calcaneus.

The calcaneus mounting plate consists of a 1 1/4" by 1 5/8" by 1/4" thick, aluminum plate which is fastened to the bone with mounting screws. The screws are #8, 2" long, self tapping Phillips head particle board screws with a course thread. The distance between the two mounting screws is 3/4" and the screws are countersunk into the mounting plate so that the surface of the plate is flush with the sensor cube. Two 3/4" long, hexagonal, nylon spacers are used to distance the mounting plate from the bone, and prevent joint motion interference.

The tibia mounting plate has the same external dimensions as the calcaneal mount but has a central, countersunk hole. A flat socket cap screw (1/4-20 × 7/8") is placed through the central mounting hole and threaded in to a 3/4" long, hexagonal, steel spacer. This unit is left intact between cadaver tests. The tibia mount is screwed into a pre-existing hole on the medial aspect of the distal tibia load cell mount after installation of the tibia load cell. Precise orientation of the mount is not crucial, but the long axis of the mount is generally aligned with the long axis of the tibia.

For neck flexion studies, the MHD Dynacubes are mounted on the posterior skull and the T1 vertebra. The procedure for attaching an angular rate sensor to the posterior skull involves removing a 5 cm X 6 cm section of scalp, centered on the median plane of the head and at the height of the head center of gravity (Figure G-3). An osteotome is used to remove the periosteum and other soft tissues from the bone. Four holes are drilled in the skull, two superior, and two inferior to the Y axis of the head. Two self-tapping wood screws are threaded into the inferior holes and tightened to an extent that makes the mounting plate orthogonal with the head axis system. An epoxy/ sand mixture (Kennett, 1995) is used as a grouting material between the mount and the skull. The epoxy/sand mixture is placed on the skull. The 0.5 cm thick, disposable mounting plate has an area of 5 cm X 6 cm and eleven holes in it; four #4-40 threaded holes for the MHD Dynacube, three through holes for screws that fasten the plate to the skull, and four #10-24 threaded holes for the protective cover to attach. The mounting plate is placed on top of the epoxy and fastened to the skull via two additional self-tapping wood screws through the superior holes in the skull. The epoxy is given 24 hours to cure at room temperature.

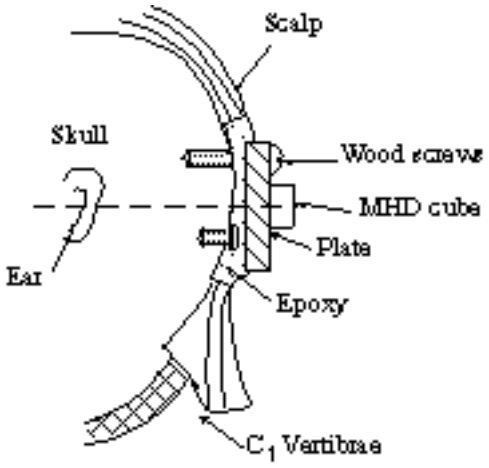

Figure G-3: Sagittal view of posterior skull mount.

A second angular rate sensor mount is attached to the proximal spine via three #8 Steinmann pins. The mount consists of a 0.25 inch thick piece of aluminum, measuring 5 cm by 6 cm. The plate has two #8 through holes spaced at 2.5 cm through which two Steinmann pins are screwed into the lateral processes of the T1 vertebrae with a hand-held drill. A third Steinmann pin is threaded into the spinous process of the T2 vertebrae through the inferior end of the mount. The third screw into the spine is necessary for limiting rotation about the Y axis of the mount. The importance of rigidity of the mount overweighs the decrease in biofidelity of the now-stiffer T1 - T2 junction. An MHD Dynacube is fastened directly to the plate via four #4-40 screws. A protective cover, measuring 5 cm X 6 cm, is fastened to the corners of the mounting plate with #10 screws and stand-offs.

G.8.4: Ligament Strain Transducers

Not currently in use.

G.8.5 Stain Gauge Application

Planar rosettes (350Ω, 5% strain) were selected as the best choice given the application to bone. Forearm incisions were intended to be minimally invasive and to limit damage to the interosseous membrane. The bone surface was prepared with Ether, and the gauges were bonded to the surface with methyl-2-cyanoacrylate. A thin latex cover was installed over the surface of the rosettes to isolate the gauges from the surrounding tissue. Gauze was placed over the latex cover before the arm was closed with sutures. Strain relief of the gauges was provided by securing the wire leads to the bone with tie-wraps, as well as suturing the wires to the skin.

G.9: Pressurization Preparation

The subject's hip is palpated and the anterior superior iliac spine is located. A line is then drawn from the iliac spine to the pubic tubercle indicating the position of the inguinal ligament. Next, an incision is made starting just inferior and parallel to the inguinal ligament exposing the superior portion of the femoral artery. Special care is made not to sever the femoral artery. Having exposed the femoral artery, the artery is lifted and nicked to facilitate the insertion of the catheter. A small wire is inserted into a Foley 30 cc balloon catheter in order to stiffen it for insertion. The wire also provides a radio opaque marker that allows confirmation of the catheter's location with x-rays. The catheter is then fed superiorly into the iliac artery and into the abdominal aorta. The balloon is then inflated using 30 cc's of air at a position just inferior to the diaphragm. It is then clamped to prevent pressurization of the lower extremities.

The neck is palpated on the left aspect to find the sterno-clavicular articulation. A line is then drawn from that articulation to a point midway between the mastoid process and the angle of the jaw. This marks the route of the left common carotid artery. Although the sterno-mastoid muscle completely covers the left common carotid, special care is taken not to transect this muscle during surgery. The cadaver’s neck is extended and turned slightly. A 7.5 cm incision is made along the anterior border of the sterno-mastoid muscle such that the center corresponds to the cricoid cartilage. The artery is then located, lifted, and nicked. If pressures are to be recorded, a Precision Measurement Model 105 pressure transducer is then fed inferiorly through the artery into the aortic arch (approximately 22 cm). A tie-wrap is placed around the artery and transducer leads and tightened in order to prevent escape of the pressurization fluid. The right common carotid is located in a similar method. Instead of inserting the pressure transducer, however, a carotid arterial injection tube is inserted. This is the location where the pressurized fluid enters the body. A string is then tied around the artery and injection tube to avoid leakage.

Pulmonary pressurization is accomplished by a tracheotomy. The subject is placed in a prone position with a head block beneath the shoulders. An incision is made perpendicular to the trachea just below the cricoid cartilage. The trachea is located and a small nick is made between the rings of the trachea. The second pressure transducer is inserted in the trachea at the approximate position of the bifurcation. A balloon tipped tracheotomy tube is placed in the trachea and the balloon is inflated.

G.10: Post-Test X-Ray

In order to provide comparable images of the cadaver, post-test radiography uses the same views as the pre-test x-rays (see Appendix G.7). In addition to these views, positioning and integrity of the instrumentation mounts are verified with the post-test x-rays. The tibia and calcaneus are filmed with the MHD mounts in place. The mounts are then removed and the tibia and calcaneus are filmed a second time. The first set of films are taken with the mounts in place in order to see radial cracks emanating from the mounting screw holes. These radial cracks are more easily identified on the films when the screws are in place, but the metal in the mounts over-exposes the film. Thus, a second set of films is taken without the mounts to reveal any previously obscured fractures.

The radiologists interpretation of the post-test x-ray views relative to the pre-test radiographs can be found in Section 3.1.3.1.

G.11: Post-Test Necropsy Procedures

Standard autopsy procedures are performed by a pathologist and autopsy specialist. Examinations of the cardiovascular system, abdomen, viscera, brain, head and neck, spine, and other skeletal elements are performed. In addition, a detailed necropsy of the lower extremities is conducted by an orthopedic surgeon. Depending on the type of impact test to which the subject was subjected, additional procedures may also be used to detail the extent of injury.

G.11.1: Autopsy Preparation

In order to minimize contamination, all tools and equipment required to perform the autopsy are prepared prior to initiation of the autopsy. All organ containers are filled with 10% buffered formalin and labeled with cadaver reference number and all instruments needed to perform the autopsy are placed on a cart next to the autopsy table.

In order to document any injuries or anomalies, the following photographic equipment is available:

35 mm Nikon Camera with Macro Lens

1 Roll 24 exp. color print film

Blue pads for photo background

A circulator is designated and the following paperwork is brought to the autopsy suite:

NHTSA Autopsy Forms

UVA Autopsy Forms

Rib fracture Report Forms

Thoracic Injury Forms

Lower Extremity Report Forms

Pre-test and post-test x-ray films are mounted on a light box in the autopsy suite. Any injuries identified by x-ray are verified during the autopsy procedures.

G.11.2 : Autopsy Procedures

An external inspection of the cadaver is performed to investigate superficial injuries. The chest is palpated for gross evidence of displacement or fractures. All sutures from incisions used to mount the instrumentation are removed. Any remaining instrumentation or mounts are removed from the subject. Initial cuts are made in the chest with a scalpel. The skin covering the chest is reflected to expose the rib cage. A bone saw is used to cut through the lateral rib cage and collar bone. The cut through the rib cage facilitates the removal of the entire breast plate and documentation of rib fractures. The pericardial sac is opened and the carotid arteries and subclavian vessels are ligated. The trachea is transected just superior to the epiglottis. The larynx is freed and retracted. Pleural effusions in the chest cavity are suctioned and the volume is recorded. The intestinal tract is removed by locating, ligating, and incising the ligament of Treitz.

A scalpel is used to cut through the mesentery. The entire length of the intestines are traced to the bowel to look for tears. The intestines are then tied off and incised. The intestinal tract is opened with a scalpel and the contents rinsed out of the intestines and colon. The genitourinary tracts are separated, lifted, and removed. The thoracic and abdominal organs (liver, kidneys, pancreas, etc.) are removed for weighing and sectioning of histology specimens. Any lacerations or abnormalities are recorded on the autopsy forms.

The hair is wetted and the scalp is cut using a scalpel. The scalp is retracted to expose the skull and a bone saw is used to penetrate through the skull. After removing the skull cap and exposing the brain, the brain is removed and weighed.

Next, the spinal cord is exposed with a bone saw. Bilateral cuts are made through the vertebral column and the sides are retracted in such a manner that the cord remains untouched.

Tissue specimens are removed from the brain, kidney, lung, heart, liver, and pancreas and placed in 10% formalin. The specimens are then dehydrated and embedded in paraffin. Thin slices are cut from these blocks and mounted on microscope slides. The paraffin is then chemically removed and the samples stained with hematoxylin and eosin. Once the slides are completed, the specimens are examined for autolysis and pathology by the pathologist.

After removing specimens for histology, the organs are placed in the body cavity and the head and chest are sutured.

G.11.3: Rib Fracture Documentation

The breast plate is examined and the number and location of rib fractures are recorded. Fractures are measured relative to the jugular notch and the mid-sagittal plane. Measurements relative to the mid-sagittal plane follow the contour of the rib to the location of fracture. Rib Fracture Report Forms are located in Section 3.1.3.3.

G.11.4: Lower Extremity Dissection

The leg and foot are separated from the body at the proximal tibia and placed with the medial surface flat on the dissection table. An incision is made distally along the posterior leg to the heel, and from the heel anteriorly to the fifth metatarsal. This incision is opened with a blunt instrument in order to allow the subcutaneous tissues to be incised, and the dermis to be removed.

Once the dermis is removed, the underlying retinaculum tissues are examined for trauma. In particular, the inferior extensor, and inferior peroneal retinaculae are examined for tears and stretching.

A posterior approach, through the superior peroneal retinaculum, is used to expose the peroneous longus, and peroneous brevis tendons. An incision along each tendinous sheath is made to allow for relocation of the tendons and exposure of the lateral ligaments. Connective tissues around the calcaneofibular, anterior talofibular, and posterior talotibular ligaments are carefully removed.

The specimen is then placed with the lateral surface flat on the dissection table. An incision in the dermis is made along the posterior leg and anteriorly to the ball of the foot. The epidermis is resected and the condition of the inferior extensor retinaculum and flexor retinaculum are noted.

The tibialis posterior, flexor digitorum longus, and flexor hallucis longus are approached posteriorly though the flexor retinaculum. Each tendinous sheath is opened and split along the length of the tendon. Then, each tendon is displaced anteriorly over the medial malleolus. Careful removal of the connective tissues around the medial malleolus reveals the deltoid ligament, which is composed of the anterior tibiotalar, tibionavicular, tibiocalcaneal, and posterior tibiotalar ligaments.

After completion of the ankle dissection, an orthopedic surgeon evaluates injury. Each tendon is examined for tears and longitudinal splits. Each ankle ligament is examined for separation from the bone and tearing. In conjunction with the physical examination, post-test x-ray information are used to evaluate changes in the bone condition and joint spacing of the ankle. Injuries that are identified on radiographs are verified during the dissection. Lower Extremity Injury Report Forms are provided in Section 3.1.3.3.

G.12: Evaluation of Skeletal Quality Test Procedures

Mechanical testing of bone from each cadaver is performed to evaluate skeletal quality. The testing permits interpretation of the hard tissue trauma with regard to the size, physiology, pathology, and age of the cadaver.

G.12.1: Rib Testing

As part of the post-test examination, sixth and seventh ribs that were not fractured in the test are removed in order to evaluate the quality of the bone. The rib segment between the anatomical mid-clavicular and the posterior axillary line is used since it exhibits the least curvature. The ribs are tested quasi-statically in a three-point bend fixture following established test protocols and guidelines (see Appendix B.8).

Appendix H: Procedures

H.1: Occupant Positioning Procedure

Adjustments are made during the course of setting up each test with the goal of maintaining a consistent spatial relationship between the occupant and various components of the passenger compartment which contributes to both a realistic interaction of the occupant with the interior of the passenger compartment and the various restraint systems. Additionally, because the kinematics of the occupant during the crash event are, to a large degree, dependent on the initial position, the consistency of results from test to test is largely a function of the consistency achieved in positioning the occupant during test set-up.

In general, the occupant is positioned according to the standard procedure outlined by NHTSA for the New Car Assessment Program (NCAP) (see reference, Appendix A.1.1) with the added consideration of maintaining a spatial relationship between the occupant and the test fixture which corresponds, as closely as possible, with that between the occupant and the passenger compartment of the 1993 Ford Taurus. Because the focus of the current test series is the interaction of the occupant's lower extremities with the intruding toepan, the initial position of the occupant's feet (which is determined largely by the angle of the toepan and its initial, un-stroked position and is held constant from test to test), and the attitude of the occupant's legs (defined by the angles of the tibia and femur), are given the highest priority in the positioning process, followed, in turn, by the remaining measured parameters describing the spatial relationship between the occupant and passenger compartment as set forth in the NHTSA Data Tape Reference Guide (see reference, Appendix B.3).

The list of positioning parameters, in order of their priority and including their corresponding target values, is summarized in the table below.

POSITIONING PARAMETER	TARGET VALUE
Tibia Angle	39 º
Femur Angle	11 º
Chest-to-Wheel Distance (CS)	30 cm
Head-to-Windshield Distance (HW)	63 cm
Head-to-Header Distance (HH)	25 cm

Once the occupant has been hoisted into the buck, centered in and allowed to settle into the seat, the feet are positioned squarely on the toepan foot plates, aligned so that their center lines fall in the vertical planes including the knee bolster piston axes and held in place with masking tape as necessary. A preliminary check is then made of the pelvic (dummy only), tibia and femur angles, as well as the distance between the chest and the center of the steering wheel to determine the nature and magnitude of the adjustments required to bring the occupant's position into compliance with the target values. The pelvic angle is then adjusted as required and the seat position (and seat back angle, if necessary) is adjusted as required to bring the tibia angle, femur angle, and chest distance into compliance with the target values if possible. The knees are then positioned 25.4 cm apart and are centered on the axis of each knee bolster piston. The occupant's hands are placed on the steering wheel and held in place with masking tape as necessary. Finally, the head angle is adjusted, the head supported and taped as required, and final adjustments to the occupant's position are made with the goal achieving an occupant position which satisfies as many of the prioritized parameters as is feasible. (Obviously, due to the often significant

anthropometric variations from dummy to cadaver and between cadavers, the consistent satisfaction of all positioning criteria is not always achievable. In these cases, great care is taken throughout the positioning process to achieve an occupant position which, given the particular anthropometric constraints, satisfies, to the greatest extent possible, both the stated dimensional priorities and the goal of consistency within the test series.)

When a satisfactory occupant position is achieved, photo targets are applied to the head and major joints of the occupant and the coordinates of the centers of the targets relative to a standard reference target on the buck are measured and recorded. The dimensions defining the spatial relationship between the occupant and the passenger compartment, including those mentioned above, and various angles relating to the position of the occupant are also measured and recorded. Further documentation of the initial conditions is provided by still photographs taken after the set-up has been completed.

H.2: Angular Rate Sensor Initial Position Measurement Procedure

The magnetohydrodynamic (MHD) angular rate sensor initial orientation relative to the inertial frame of reference is determined by using a three dimensional position-measuring device. The device measures three independent rotations about an orthogonal set of axes aligned with the global axes of the test fixture. These angles are the Euler angles of the sensor cube, and are used to calculate the initial conditions for integration of the data. (See Appendix I.6 for a description of the data processing procedure.)

The measurement device consists of a fixture which fits over the sensor cube and to which are attached three independent 360-degree rotary dials. Pointers on the Y- and Z-axis dials can be aligned with the inertial reference frame by means of a circular bubble level. The X-axis pointer extends beyond the edge of its dial and can be visually aligned parallel to one of several X-axis members of the toepan structure. The fixture is held in place on each sensor cube and the dials are rotated until the pointers are aligned with the inertial reference frame. The fixture is then removed and the Euler angles are read and recorded.

H.3: Chestband Installation and Verification Procedure

Before the test, the locations of the active gauges being used in each chestband are marked on tape attached to the outer surface and upper edge of the band. Chestbands are installed before the occupant is placed in the seat of the test fixture. On a gurney located next to the test sled, the occupant is held in a seated position by the lifting hoist. The arms are secured above the head by taping the hands to the hoist chain. The lower chestband is installed first, wrapped around the thorax at the location of the specified rib and held in place by duct tape. The appropriate gauge is aligned with the spine, and measurements are taken of the overlap of the band ends and of the distance from the nearest active gauge to the center of the sternum. Next, the verification procedure, described below, is performed. While the verification data is being processed, the lower band is securely taped in place with duct tape and the installation process is begun for the upper chestband. The test procedure continues after the verification procedure has been satisfactorily completed for both chestbands. Long strips of duct tape are placed diagonally across the chest, over the chestbands, in the area where the shoulder belt will be located, to keep belt friction from displacing the chestbands.

The chestband verification procedure is a full-system check of the chestbands and the data channels to which they are connected. This procedure is performed because chestband status can not be readily determined by monitoring individual gauge outputs. After each chestband is installed, chest breadth and chest depth are measured using a large caliper. When the measurements have been recorded, a small set of data is recorded (with the data acquisition system) from each chestband. The average of the recorded data for each gauge and the measured sternum-location and circumference information are then transferred to the RBANDS_PC computer program, which generates contour files. Special software is used to calculate chest depth and breadth, based on the contour files, and compare them to the measured lengths. If differences between calculated and measured lengths greater than 10% are observed, the measurements and the verification data processing are repeated. If these differences persist and can not be explained, the test is postponed until the cause can be determined.

H.4: Cardiovascular and Pulmonary Pressurization Procedure

Just prior to the launch of the test sled, the cardiovascular and pulmonary pressurization systems are activated, to simulate in the cadaver, the conditions present in a living person. The onboard air tank is connected by hose to the laboratory air system and filled to a pressure of approximately 1000 kPa. The air in this tank is the source of pressure for both pressurization systems. The supply hose is left connected until just before the sled launch and sufficient air is stored in the tank to maintain pressure in both systems during the sled run and impact.

The fluid reservoir, filled with approximately 4 liters of a 1:1 solution of glycerin and saline, is pressurized with air from the air tank, by opening a valve. After pressurized fluid has pushed all the air from the fluid reservoir output hose, the fluid flow is stopped and the pressure regulator is adjusted to maintain approximately 3.5 kPa of pressure, measured at the point where the hose leading to the cardiovascular system of the cadaver will be connected. The cadaver hose is then connected and the pressurized fluid is applied to the cardiovascular system. If necessary, the pressure is readjusted, to compensate for any pressure-drop resulting from the flow of fluid into the cadaver.

The hose leading to the trachea of the cadaver is connected and the pulmonary system is pressurized to a regulated pressure of approximately 3.5 kPa. The back-flow bleeder valve is set to begin relieving pressure at this value. The additional pulmonary pressure generated by the impact is vented through the back-flow bleeder.

Pressure gauges, used in making the adjustments mentioned above, are disconnected and removed from the test fixture before the sled is launched. After the impact, valves are closed, to relieve the pressure on both systems, and prevent the flow of additional fluid into the cardiovascular system.

H.5: Restraint Belt Spool-Out Measurement Procedure

When a retractor-type restraint belt is used, an approximate measurement of the maximum amount of belt webbing which was pulled out of the retractor assembly is taken by comparing the position of the webbing, relative to the retractor, before the launch and after the impact. When a retractor pre-tensioning device is used, a similar measurement is taken of the maximum amount of belt webbing retracted.

For either measurement, a string is sewn to the belt webbing, at a location which will be near the retractor when the belt is in position around the occupant. A small block of polystyrene foam is attached to the test fixture close to the retractor spool and in line with the vertical section of the belt between the retractor and the D-ring. The free end of the string is pushed through the foam block, using a needle. Immediately before the launch (after all occupant positioning procedures have been completed and after cadaver pulmonary pressurization has been initiated), the string is pulled taut and marked at the edge of the foam block. After the impact, before the occupant is disturbed, the string is marked again. The distance between the two marks is measured and recorded after the test.

Appendix I: Data Processing Procedures

I.1: Sensor Data Post-processing

The IMPAX data acquisition software produces output files consisting of raw binary data, with sensor, test and scaling information in a text header. There is one file for each data channel. Before any subsequent processing takes place, these files are converted to ASCII text in a scaled floating-point format. The frequency content of the data at this stage results from the use of 8-pole Butterworth 3300 Hz hardware low-pass filters in the data channel amplifier modules when the data was recorded. The data is further low-pass filtered to meet the SAE-J211 standard for Channel Frequency Class (CFC) 1000, using a NHTSA-supplied two-pass (forward and backward) 4-pole Butterworth software filter algorithm. The record length is truncated to 5120 samples, of which 100 samples are pre-trigger.

It should be noted that the combination of hardware and software filtering described above has been verified to adhere to the SAE J211 CFC 1000 standard by analysis, done by NHTSA, of SWG test results. See Appendix A.1.2 for reference to the SAE J211 standards. See Appendix B.4 for reference to a description of the SWG testing procedure.

I.2: Data Tape Generation

All data to be included on the data tape is initially processed as described above. The data from some sensors is processed additionally, as described elsewhere in this Appendix. Any filtering to a lower Channel Frequency Class is accomplished by using the filter algorithm mentioned above. Finally, all the data is converted to the NHTSA data tape format, and written onto high-density 3.5” diskettes for delivery to NHTSA. The various header files are generated by the NHTSA-supplied program ENTREE, except the GROUP 5 header, which is written using a text editor, and checked with the BIOCHECK program. The set of diskettes with header and data files constitutes the “data tape” as referred to in this report.

I.3: Generation of Resultants

Data is first filtered to the appropriate Channel Frequency Class, as specified in SAE J211. Resultant data is generated by taking the square root of the sum of the squares of the data from each of the three component axes, for each data sample. Resultant data of this type does not generally appear on the data tape, but is reported and plotted.

I.4: Inertial Compensation of Load Cell Data

Some load cells carry structures of significant mass mounted between the cell and the point where external force is applied. The data from these load cells is compensated for the force imposed as a result of the inertia of the structure mass moving with the test fixture. For each data sample, the mass of the structure and data from an accelerometer, mounted on the structure, are used to compute the inertial component of the force applied to the load cell, which is then subtracted from the load cell data.

The data from the accelerometer is generally included on the data tape, as well as the inertially-compensated load cell data.

I.5: Footplate Data Processing

The data from the four load cells in each footplate is added together and then inertially-compensated, as described above. The results, which consist of a single contact-force curve for each footplate, are included on the data tape.

I.6: Ankle Rotation Data Processing

During the pre-launch preparations, the three Euler angles that describe the initial orientation of each magnetohydrodynamic (MHD) angular rate sensor are measured directly. These Euler angles, in combination with the initial foot and tibia flexion angles, determine the rotational transformation matrices that relate the foot, tibia, foot sensor, and tibia sensor to the inertial reference frame.

The angular velocity data from each sensor is first low-pass filtered to SAE J211 Channel Frequency Class 180 and the offset is removed by subtracting the average of the pre-trigger data from the remaining data. Velocity data is then transformed from the inertial frame of reference to the respective local anatomical reference frame by using the initial rotational transformation matrices. The transformed angular velocity data appears on the data tape.

The data is then integrated using the trapezoidal rule to yield incremental angular rotations for each data sample time. At each time, t, the transformation matrix of each segment with respect to it's position at t-1 is calculated based on the incremental angles for that time. These angles are used as sequential Euler angles, but are not sequence dependent due to their small magnitude. The incremental transformation matrices for each sample time are used to determine the transformation matrix from the local anatomical frame to the inertial reference frame. These final transformation matrices are then manipulated in order to determine the angles of dorsi/plantar flexion, eversion/inversion, and internal/external rotation for every data sample. Flexion angles are calculated about a set of orthogonal axes, located at the center of the ankle, and the results are reported and plotted.

I.7 Elbow Flexion Data Processing

During the pre-launch preparations, the three Euler angles that describe the initial orientation of each magnetohydrodynamic (MHD) angular rate sensor are measured directly. These Euler angles, in combination with the initial flexion and pronation angles, are used to determine the rotational transformation matrices that relate the humorous, ulna, and radius to the inertial reference frame.

The angular velocity data from each sensor is low-pass filtered to SAE J211 Channel Frequency Class 1000 and the offset is removed by subtracting the average of the pre-trigger data from the remaining data. Velocity data is measured with respect local body segment coordinate frames, thus no coordinate system transformations are necessary.

The humorous angular rate data is integrated using the trapezoidal rule to yield incremental angular rotations for each time, *t*. At each time, *t*, the transformation matrix of the humorous with respect to it's position at *t-1* is calculated based on the incremental angles for that time. These angles are used as sequential Euler angles, but are not sequence dependent due to their small magnitude. The incremental transformation matrices for each sample time are used to

determine the transformation matrix from the local humorous frame to the inertial reference frame.

The amount of elbow flexion at each time point is calculated as the integral of the difference between the angular rate about humorous *y* and ulna *y*. The orientation of the ulna with respect to the inertial reference frame is calculated by rotating the humorous coordinate frame about the humorous *y* axis for each time, *t*, by the elbow flexion angle. The angular velocity vector of the ulna is calculated as the difference between the humorous angular rate vector and the ulna *y* angular rate vector, in the local ulna coordinate frame. The amount of elbow pronation at each time point is calculated as the integral of the difference between the angular rate of the ulna about forearm *x* and the angular rate of the radius about forearm *x*.

I.7.1 Neck Flexion Data Processing

During the pre-launch preparations, the three Euler angles that describe the initial orientation of each magnetohydrodynamic (MHD) angular rate sensor are measured directly. These Euler angles, in combination with the initial head and spine flexion angles, determine the rotational transformation matrices that relate the head, T1 vertebra, head sensor, and T1 sensor to the inertial reference frame.

The angular velocity data from each sensor is first low-pass filtered to SAE J211 Channel Frequency Class 180 and the offset is removed by subtracting the average of the pre-trigger data from the remaining data. Velocity data is then transformed from the inertial frame of reference to the respective local anatomical reference frame by using the initial rotational transformation matrices. The transformed angular velocity data appears on the data tape.

The data is then integrated using the trapezoidal rule to yield incremental angular rotations for each data sample time. At each time, t, the transformation matrix of each segment with respect to it's position at t-1 is calculated based on the incremental angles for that time. These angles are used as sequential Euler angles, but are not sequence dependent due to their small magnitude. The incremental transformation matrices for each data sample time are used to determine the transformation matrix from the local anatomical frame to the inertial reference frame. These final transformation matrices are then manipulated in order to determine the angles of Y-flexion, X-version, and Z-rotation for every data sample. Neck Flexion angles are calculated about a set of orthogonal axes located at the center of the ankle with polarity consistent with the right hand rule.

I.8: Head Center of Gravity Acceleration Calculation

The head is instrumented with three uniaxial accelerometers, located on the X, Y, and Z axes of the head. This mounting scheme eliminates the effects of angular accelerations of the head on the sensor data. Centripetal accelerations of the head are calculated, based on the angular rate vector of the head and anthropometric data. Accelerations at the center of the gravity of the head are determined in a spreadsheet with the following equation:

$$\vec{a}_{cg} = \vec{a}_{measured} - \vec{w} \times \left(\vec{w} \times \vec{r}\right)$$

where;

$\vec{a}_{cg}$ = the acceleration vector at the center of gravity of the head,

$\vec{a}_{measured}$ = the measured acceleration at a point on the skull,

$\vec{w}$ = the angular velocity vector of the skull, as measured via MHD Dynacube,

and $\vec{r}$ = the radial vector from the center of gravity to the measurement point.

I.9: High Speed Motion Picture Analysis

Motion analysis is performed on a high speed motion picture image of the test recorded by the offboard driver's side camera, using a NAC Inc. model 160F film motion analyzer and Concurrent Processing Inc. Motion Analysis Package (MAP) software.

The software determines the effective frame rate of the camera, by measuring the relative positions of the timing marks on several frames of the film image. The timing mark images are identified to the program using the digitizing screen of the analyzer. The T_0 frame, as indicated by the special timing mark and the strobe flash, is also identified to the program. All subsequent frames are then indexed to the T_0 frame. The distance scale of the film image is calculated by the software after the images of two points on the test fixture, of a known distance apart, are identified on the analyzer screen.

During the pre-launch preparations, adhesive-backed crosshair-type photo targets are attached to various points on the test fixture and on the occupant, to facilitate accurate identification of the points of interest during film analysis. Within the T_0 frame image, the points of interest, including a fixed point on the test fixture, are identified to the program using the digitizing screen of the film analyzer. The same points are also identified in subsequent frames, incremented by a fixed time interval, through the whole event. After all required points are recorded, kinematic data is calculated and reported by the program and plots are generated.

I.10: Data Plotting

For the time-history plots which appear in this report, the data is first low-pass filtered to the appropriate Channel Frequency Class (CFC), as defined in SAE J211, using a NHTSA-supplied two-pass (forward and backward) 4-pole Butterworth software filter algorithm. The record length is truncated, as necessary, to expand the region of interest. The plots are then generated by a spreadsheet program.

Chestband data is processed by the NHTSA-supplied program RBANDS_PC, after being low-pass filtered to CFC 180, and stripped of pre-trigger points. The plots are generated by a local ASL program PLOTIT.

String pot chest data is processed by the NHTSA-supplied program STRING2, after being low-pass filtered to CFC 180, and stripped of pre-trigger points. The plots are generated by a local ASL program STRINGPT.

I.11 Strain Gauge Processing

Rectangular rosette strain gauges are mounted on forearm bone surface. Two strain gauges are mounted on the radius, and two are mounted on the ulna, generally in the same bone section in the midshaft region of each bone. Location and orientation measurements are taken for each gauge and are tabulated in Table 2.2.3.2. During testing, strain gauge data is taken for each of the three gauges per rosette. This data is filtered to SAE J211 Channel Frequency Class 1000 for further processing.

The strain gauge data from each rosette strain gauge is processed so that the strain gauge data from each rosette axis (denoted 1,2,3) is transformed to strain in principle orthogonal axes ε_P, $\varepsilon_{Q,}$ and an angle, θ. The angle θ is measured from the P direction to the bone long axis. The original rosette strain gauge is generally oriented along 2 strain gauge direction. These principle axes P and Q denote the directions of maximum and minimum strain respectively. The relationship between bone axes, strain gauge axes, and principle strain axes are shown in *Figure I.11.1*.

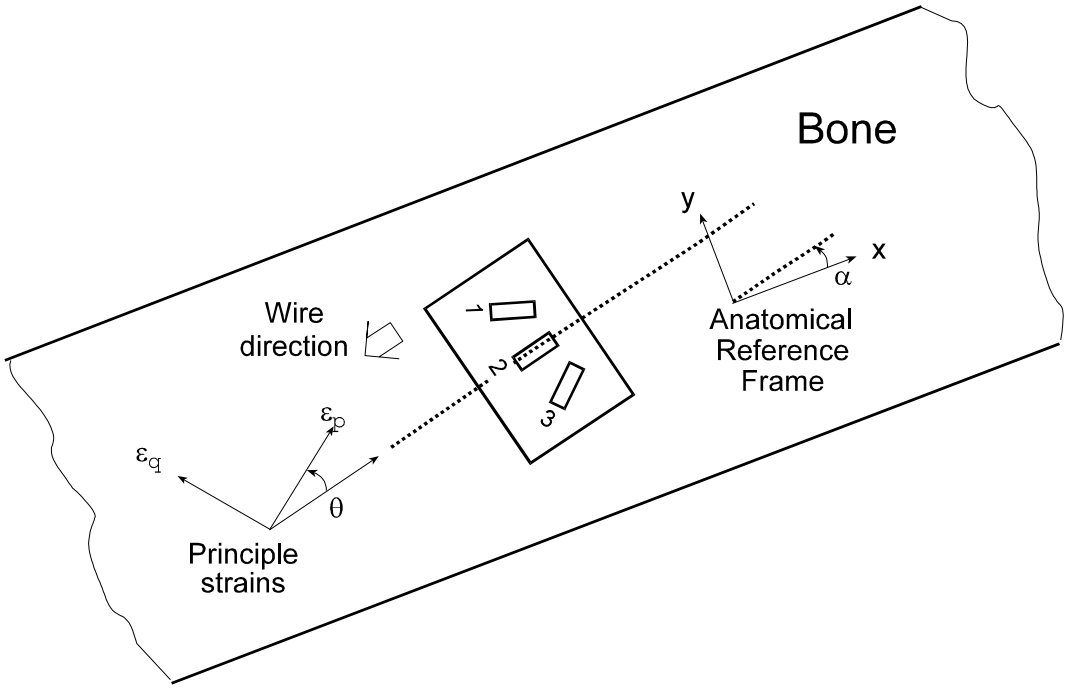

Figure I.11.1: Strain gauge and bone axes systems

Bone elastic properties are derived from Computer Tomography (CT) scans as outlined in Section 2.1.5.2. A forearm calibration procedure is used to confirm the computed properties. In this procedure, the forearm is initially pronated and placed in a quasistatic 3-pt bend. The Measured stiffness properties are used to confirm the calculated values.

From the strain data, anisotropic stresses are calculated in the bone material directions (i.e. the long bone axis is direction 1, the surface normal to the long bone axis is direction 2) using an analysis of Carter. Anisotropic properties data is derived from CT scans as outlined in Section 2.1.5.2. Using the anisotropic stresses, beam theory is used to calculate the sectional moments both in the radius and in the ulna. Assumptions used in this analysis include, 1) no torsional bending under airbag load, 2) the state of stress is induced by a two-axis bending and a two-axis shear, 3) the section of the beam analyzed is prismatic and convex with dimensions of the bone section on which the two strain gauges are mounted, 4) bone material is assumed linear and elastic with constant sectional properties. Sectional properties and physical characteristics such as cross-sectional areas and moments of inertia are derived from pre-test CT scans.